Corrosion-induced Cracking in Reinforced Concrete Structures -a numerical study

Thybo, Anna Emilie Anusha

Publication date:
2018

Document Version
Publisher's PDF, also known as Version of record

Corrosion-induced Cracking in Reinforced Concrete Structures - a numerical study

Anna Emilie Anusha Thybo

PhD Thesis

Department of Civil Engineering
Technical University of Denmark

2018

Figure front page:

Xxx

Corrosion-induced Cracking in Reinforced Concrete Structures - a numerical study

Printed by xxx

Department of Civil Engineering

Technical University of Denmark

ISBN: xxx

ISSN: xxx

Report: xxx

Preface

This thesis is submitted as a partial fulfilment of the requirements for the Danish Ph.D. degree. The thesis is based on numerical investigations carried out as part of the Ph.D. project "Corrosion-induced Cracking in Reinforced Concrete Structures - a numerical study", undertaken at the Department of Civil Engineering at the Technical University of Denmark (DTU Byg), Kgs. Lyngby, Denmark.

An external research stay at Concrete Laboratory, Department of Civil Engineering, Nagoya University, Nagoya, Japan formed part of the Ph.D project.

The principal supervisor of the Ph.D. project was Professor Henrik Stang from DTU Byg with co-supervisors postdoc Alexander Michel, also from DTU, Professor Mette Rica Geiker, from Norwegian University of Science and Technology, and Lars Nyholm Thrane from Danish Technological Institute.

Financial support was provided by the Danish Expert Centre for Infrastructure Constructions.

Aarhus the 1st of May 2018

Anna Emilie A Thybo 1/5 - 2018

Anna Emilie Anusha Thybo

Acknowledgments

First, I would like to express my gratitude for the support and advices from my supervisors Henrik Stang and Alexander Michel at the Technical University of Denmark, Mette Rica Geiker at Norwegian University of Science and Technology, and Lars Nyholm Thrane at the Danish Technological Institute. Also thanks to Alexander Michel for providing me with experimental data and helping me with experimental setup.

Further, I would like to thank Professor Nakamura and his research group at the Concrete Laboratory at Nagoya University for an interesting and educating stay. I was welcomed in the friendliest and most helpful way I could wish for. Through professional and social activities I experienced and learn so much for which I am very grateful.

I would like to acknowledge the financial support of the Danish Expert Centre for Infrastructure Constructions, DTU for funding this PhD. Financial contributions supporting external research stays and attendance of conferences, provided by IDAs og Berg-Nielsens Studie- og Støttefond, Oticon Fonden, Otto Mønsteds Fund, Rudolpf Als Fondet, and the DTU were very much appreciated.

Thanks to my colleagues and fellow PhD students for the time at DTU. Special thanks to postdoc Bradley Justin Pease who provided me with data from experimental observations. Furthermore, I appreciate the interesting discussions with and constant support from Anders Ole Stubbe Solgaard, Ieva Peagle, Jan Winkler, Joan Hee Roldsgaard, Kenneth Kleissl, Mads Mønster Jensen, Nina Gall Jørgensen, Rocco Custer and Sebastian Andersen.

Finally I would like to thank my family and friends without whom I would never have finished due to their continuing support and general understanding of my absence. Special thanks to my husband Mads who has always supported me in any possible way during this process.

Abstract

Buildings and infrastructure constructions represent a major part of the investments made today and thus, the owners make severe demands on the economy when building new structures. Durability and service life of structures are two key parameters strongly related to the economy. Increased durability and longer service life decreases the total amount of materials needed when considering construction and maintenance of structures decreasing the total costs. Further optimisation of material usages is beneficial when considering sustainability as extraction of raw materials, production of structural members, repair and disposal constitute a large part of the total amount of carbon dioxide emission during the life cycle of a structure. One of the most decisive factors controlling the durability and service life of a structure - designed and constructed without flaws and deficiencies - is deterioration of the structure due to environmental effects. Reinforced concrete structures comprise a great part of the structures taking form today and in structures, such as bridges, tunnels, parking garages etc. Corrosion of the reinforcing steel is the most significant deterioration mechanism in reinforced concrete structures. Reinforcement corrosion is therefore a major concern during design and service life.

The aim of the present work was to further develop the knowledge within the field of service life of reinforced concrete structures. To be exact further development of service life modelling based on reinforcement corrosion.

First an existing finite element model simulating corrosion-induced cracking was taken a step further. The existing deterministic model, which was developed at DTU, is divided into five distinct domains; concrete, reinforcement, a corrosion layer, cracking, and debonding domain (crack opening and sliding at reinforcement surface). Applying a fictitious thermal load to the elements in the corrosion layer expansion of the corrosion products was simulated applying a discrete crack modelling approach. Due to expansion of the corrosion products the stresses in the reinforcement/concrete interface increases reaching at some point the tensile strength of the concrete initiating cracking. Penetration of corrosion products into the surrounding concrete was included in the modelling postponing the initiation of the crack following

experimental observations of the corrosion process. With further expansion of the corrosion products the crack continues to develop in the concrete cover layer towards the concrete surface. As several studies have shown that corrosion products precipitate non-uniformly along the circumference of the reinforcement the model was further developed changing the precipitation of corrosion products along the circumference of reinforcement from uniform to non-uniform varying the corrosion current density along the circumference of the reinforcement.

Secondly a new corrosion-induced damage model was developed. Applying a smeared crack modelling approach the new model is cable of modelling the initiation and propagation of multiple micro- and macrocracks. The model is based on finite element theory and is divided into three domains: a concrete domain surrounding a corroding and a non-corroding steel domain. To simulate the expansive nature of solid corrosion products a thermal expansion coefficient was applied to the corroding steel elements. Similar to the discrete crack model cracking was initiated when stresses in the reinforcement/concrete interface exceeded the tensile strength of the surrounding concrete. Besides non-uniform precipitation of corrosion products along the circumference of the reinforcement the modelling also included effects such as penetration of corrosion products into the surrounding concrete and creep.

Parallel to the modelling the simulated results were compared to experimental data. The applied experimental data was results of experiments produced at DTU and observations described in the literature. The comparison showed good estimates of both deformations in the reinforcement/concrete interface and crack width. Comparing with experimental data the discrete and the smeared crack modelling approach was also compared indicating that a smeared crack modelling approach show more realistic cracking pattern however this modelling approach is strongly depend on the number of steps during simulations.

Finally both model approaches was used to numerically study the influence of different mechanisms and geometrical parameters on corrosion-induced cracking. Among others the influence of non-uniform precipitation of corrosion products was investigated. The investigation showed that the crack pattern and the development of a surface crack width strongly depend on the formation of the precipitated corrosion products and that the degree of reinforcement corrosion varies at time-to surface crack initiation.

Resumé

Bygninger og konstruktioner til infrastrukturen udgør en stor del af de investeringer, der foretages i dag og derfor stilles der store krav til anlægsøkonomien fra bygherrens side. Holdbarhed og levetid af konstruktioner er to nøgleparametre stærkt relateret til økonomien. Øget holdbarhed og længere levetid reducerer den samlede mængde materialer, der er nødvendig, til opførelse og vedligeholdelse af byggeriet, hvormed de samlede omkostninger reduceres. Yderligere er optimering af materialeanvendelse essentiel, når der fokuseres på byggeriets bæredygtighed og kuldioxidemission i konstruktionens livscyklus ved både udvinding af råmaterialer og produktion af strukturelle elementer samt reparation og bortskaffelse. En af de mest afgørende faktorer, der styrer holdbarhed og levetid af en konstruktion - projekteret og konstrueret uden fejl og mangler - er nedbrydelse af konstruktionen på grund af miljøpåvirkninger. Armerede betonkonstruktioner udgør en stor del af de konstruktioner, der benyttes i infrastrukturen i dag, såsom broer, tunneller, parkeringshuse mv. Korrosion af armeringen er den væsentligste mekanisme i nedbrydningen af armerede betonkonstruktionerne. Armeringskorrosion har derfor meget stor fokus under projektering og vedligeholdelse.

Formålet med nærværende arbejde var at videreudvikle viden inden for levetid for armerede betonkonstruktioner, nærmere bestemt videreudvikling af levetidsmodellering baseret på armeringskorrosion.

Til at begynde med blev en eksisterende, finite elementmodel, der simulerer revner forårsaget af korrosion videreudviklet. Den eksisterende deterministiske model, som blev udviklet på DTU, er opdelt i fem forskellige områder; beton, armering, et korrosionslag samt et revne- og debondingområde (revneåbning og glidning ved armeringsoverfladen). Ved anvendelse af en fiktiv termisk belastning på elementerne i korrosionslaget simuleres udvidelsen af korrosionsprodukterne ved anvendelse af en deterministisk revnemodelleringsmetode. Grundet udvidelsen af korrosionsprodukterne øges spændingerne i armering/betonkontaktfladen og når på et tidspunkt trækstyrken af betonen hvormed en revne initieres. Indtrængning af korrosionsprodukter i den omgivende beton blev medtaget i modelleringen, hvilket udsatte initieringen af revnen stemmende overens med eksperimentelle observationer

af korrosionsprocessen. Ved yderligere udvidelse af korrosionsprodukterne fortsætter revnen med at udvikle sig i dæklaget bevægende sig mod betonoverfladen. Da flere studier har vist, at korrosion af armering ikke korroderer jævnt fordelt over armeringsoverfladen, blev modellen videreudviklet. Fordelingen af korrosionsprodukterne langs armeringsomkredsen blev ændret fra jævnfordelt til ikke-jævnfordelt ved at variere korrosionens strømningsdensitet langs omkredsen af armeringen.

Dernæst blev en ny brudmekanisk korrosionsmodel, til beskrivelse af skadesudviklingen i en betonkonstruktion, udviklet. Ved at anvende en smeared revnemodellering blev det muliggjort for den nye model, at medtage begyndelsen og udviklingen af flere mikro- og makrorevner. Modellen er baseret på finite element teori og er opdelt i tre områder: Et betonområde, der omgiver et korroderende og et ikke-korroderende stålområde. For at simulere de faste korrosionsprodukters ekspansion blev der anvendt en termisk ekspansionskoefficient på de korroderende stålelementer. På samme måde som den deterministiske revnemodel initieres revner ved højere spændinger i armering /betonkontaktfladen end trækstyrken af den omgivende beton. Udover ikke-jævnt fordelt korrosionsprodukter langs armeringens omkreds omfattede modelleringen også effekter såsom indtrængning af korrosionsprodukter i den omgivende beton og krybning.

Parallelt med modelleringen blev de simulerede resultater sammenlignet med eksperimentelt data. Det anvendte eksperimentelle data var resultater af forsøg udført på DTU og observationer beskrevet i litteraturen. Sammenligningen viste gode estimater af både deformationer ved armering/betonkontaktflade og revnevidde. Sideløbende med sammenligningen med eksperimentelle data blev også den deterministiske model sammenlignet med modellen, der anvendte en smeared revnemodelleringsmetoden. Sammenligningen indikerede at en smeared revnemodel bedre simulerer et realistisk revnemønster, men at denne modelleringsmetode er stærkt afhængig af antallet af beregningstrin under simuleringen.

Endeligt blev begge modeller brugt til numerisk at studere indflydelsen af forskellige mekanismer og geometriske parametre på korrosionsinitieret revnedannelse. Blandt andet blev indflydelsen af ikke-jævnt fordelte korrosionsprodukter undersøgt. Undersøgelsen viste, at revnemønsteret og udviklingen af en revne i betonoverfladen afhænger stærkt af fordelingen af korrosionsprodukter, og at graden af armeringskorrosion varierer for tidspunktet, hvor revnen når betonoverfladen.

Table of Contents

Chapter 1

Introduction

1.1 Reinforced concrete structures

A considerable part of the civil infrastructure is made from reinforced concrete. Concrete is a cheap material compared to other building materials, such as steel or wood. Concrete can be produced in most parts of the world as in principle only water, cement and aggregates are necessary. Further, concrete is a versatile material and engineers, depending on the purpose, can decide to cast on site or use pre-casted elements. Due to the liquid texture prior to hardening, it is possible to cast concrete in almost any kind of shape. This is an advantage considering aesthetics as well as optimising material use to create shapes that follow variation in load [*Dansk Betonforening, 2014*].

One of the main characteristic of concrete is its compressive strength, which is mainly controlled by the water-to-cement ratio (w/c) [*Bertolini et al., 2013*; *Aalborg Portland, 2012*]. Decreasing the w/c increases the compressive strength. A high compressive strength is beneficial when building for example large structures such as bridges, tunnels and high rise buildings. On the other hand, one of the main drawbacks of concrete is its low tensile strength. However, combined with steel, which is known for its excellent tensile and ductile characteristics, the composite material is suitable for almost any construction purposes. The high tensile strength of steel allows to overcome the main drawback of concrete, i.e. low tensile capacity, and the good ductility prevents brittle failure of the composite material.

In general, (reinforced) concrete is also known for its good durability. Concrete does not need surface treatment compared to other building materials, such as steel or wood, even if placed in water or below ground level. Further, concrete provides protection of the embedded steel considering durability and deterioration [*Aalborg Portland, 2012*; *Dansk Betonforening, 2014*]. In concrete, the alkaline level is very high, i.e. the pH is very high. The alkaline environment protects the embedded steel

(from harmful substances such as carbon dioxide or chlorides) surrounding the reinforcement with a passive layer [*Bardal, 2004*]. However, under certain circumstances this protective "symbiosis" can be destroyed leading to deterioration of reinforced concrete structures. Nowadays, deterioration is the governing factor considering service life of structures and reinforcement corrosion is one of the most significant deterioration mechanisms in reinforced concrete structures [*Rendell et al., 2002*]. The two main causes for reinforcement corrosion are in general the ingress of carbon dioxide or chlorides though the concrete. Carbonation describes thereby the loss of alkalinity due to the reaction of alkaline constituents with carbon dioxide in the concrete surrounding the reinforcement and subsequently initiating the corrosion process. Also, penetration of chloride ions through the concrete cover and the accumulation beyond a certain critical concentration near the reinforcement surface can lead to the destruction of the passive film and thus initiation of reinforcement corrosion. Propagation of reinforcement corrosion may lead to corrosion-induced damages, such as concrete cracking, spalling, delamination, and cross sectional reduction of the reinforcement, which may cause aesthetic damages, decrease of the load bearing capacity, and in the worst-case lead to fatal structural consequences, such as failure.

1.2 Service life of reinforced concrete structures

The service life of a reinforced concrete structure may be defined as the length of time during which a desired level of functionality is maintained. The end of service life is then usually defined by the owner of the structure depending on general requirements concerning e.g. structural safety as well as aesthetics and comfort. Among others, rising awareness for the need of more sustainable design led to service life requirements for modern concrete structures of at least 100 years e.g. Great Belt [*Bertolini et al., 2013*]. In doing so, designers typically use standards e.g. [*Eurocode, 2008*] or simply experience, which are often based on oversimplified assumptions and neglect important phenomena, for the service life design of reinforced concrete structures. The standards and codes only provide information on concrete cover thickness and maximum crack width, based on an expected service life of 50 years. In order to provide additional information when estimating the service life of a structure, service life models such as DuraCrete [*DuraCrete, 2000*], fib [*fib, 2006*], 4sight [*Synder, 2001*], Hetek *[Nilsson et al. 1996*] and DuCOM [*Maekawa et al., 1999*] are sometimes used by designers.

In general, the service life of reinforced concrete structures may be divided into two stages: 1) the initiation phase and 2) the propagation phase. The initiation phase is characterised by the ingress or leaching of substances through the concrete cover layer. Eventually, de-passivating substances, such as e.g. carbon dioxide and chloride, penetrate through the concrete cover layer and may at some point (when a critical amount is reached) lead to a breakdown of the passive layer (de-passivation of the

reinforcement). At this stage, the initiation phase is finished and the propagation phase begins.

The underlying concept employed in all of the aforementioned standards, recommendations and models for the service life design of reinforced concrete structures is seen in Figure 1.1. The figure is a schematic illustration of the different deterioration stages of a structure and was developed by [*Tuutti, 1982*]. For the case of deterioration due to reinforcement corrosion, the figure describes age and condition of a structure along with two corrosion phases – initiation and propagation. The blue solid line describes the typical service life model and the red dashed line describes a modified service life model that includes part of the propagation phase until the end of service life.

The rate of concrete deterioration increases greatly in the propagation phase compared to the initiation phase, see Figure 1.1. Due to the corrosion process, the cross section of the reinforcement is reduced, which may lead to a decreased structural capacity. Moreover, the corrosion process leads to the formation of corrosion products, which are taking up more volume than the consumed steel. This process may lead to internal damage in the concrete initiating at the reinforcement surface, which can, with continuing corrosion, lead to cracking, delamination and spalling in the concrete cover [*Wong et al., 2010*; *Tran, 2012*; *Pease et al., 2012*; *Michel et al., 2013*]. Prediction of the corrosion process in the propagation phase is uncertain as several parameters may influence the rate of deterioration. Among others, humidity, the present of oxygen and transport and material properties of the concrete [*Bardal, 2004*] are known to be important parameters that affect the corrosion process in uncracked concrete.

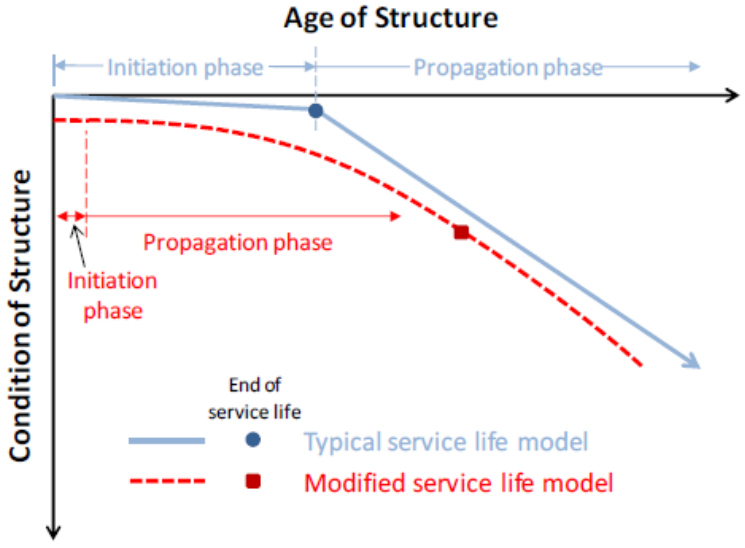

Figure 1.1 *Traditional service life model based on* [*Tuutti, 1982*] *compared to service life model including part of the propagation phase in the service life, from* [*B.J. Pease et al., 2012*]

At present, the remaining service life of existing reinforced concrete structures is commonly based on visual inspections, i.e. the appearance of rust stains or presence of corrosion-induced cracks. The visual observations may then be linked to a mechanical model to relate e.g. surface crack width to cross sectional reduction of reinforcement and thus amount of corrosion, which may allow for estimation of the residual load bearing capacity. However, the accuracy of the mechanical model plays then an important role in the evaluation of the remaining service life as e.g. severe corrosion may be possible without visible cracking. Thus, in-depth knowledge on mechanisms and parameters related to corrosion-induced damage is needed to allow for more accurate determination of the remaining service life.

1.3 Corrosion-induced damage modelling - state of the art

Within the industry and academia, a considerable effort is done in order to understand and predict the service life and associated deterioration mechanisms of reinforced concrete structures. Assuming an ideal situation with homogenous reinforced concrete as well as symmetric and non-varying exposure conditions (i.e. no variations due to seasonal changes in temperature, humidity, etc.), yielding a uniform deposition of corrosion products at the reinforcement/concrete interface, corrosion-induced damage generally depends on the cover thickness as well as reinforcement diameter and spacing i.e. geometry [*Jamali et al., 2013*]. However, this ideal situation does rarely exist in situ, which leads to the need for more complex modelling approaches to describe reinforcement corrosion and corrosion-induced damages. Several parameters affect the corrosion as discussed in the previous sections giving rise to questions such as “Where does reinforcement corrosion initiate?”, “How does reinforcement corrosion propagate?” and “How is the reinforcement corrosion process modelled?” Additionally, modelling of corrosion-induced damage of the surrounding concrete has to be considered, increasing the number of parameters and questions to be answered including among others “How does reinforcement corrosion affect the surrounding concrete?”, “When does corrosion-induced cracking initiate?”, “How does corrosion-induced cracking propagate” and “How can corrosion-induced damage processes be modelled?”

A vast amount of studies can be found in the literature in the quest of answering the above-mentioned questions and to predict the time at which the service life ends. The proposed models focus thereby on different aspects in relation to the service life of a reinforced concrete structure. Based on the theoretical background, the proposed models can be divided into three different groups: transport, corrosion and mechanical models. While transport processes, e.g. [*Jensen, 2014*], are typically related to the ingress of various substances and heat, a study seen from a corrosion perspective describes the electrochemical processes, e.g. [*Michel, 2012*], taking place at the reinforcement surface due to the ingress of corrosion-initiating substances. Both mechanisms are primary related to material technology and chemistry.

The mechanical process (in this context) is a consequence of the reinforcement corrosion i.e. corrosion-induced damage – both with regard to concrete and reinforcement. As the emphasis of this thesis is on the modelling of corrosion-induced damage, in the following, focus will be placed on the review of modelling approaches related to this topic. In general, models dealing with corrosion-induced damage can be divided into three approaches i.e. analytical [*Bazant, 1979*; *Pantazopoulou, S. J., & Papoulia, 2001*; *Bhargava et al., 2006*; *Chernin et al., 2010*; *Balafas and Burgoyne, 2011*], empirical [*Andrade et al., 1993*; *Rodriguez et al., 1996*; *Liu and Weyers, 1998*; *Alonso et al., 1998*; *Vu et al., 2005*] and numerical [*Molina et al., 1993*; *Suda et al., 1993*; *Lundgren, 2005b*; *Isgor and Razaqpur, 2006*; *Richard et al., 2010*; *Tran, 2012*; *Ožbolt et al., 2012*; *Strauss et al., 2012*; *Bohner, 2012*; *Solgaard et al., 2013*; *Fahy et al., 2017*; *Guzmán and Gálvez, 2017*] and are therefore discussed more detailed in the following.

1.3.1 Analytical approach

Closed form solutions are applied in the modelling scheme of analytical models. The approach makes the models more flexible, compared to for example empirical models. However, the geometry is fixed and often only one reinforcement bar is considered. Analytical approaches, e.g. [*Pantazopoulou, S. J., & Papoulia, 2001*; *Bhargava et al., 2006*; *Balafas and Burgoyne, 2011*], are generally applying the theory of a thick-walled cylinder simplifying the geometry and determining the state of stress in the surrounding concrete. Both [*Balafas and Burgoyne, 2011*] and [*Pantazopoulou, S. J., & Papoulia, 2001*] partially applies the theory of a thick-walled cylinder in combination with an empirical or numerical approach respectively, to overcome some of the aforementioned analytical challenges.

One of the first models developed, based on the theory of a thick-walled cylinder, was presented in [*Bazant, 1979*]. [*Bazant, 1979*] assumed that the cover fails at the first appearance of cracking. However, the model was not experimental validated and it was later shown that the model underestimated the time to corrosion-induced cracking [*Liu and Weyers, 1998*].

The geometry of a thick-walled cylinder induces a uniform distribution of internal pressure and therefore uniform distribution of corrosion products in the reinforcement/concrete interface is commonly assumed. [*Balafas and Burgoyne, 2011*] acknowledged localized corrosion but neither [*Balafas and Burgoyne, 2011*] nor [*Bazant, 1979*; *Pantazopoulou, S. J., & Papoulia, 2001*; *Bhargava et al., 2006*] included non-uniform precipitation of corrosion products in the modelling scheme. The thickness of the thick-walled cylinder is determined by the concrete cover around the reinforcement. However, crack propagation and type of cracking mechanism (spalling or delamination) is also determined by the distribution of corrosion products.

Each of the models previously mentioned has its benefits. [*Balafas and Burgoyne, 2011*] included long terms properties of concrete (creep and shrinkage) due to the slow process of corrosion and considered an equivalent rust thickness accounting for the compaction of rust. However [*Balafas and Burgoyne, 2011*] only considered concrete spalling. Both [*Pantazopoulou, S. J., & Papoulia, 2001*] and [*Bhargava et al., 2006*] took concrete softening into account. [*Bhargava et al., 2006*], focusing on cover cracking and weight loss of the reinforcement bar, further included the stiffness of the remaining steel and corrosion products. [*Pantazopoulou, S. J., & Papoulia, 2001*] took the presence of cracks into account and applied finite differences in the analysis of the concrete cover.

1.3.2 Empirical approach

A generally accepted model is the semi empirical model described in [*Liu and Weyers, 1998*]. The model is used as a basis in several studies and is a further development of the analytical corrosion-induced cracking model originally presented in [*Bazant, 1979*]. As described it was shown that [*Bazant, 1979*] underestimated the time to corrosion-induced cracking [*Liu and Weyers, 1998*]. [*Liu and Weyers, 1998*] explained the deviation introducing the phenomenon of the “porous zone”. The porous zone, as a result of the porous nature of concrete, allows for corrosion products to penetrate from the surface of the reinforcement into the surrounding concrete postponing the time to cracking. However, an actual study of this phenomenon was not conducted in the study and the phenomenon was implemented as a fitting factor applying a semi experimental value to the thickness of the porous zone. Further the modelling focused on the development of one vertical crack due to expansion of uniform corrosion, even though localized corrosion was observed in the experiments. In [*Vu et al., 2005*] localized corrosion was also neglected in the modelling even though localized corrosion was observed in experiments. Though, [*Vu et al., 2005*] further introduced a factor varying the corrosion current density accounting for the deviation in crack propagation between accelerated corrosion testing and real life corrosion currents. Generally seen the models presented in [*Liu and Weyers, 1998*] and [*Vu et al., 2005*] provided reasonable predictions of corrosion-induced cracking. However, due to the fixed geometry and material parameters empirical approaches are in general not very flexible and therefore these types of models are typically only applicable for the cases they were calibrated for.

1.3.3 Numerical approach

A numerical approach is often chosen overcoming the challenges (e.g. fixed geometry) of an analytical modelling approach and at the same time maintaining flexibility and accuracy, which is the drawback of an empirical modelling approach. The finite element (FE) method is a frequently applied numerical approach. Applying a FE approach elements form the geometry and are divided into domains typically

representing concrete, steel and corrosion. It is possible to categorise the main part of the models presented in the literature into discrete and smeared cracking approaches.

[*Molina et al., 1993*] suggested, as one of the first, a 2D finite element model for simulation of cracking in concrete specimens subjected to reinforcement corrosion. A smeared cracking approach was applied simulating cracking based on geometrical and material criteria and including the effect of microcracking. A thermal analogy was used to account for the expansive nature of corrosion products. Assuming corrosion products could be treated as a fluid, [*Molina et al., 1993*] considered the properties of the corrosion products nearly equal to liquid water. Penetration of corrosion into the porous concrete and long term properties of concrete, such as creep and shrinkage, was not implemented in the modelling. Reliable results of the main characteristics of the experimental behaviour were shown, but a definitive validation of the numerical model was not possible at the time being. Like [*Molina et al., 1993*] also [*Lundgren, 2005a*; *Ožbolt et al., 2012*; *Sanz et al., 2017*] applied a smeared cracking approach and included, in addition, penetration of corrosion products into the porous concrete in the modelling scheme. [*Lundgren, 2005a*] however, concluded that excluding the effect of penetration into the porous concrete was giving a more correct result. Further, the 3D model presented in [*Lundgren, 2005a*] was considering uniform precipitation of corrosion products. [*Ožbolt et al., 2012*] also presented a 3D model but contrary to [*Lundgren, 2005a*] included the effect of non-uniform precipitation of corrosion products, shrinkage and diffusion of corrosion products into cracks. Tough, [*Ožbolt et al., 2012*] neglected the effect of concrete softening. [*Sanz et al., 2017*] included both the effect of concrete softening as well as penetration of corrosion products into the porous concrete but not long-term properties of concrete. Further, [*Sanz et al., 2017*] assumed uniform precipitation of corrosion products.

Applying a discrete modelling approach both location of crack initiation and the crack propagation path(s) are predefined. Corrosion and therefore most likely corrosion-induced cracks, initiate at weak locations (due to e.g. flaws, debonding etc.) at the reinforcement/concrete interface, which are difficult to predict. One drawback of applying a discrete cracking approach is therefore, that the governing macrocrack in reality may be initiating and propagating somewhere else than expected giving incorrect predictions. Further, the effect of microcracking is not included in the modelling approach, which may affect both the stiffness and behaviour of the structure. Despite the drawbacks, the discrete cracking approach is a commonly applied and well-presented approach in the literature [*Isgor and Razaqpur, 2006*; *Richard et al., 2010*; *Biondini and Vergani, 2012*; *Tran, 2012*; *Fahy et al., 2017*; *Guzmán and Gálvez, 2017*]. The main reason for applying a discrete cracking approach is the reduced complexity compared to a smeared cracking approach. Generally, the suggested models described in the literature vary implementing different mechanisms and characteristics. [*Isgor and Razaqpur, 2006*; *Fahy et al., 2017*] both presented a 2D coupled model focusing on the corrosion rate and the

connected propagation of cracking however long term properties of concrete were not included in the modelling. [*Biondini and Vergani, 2012*] and [*Tran, 2012*] considered non-uniform precipitation of corrosion products and penetration of corrosion products into the porous concrete but the 3D models were not coupled to a corrosion model and long-term properties of concrete were not implemented in the modelling scheme. Contrary, [*Fahy et al., 2017*] included long-term properties of concrete and considered corrosion products as a fluid explaining penetration due to radial pressure. However, uniform precipitation of the corrosion products was assumed. [*Guzmán and Gálvez, 2017*] neither included penetration of corrosion products into the porous concrete nor long-term properties of concrete but included non-uniform precipitation of corrosion products in a 2D modelling scheme. [*Richard et al., 2010*], stands out, suggesting, among few, a coupled 3D model. Focusing on the reinforcement/concrete interface the model applied continuum damage mechanics setting up a number of constitutive equations to model the bond strength as well as the corrosion and uniform expansion of the corroding reinforcement. The corrosion was coupled with irreversible thermodynamic processes however, the reduction in reinforcement radius and effects of corrosion in the reinforcement/concrete was not considered.

1.3.4 Parameters affecting crack initiation and propagation

Several parameters affect the corrosion-induced damage. [*Jamali et al., 2013*] suggested five parameters to be considered predicting corrosion-induced damage: 1) Corrosion rate, also known as the corrosion current density, which is a function of the environment and exposure conditions and depends on material and geometrical properties such as concrete strength and cover layer. Under natural conditions the corrosion current density is typically around 1 $\mu A/cm^2$ [*Jamali et al., 2013*]. For testing, the corrosion current density is often increased by means of impressed current (e.g. 100 $\mu A/cm^2$) to reduce the time frame. 2) Type of corrosion products, which is also a function of the environment and exposure conditions. For example, characteristics (such as volume expansion and morphology etc.) of the corrosion products vary depending on the presence of carbon dioxide or chloride [*Jamali et al., 2013*]. 3) Corrosion accommodating region, which is capable of depositing corrosion products without inducing expansive stresses [*Michel et al., 2014*], in the porous concrete at the reinforcement/concrete interface. The porosity of the concrete primarily depends on the water-to-cement ratio (w/c) and the degree of hydration [*Pease et al., 2012*]. However, e.g. casting also affects the porosity and presence of voids at the reinforcement/concrete interface. 4) Mechanical properties of materials. Corrosion-induced damage depends on the concrete strength and tension softening, however, also other material properties of concrete, such as e.g. alkaline characteristics, affect the time to corrosion initiation. 5) Geometry. Parameters such as concrete cover layer, reinforcement diameter, reinforcement spacing and corrosion

morphology affect both time of crack initiation and the following crack propagation and should therefore be considered.

In particular, two parameters are worth discussing further when considering corrosion-induced damage models, i.e. penetration of corrosion products into the surrounding (porous) concrete and the distribution of corrosion products (corrosion morphology) at the reinforcement/concrete interface (along the circumference of the reinforcement when considering 2D modelling).

1.3.4.1 Penetration of corrosion products

[*Molina et al., 1993*; *Liu and Weyers, 1998*] were among the first to consider penetration of corrosion products into the surrounding concrete introducing the term "porous zone" (in the present work also referred to as corrosion accommodating region (CAR) [*Michel et al., 2013*]). The porous zone was referred to as a zone in which corrosion products could penetrate/diffuse due to the porosity (pores and voids) of the concrete. As a consequence, the pressure, due to penetration of some of the expanding corrosion products, is delayed [*Andrade et al., 1993*] postponing the time to crack initiation. Experimental investigations, on this subject, are few and the effect and modelling of penetration of corrosion products into the surrounding concrete is therefore an ongoing discussion and questions such as "Should the modelling of corrosion-induced damage include penetration of corrosion products?", "How is the mechanism implemented?" and "What are the effects of the implementation?" arise. With respect to the first question, results of experimental investigations, such as visual inspection [*Tran, 2012*; *Wong et al., 2010*], scanning electron microscope (SEM) [*Zhao et al., 2013*] and x-ray attenuation measurements [*Michel et al., 2013*], strongly indicate that corrosion products indeed penetrate into the surrounding concrete and the mechanism is generally accepted in recent modelling approaches [*Pantazopoulou, S. J., & Papoulia, 2001*; *Bhargava et al., 2006*; *Ožbolt et al., 2012*; *Fahy et al., 2017*; *Sanz et al., 2017*]. In one of the first attempts, to include penetration of corrosion products into the porous zone, the mechanism was implemented as a fitting parameter based on the deviation between modelled results and experimental observations [*Liu and Weyers, 1998*]. [*Pantazopoulou, S. J., & Papoulia, 2001*; *Bhargava et al., 2006*; *Richard et al., 2010*; *Balafas and Burgoyne, 2011*] all assumed penetration of corrosion products into the porous concrete. In [*Solgaard et al., 2013*; *Guzmán and Gálvez, 2017*] the mechanism was acknowledged but the effect was not included in the modelling scheme due to insufficient information and experimental data. Also [*Lundgren, 2005a*] and [*Jamali et al., 2013*] discuss the influence of the mechanism. [*Lundgren, 2005a*] implemented penetration of corrosion products into the surrounding concrete. However, due to lack of information, at the time being, regarding size of the porous layer and mechanical properties of the corrosion products, the model predicted unsatisfying results and it was decided not to include penetration of corrosion products in the modelling. [*Jamali et al., 2013*] claimed that it was not

possible to measure the thickness of the porous zone due to an unclear boundary between the porous zone and the remaining concrete. Though, in [*Michel et al., 2013*] it was possible to distinguish between the different materials i.e. corrosion products, steel and concrete, using x-ray attenuation measurement. Further, [*Jamali et al., 2013*] was critical of the influence of the corrosion current density on penetration of corrosion products suggesting that increased current density decreased the effect of penetration. However, in [*Michel et al., 2013*] the penetration depth was not affected by the corrosion current density. Independent on corrosion current density, the penetration depth was the same, considering the same amount of corrosion (the time at which the amount was reached differed). This tendency was shown for different w/c ratios as well. In [*Michel et al., 2013*] modelled results, including the effect of penetration, were compared to experimental observations. Comparing deformations and cracking satisfying results were obtained.

1.3.4.2 Distribution of corrosion products at reinforcement/concrete interface

Whether or not the distribution of corrosion products at the reinforcement/concrete interface is uniform or non-uniform is a discussed issue. Experimental observations [*Vu et al., 2005*; *Wong et al., 2010*; *Tran, 2012*] indicated a random and non-uniform distribution of corrosion products. However, the majority of models found in the literature e.g. (Molina et al. 1993; Suda et al. 1993; To and Pantazopoulou 2001; Bhargava et al. 2006;El Maaddawy and Soudki 2007; Richard et al. 2010; Fahy et al. 2017) assumed uniform distribution of corrosion products. The primary reasons for this assumption were reduced complexity and insufficient experimental data describing the distribution of the corrosion products. [*Liu and Weyers, 1998*] claimed that the non-uniformity evens out with time suggesting uniform distribution of corrosion products. Though, technology and measurement technics [*Michel et al., 2013*; *Pease et al., 2012*] have been developed, improving the understanding of the distribution of corrosion products, showing that the non-uniformity does not even out with time [*Pease et al., 2012*]. [*Lundgren, 2005a*; *Bohner E., 2010*; *Qiao et al., 2012*; *Ožbolt et al., 2012*; *Guzmán and Gálvez, 2017*] included the effect of local corrosion/pitting corrosion i.e. accumulation of corrosion products in *one* area of the reinforcement surface. However, actual modelling of a random distribution (several vertices) of the corrosion products, seen from a mechanical point of view, has to the authors knowledge not been presented.

Several models are suggested in the literature - all contributing to improve the knowledge within service life modelling. Experiments show that the distribution of corrosion products is random even in controlled environments during testing. Despite of these observations, only few models include non-uniform distribution of corrosion products in the modelling scheme. The corrosion-induced pressure, which is a function of the distribution of corrosion products, determines the predicted location of

crack initiation and crack propagation. Neglecting non-uniform distribution of corrosion products may therefore lead to incorrect predictions of time to crack initiation and deterioration. Depending on geometry (arrangement of reinforcement and cover layer), delamination may occur indicating no visible warning of ongoing deterioration in the concrete cover layer.

To improve the versatility of corrosion-induced damage predictions, non-uniform distribution of corrosion products should therefore be included in the modelling scheme. Further, applying a smeared cracking approach may emphasise the influence of non-uniform distribution of corrosion products, as the cracking path is not fixed (compared to a discrete cracking approach). Applying a smeared cracking approach also includes the influence of microcracking in the modelling scheme.

1.4 Research objectives

A state of the art finite element based service life model for reinforced concrete subjected to chloride-induced corrosion was developed [*Michel, 2012*; *Solgaard, 2013*]. Based on electrochemical and mechanical modelling the model is capable of predicting the extent and kinetics of a corrosion cell as well as corrosion-induced cracking. The model was developed using a combination of theoretical and experimental studies and includes mass transport mechanisms and the simulation of the development of macro cell corrosion in a homogeneous defect free system.

The developed service life model is based on stringent physical principles and has been shown to be applicable for the design of durable reinforced concrete structures. Although, several key issues remain that must be included in service life modelling for a more accurate qualification and quantification of the service life of concrete structures. In particular, with respect to the assessment of the remaining service life of reinforced concrete structures several challenges remain. At present, the remaining service life of reinforced concrete structures is commonly based on visual inspections, i.e. the appearance of rust stains or presence of corrosion-induced cracks. The visual observations may then be linked to a mechanical model to relate e.g. surface crack width to cross sectional reduction of reinforcement and thus amount of corrosion, which may allow for estimation of the residual load bearing capacity. However, the accuracy of the mechanical model plays then an important role in the evaluation of the remaining service life as e.g. severe corrosion is possible without visible cracking. Thus, in-depth knowledge on mechanisms and parameters related to corrosion-induced damage is needed to allow for more accurate determination of the remaining service life.

Taking the aforementioned considerations into account, the objective of this PhD project was to:

Develop a theoretical framework for corrosion-induced damage in reinforced concrete to improve the basis for assessment of service life of structures based on visual assessment.

Based on a review of state of the art modelling approaches for corrosion-induced damage in reinforced concrete structure, the main work is related to:

- modelling and investigation of non-uniform distribution of corrosion products along the circumference of the reinforcement,
- modelling and investigation of penetration of corrosion products into the corrosion accommodating region and
- modelling and investigation of corrosion-induced multiple cracking in reinforced concrete structures applying a smeared cracking model.

A basic hypothesis is that non-uniform distribution of corrosion products along the circumference of the reinforcement has a considerable influence on the actual corrosion-induced damage mechanism. Depending on the damage mechanism (spalling or delamination) cracking may not be visible at the surface. Warning of deterioration and estimation of remaining service life is therefore unreliable. The second hypothesis is that applying a smeared crack modelling approach predicts more realistic corrosion-induced damage, compared to a discrete cracking approach. Applying a smeared cracking approach is further assumed enhancing the effect of non-uniform distribution of corrosion products as the location of crack initiation and subsequent cracking path is not predefined.

Based on the objective and focus area the following research questions were formulated:

i. What is the relation between the non-uniformity of distribution of corrosion products at the reinforcement/concrete interface and prediction of corrosion-induced damage in reinforced concrete structures?

ii. What is the relation between the crack modelling approach and the prediction of corrosion-induced damage in reinforced concrete structures?

iii. What is the relation between parameters such as arrangement of reinforcement, geometry of concrete member, distribution of corrosion products, etc. and prediction of corrosion-induced damage in reinforced concrete structures when considering multiple cracking?

1.5 Limitations and assumptions

As several mechanisms as well as geometrical parameters and material characteristics affect the service life of the structure, some limitations and assumptions are made to limit the scope of the study. General limitations and assumptions are described in the following; however, more specific limitation and assumptions are described in the different chapters.

This study is focusing on the mechanical perspective when considering service life prediction and modelling of corrosion-induced cracking, while the exact reason for non-uniform distribution of corrosion products is not investigated.

Complexity and applicability are often related and, as a simplification, it was decided to consider a cross section with one reinforcement bar in the modelling scheme. The complexity, when modelling corrosion-induced cracking in a cross section with multiple reinforcement bars, is increased due to the interaction between cracks and corrosion of several reinforcement bars. It is assumed that corrosion-induced damage based on corrosion of one reinforcement bar – and describing the interaction between adjacent bars implicitly – is sufficient to represent the influence on service life cracking which is studied in the present work.

In the modelling neither cracking nor corrosion along the length of the reinforcement is considered as a 2D modelling approach was applied. Further, as the numbers of equations, which have to be solved, are drastically decreased, when modelling in 2D compared to e.g. 3D, the computational time is reduced. Finally, it is assessed that applying a 2D model simplifies the output information (due to a decreased number of variable parameters) making it easier to identify certain trends and patterns and thereby drawing conclusions. Modelling in 3D probably affects the simulation of both the corrosion and subsequent cracking; however, it is assumed that tendencies and general conclusions presented in this study are not affected.

A number of different mechanisms can cause concrete cracking e.g. mechanical loading, shrinkage and settlement of the structure. However, only corrosion-induced loading and corrosion-induced cracks are considered. Further it is assumed that sufficient reinforcement, following the design codes and expected loading, is present in the structures and the structure was built without flaws and deficiencies.

1.6 Organization of Thesis

This thesis consists of six chapters. Through the chapters, the studied model is further developed implementing different mechanisms affecting the initiation, propagation and pattern of corrosion-induced cracking. Chapters 2 to 4 are comprised of papers published in conference proceedings and a paper published in a peer-reviewed scientific journal. Chapter 5 is comprised of a paper prepared for submission in a

peer-reviewed scientific journal. As these four chapters are individually written some repetition of each paper do occur.

Chapter 6 is putting the research, described in the previous chapters, into perspective and summing up the conclusions made during the study. Further ideas and suggestions for future research are discussed.

In Chapter 2 (Paper I), a model simulating corrosion-induced concrete damage is presented. The presented model is a further development of an existing finite element based model [*Michel, 2012*; *Pease et al., 2012*; *Solgaard et al., 2013*]. The model simulated corrosion-induced cracking in a reinforced semi-infinite concrete body applying a discrete crack modelling approach. The crack was initiated at the reinforcement/concrete interface developing towards the concrete surface at top of the specimen. In the original model, penetration of corrosion products was accounted for; however, the precipitation of corrosion products was assumed uniform along the circumference of the reinforcement. Introducing a vector with varying corrosion current density non-uniform precipitation of corrosion products is implemented in the modelling. The implementation of non-uniform precipitation in the modelling was tested comparing numerical results with experimental data.

In Chapter 3 (Paper II), the influence of accounting for non-uniform precipitation of corrosion products along the circumference of the reinforcement was investigated. Further, the influence of cover layer, reinforcement diameter and water-to-cement ratio on the damage and cracking limit state was investigated. During the study, penetration of corrosion products into the surrounding concrete and creep was taken into account. A discrete crack model approach was applied in the developed finite element model during this study. The predefined cracking path was modelled initiating at the reinforcement/concrete interface propagating vertically towards the concrete surface. Two different distributions of the corrosion current density were chosen for the study when varying the three parameters: cover layer, reinforcement diameter and water-to-cement ratio.

In Chapter 4 (Paper III) the applied crack modelling approach was changed from discrete to smeared. This was mainly done to overcome the limitations of the discrete crack modelling approach i.e. in terms of predefining the cracking path and predefining the number of cracks. Mechanisms such as penetration of corrosion products into the surrounding concrete, non-uniform precipitation of corrosion products along the circumference of the reinforcement and creep were maintained and implemented in the smeared crack modelling approach. Multiple cracking affects the description of stiffness of both the complete modelled body and each element in the modelled body as each crack contribute to decrease in stiffness. Applying a smeared crack modelling approach therefore increases the complexity of the calculation and thereby the computational time compared to applying a discrete crack modelling approach. To study the applicability of applying a smeared crack modelling approach,

despite the drawbacks, results were compared both to results simulated applying a discrete crack modelling approach and experimental data from two different studies. The influence of implementing penetration of corrosion product into the surrounding concrete and the elastic modulus of corrosion products when applying a smeared crack modelling approach is also discussed in this chapter.

In Chapter 5 (Paper IV), the influence of simulating multiple cracking combined with non-uniform precipitation of corrosion products along the circumference of the reinforcement was studied. Focusing on surface crack initiation and reduction in reinforcement radius the influence of the concrete cover layer, reinforcement diameter and size of specimen was investigated. The different geometrical parameters were varied simultaneously with varying distribution of the corrosion current density along the perimeter of the reinforcement bar to highlight the uncertainty within this field. The modelled results were compared to experimental data from two different studies found in the literature.

In Chapter 6, conclusions are made based on the work presented in the papers. In addition, recommendations for future work are discussed based on the results and limitations of the presented work.

Chapter 2
Modeling of Corrosion-induced Concrete Damage
(Paper I)

Anna Emilie A. Thybo

Department of Civil Engineering, Technical University of Denmark, Kgs. Lyngby, Denmark

Alexander Michel

Department of Civil Engineering, Technical University of Denmark, Kgs. Lyngby, Denmark

Henrik Stang

Department of Civil Engineering, Technical University of Denmark, Kgs. Lyngby, Denmark

In Proceedings of the 8th International Conference on Fracture Mechanics of Concrete and Concrete Structures 2013

Abstract

In the present paper a finite element model is introduced to simulate corrosion-induced damage in concrete. The model takes into account the penetration of corrosion products into the concrete as well as non-uniform formation of corrosion products around the reinforcement. To account for the non-uniform formation of corrosion products at the concrete/reinforcement interface, a deterministic approach is used. The model gives good estimates of both deformations in the concrete/reinforcement interface and crack width when compared to experimental data. Further, it is shown that non-uniform deposition of corrosion products affects both the time-to cover cracking and the crack width at the concrete surface.

Keywords

Non-uniform corrosion, Durability, Reinforced concrete, Concrete cover cracking.

2.1 Introduction

Infrastructure constructions represent major investments for society and consequently vast efforts are made to understand and predict the service life and associated deterioration mechanisms of infrastructure constructions. A major part of these infrastructure constructions is made of reinforced concrete. One of the most important deterioration mechanisms in rein-forced concrete structures is reinforcement corrosion [1]. Corrosion-induced damages, such as concrete cracking, spalling, delamination, and cross sectional reduction of the reinforcement, may cause aesthetic damages, decrease the load bearing capacity of a structure, and in the worst case lead to fatal structural consequences, such as failure.

In particular, the formation of cracks in the concrete cover as well as cross sectional reduction of reinforcement area is affecting strength and serviceability of reinforced concrete structures. Hence, corrosion-induced cover cracking has been studied to a great extent, see e.g. [*Alonso et al., 1998*; *Andrade et al., 1993*], and various models such as analytical, see e.g. [*Liu and Weyers, 1998*; *Chernin et al., 2010*], empirical, see e.g. [*Molina et al., 1993*; *Noghabai, 1999*], and finite element based, see e.g. [*Biondini and Vergani, 2012*; *Isgor and Razaqpur, 2006*; *Michel et al., 2010*; *Solgaard et al., 2013*], models have been suggested over the years. In general, these models are consistent with experimental data, however, recent application of experimental techniques such as x-ray attenuation [*Michel et al., 2012*; *Bradley Justin Pease et al., 2012*; *Michel et al., 2011*] and digital image correlation [*Pease et al., (2012)*] have highlighted that (i) corrosion products penetrate into the concrete matrix and (ii) corrosion products form non-uniformly around the circumference of the reinforcement leading to non-uniform deformations - both topics are so far relatively

uncharted. The majority of the proposed models neglect these mechanisms, which may cause misleading and unrealistic results. Therefore, the influence of penetration of corrosion products as well as non-uniform formation in the concrete/reinforcement inter-face should be further investigated.

In the present paper an existing finite element based model [*Pease et al., (2012)*], which simulates the expansion of uniformly deposited corrosion products - taking into account the penetration of corrosion products into the concrete matrix - and predicting the propagation of corrosion-induced damage, is taken one step further al-lowing for non-uniform formation of corrosion products around the circumference of the rein-forcement. The model is accounting for the expansion of corrosion products utilizing a thermal analogy. Non-uniform corrosion is introduced assigning a specific thermal expansion to each element in the corrosion layer. Initially, the modeling approach to account for non-uniform formation of corrosion products is tested comparing numerical results with experimental observations presented in [*Pease et al., (2012)*].

Finally, a numerical example is given to demonstrate the influence of non-uniform corrosion on the time-to corrosion-induced cover cracking.

2.2 Modeling Approach

The proposed modeling approach is based on an existing finite element method (FEM) model [*Michel et al., (2010); Solgaard et al., (2013); Pease et al., (2012)*] that simulates the formation and propagation of corrosion-induced damage in a reinforced concrete body applying a discrete cracking approach. Neither micro-cracking nor the influence of cracks on the transport properties of concrete is currently included in the model.

To simulate the formation and propagation of corrosion-induced damage, the proposed model is divided into five distinct domains; concrete, reinforcement, a corrosion layer, cracking, and debonding domain (crack opening and sliding at reinforcement surface). Crack propagation along with the different domains is illustrated in Figure 2.1 for two different times, t_1 and t_2. The crack initiates at or near the surface of the reinforcement and sub-sequently propagates towards the concrete surface as observed in [*Michel et al., (2012); Pease et al., (2012); Michel et al., (2011); Pease et al., (2012)*]. The concrete domain is described by a semi-infinite concrete body with elastic material behavior. Zero-thickness cohesive interface elements are implemented perpendicular (simulating mode-I crack propagation in the concrete cover) and circumferential (simulating mixed-mode crack propagation) to the reinforcement allowing only for crack propagation in the implemented interface elements. However, corrosion-induced crack patterns obtained from experimental investigations (see e.g. [*Alonso et al., 1998*; *Andrade et al., 1993*; *Val et al., 2009*]) support the assumption of a prescribed crack path.

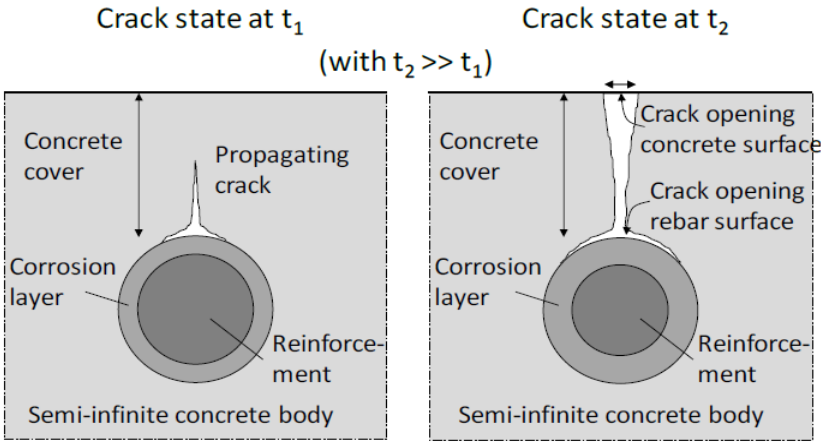

Figure 2.1 *Crack propagation in proposed FEM model, from* [*Solgaard et al., 2013*].

Cracking in the concrete cover layer is induced once tensile stresses (which are caused by the expansion of corrosion products) exceed the tensile strength of the concrete. To simulate corrosion-induced damage in the model two steps are implemented; a) calculation of the reduction of the reinforcement radius and b) calculation of the expansion of corrosion products.

Figure 2.2 illustrates the confined and free expansion mechanism of the corroding reinforcement assuming uniform formation of corrosion products. R_2 is the free expanding radius of the corroded reinforcement, R_1 the radius of the non-corroded part of the reinforcement and R_0 the radius of the original non-corroded reinforcement.

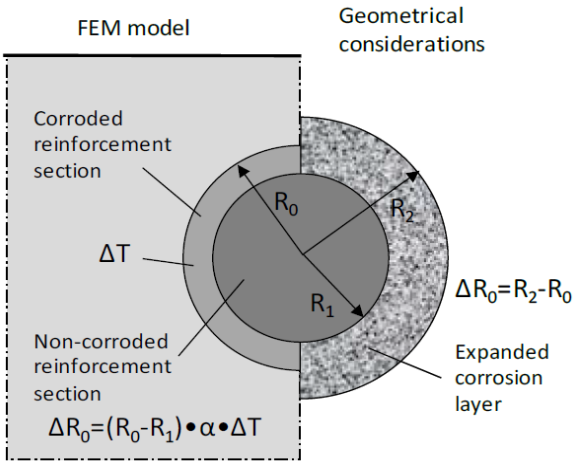

Figure 2.2 *Load application in FEM model (left) and basic geometrical considerations of the free expansion of the corroding reinforcement (right) in crack propagation model, from* [*Solgaard et al., 2013*].

From Faraday's law the reinforcement radius reduction due to corrosion i.e. the thickness of the corrosion layer is determined:

$$X(t) = R_0 - R_1 = \frac{M\, i_{corr}\, \Delta t}{z\, F\, \rho} \tag{2.1}$$

where M is the molar mass of the metal [g/mol], i_{corr} the corrosion current density [A/mm2], Δt the duration of current application [s], z the anodic reaction valence [-], F Faraday's constant [96485 As/mol] and ρ the density of the metal [g/mm3].

Considering Figure 2.2, the thickness of the free expanding corrosion products can be ex-pressed as:

$$\Delta R_0 = R_2 - R_0 \tag{2.2}$$

The expansion of corrosion products is included in the model applying a fictitious thermal load to the corrosion layer as described in the following equation:

$$\Delta R_0 = (R_0 - R_1)\eta_{lin} \tag{2.3}$$

where η_{lin} is the linear expansion coefficient depending on the type of corrosion products formed. The linear expansion coefficient is described by a fictitious thermal expansion coefficient, α [K^{-1}], and a corresponding temperature increment, ΔT [K], see Eq. (2.4).

$$\eta_{lin} = \alpha\, \Delta T \tag{2.4}$$

2.2.1 Penetration of corrosion products into the concrete matrix

Figure 2.3 illustrates experimental results of accelerated corrosion tests observed by x-ray attenuation measurements in [*Michel et al., 2012*]. The figure clearly shows that corrosion products form in a non-uniform manner around the reinforcement and furthermore penetrate the surrounding concrete matrix and thereby delaying stress formation. Therefore, the penetration of corrosion products into the concrete matrix was included in the modeling scheme in [*Michel et al., (2012); Pease et al., (2012)*] to reduce the effect of corrosion-induced expansion. The model was based on experimental data obtained from x-ray attenuation [*Michel et al., (2012); Pease et al., (2012); Michel et al., (2011)*] and digital image correlation measurements *[Pease et al., (2012)*] describing the penetration (time and depth) of corrosion products. From the experimental data a conceptual model (see Figure 2.4) to describe the penetration of corrosion products into the cementitious matrix was developed.

Based on the experimental results presented in *[Michel et al., (2012); Pease et al., (2012); Michel et al., (2011); Pease et al., (2012)*], it is assumed that an initial corrosion accommodating region (CAR) around the reinforcement exists, denoted CAR_0, which delays stress formation while filling with solid corrosion products.

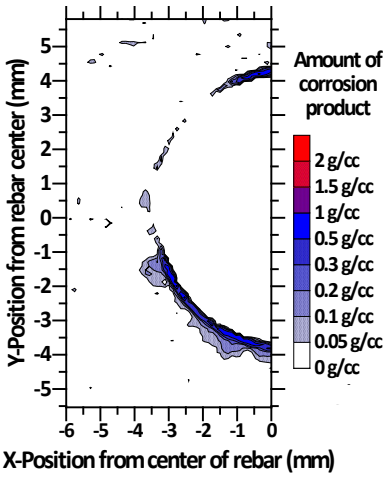

Figure 2.3 *Contour plots highlighting penetration of corrosion products into mortar, from* [*Michel et al., 2011*].

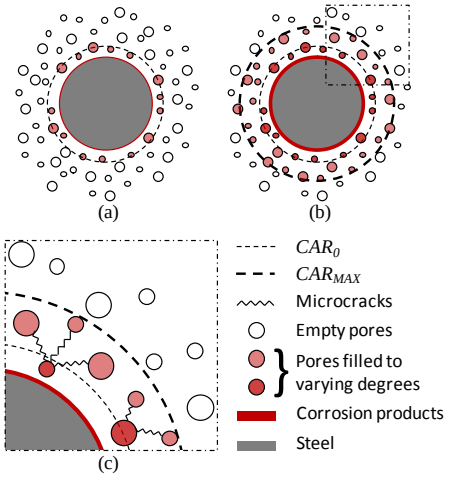

Figure 2.4 *Conceptual schematic of idealized filling process of capillary porosity with corrosion products: (a) shows the initial CAR,* CAR_0*, (b) the subsequent increase in CAR size to a maximum,* CAR_{MAX} *and filling of additional pores due to (c) formation of micro-c racks between pores allowing movement of corrosion products, from [Pease et al., (2012)].*

Once this initial CAR_0 is filled with corrosion products, tensile stresses in the surrounding cementitious material will increase and potentially lead to the formation of micro-cracks. These micro-cracks allow solid corrosion products to penetrate additional pore spaces and further delay corrosion-induced stresses. At some point a maximum size of the CAR, denoted as CAR_{MAX}, is reached. No corrosion products can penetrate the matrix of the cementitious material beyond that point and all additionally formed corrosion products will introduce tensile stresses and potentially lead to the formation of a macro-crack.

Eqs. (2.5) and (2.6) express the observed characteristics of the CAR. κ describes the change in connectivity of capillary pores inside the CAR, t_{CAR_min} the time until CAR_0

is filled with corrosion products, t_{CAR_max} the time until CAR_{MAX} is filled with corrosion products, and t the time.

$$\kappa = \begin{cases} 0 & \text{if } t \leq t_{CAR\_min} \\ t_c & \text{if } t_{CAR\_min} < t \leq t_{CAR\_max} \\ 1 & \text{if } t > t_{CAR\_max} \end{cases} \quad (2.5)$$

where

$$t_c = \frac{t - t_{CAR\_min}}{t_{CAR\_max} - t_{CAR\_min}}$$

$$CAR = CAR_0 + (CAR_{MAX} - CAR_0)\kappa \quad (2.6)$$

Assuming the CAR consists of the capillary porosity of the cementitious material, φ, the CAR volume, V_{CAR}, may be determined as follows:

$$V_{CAR} = \varphi V_{CM} \quad (2.7)$$

where V_{CM} is the accessible volume of the cementitious matrix.

As mentioned before, a thermal analogy is used in the model to mimic the expansion of the corrosion products. The variation of the temperature increment in time is thereby calculated as shown in Eq. (2.8), where ΔT_{CAR} is an adjusted equivalent temperature increment accounting for the impact of the CAR on corrosion-induced deformations and is applied in the FEM analysis instead of ΔT.

$$\Delta T_{CAR} = \lambda_{CAR} \Delta T \quad (2.8)$$

where λ_{CAR} describes the penetration of corrosion products into the accessible space of the cementitious matrix, V_{CAR}, and is described as follows:

$$\lambda_{CAR} = \begin{cases} \left(\frac{V_{cp}}{V_{CAR}}\right)^n & \text{if } V_{cp} < V_{CAR} \\ 1 & \text{if } V_{cp} \geq V_{CAR} \end{cases} \quad (2.9)$$

where n is an empirical parameter estimated to be 1.3 in *[Pease et al., (2012)]*. Both the volume of the corrosion products, V_{cp}, and the volume of the CAR, V_{CAR}, are time dependent parameters, see e.g. Eqs. (2.1) and (2.5).

2.2.2 Creep

The effect of creep was implemented in the model in [*Pease et al., (2012)*] according to Eurocode 2 [*Standard and DS, 1993*] where the effective Young's modulus of the concrete matrix is adjusted at each time step according to Eq. (2.10).

$$E_{c,eff} = \frac{E_c}{1 + \varphi(t, t_0)} \quad (2.10)$$

where $E_{c,eff}$ and E_c are the effective and secant Young's modulus [MPa], respectively, $\varphi(t,t_0)$ is the creep coefficient, which is a function of time, t the age of the concrete matrix [days] and t_0 the time at loading [days].

In the following a description of the modifications made to include the non-uniform formation of corrosion products is found.

2.2.3 Implementing non-uniform corrosion

Figure 2.5 illustrates the expansion mechanism of non-uniformly deposited corrosion products. The non-uniformity is implemented varying the corrosion current density around the circumference of the reinforcement and thereby generating different degrees of corrosion of the reinforcement - maintaining the same total corrosion current as in the uniform case. Mathematically the non-uniformity is modeled changing the corrosion current density from a scalar to a vector. This implies that Eq. (2.1) is changed to Eq. (2.11) in which the reinforcement radius reduction not only depends on time but also on the location.

The new vector describes the change in corrosion current density around the circumference of the reinforcement and thereby the shape of the corrosion layer. The shape is considered constant over time, which corresponds well to experimental observations made in [*Michel et al., (2012); Pease et al., (2012); Pease et al., (2012)*].

$$\overrightarrow{X(t)} = \overrightarrow{R_0} - \overrightarrow{R_1} = \frac{M\,\overrightarrow{i_{corr}}\,\Delta t}{z\,F\,\rho} \tag{2.11}$$

As Eq. (2.11) is dependent on Equations (2.8) and (2.9), the partial penetration coefficient, λ_{CAR}, and the adjusted temperature increment, ΔT_{CAR}, are also dependent on the location.

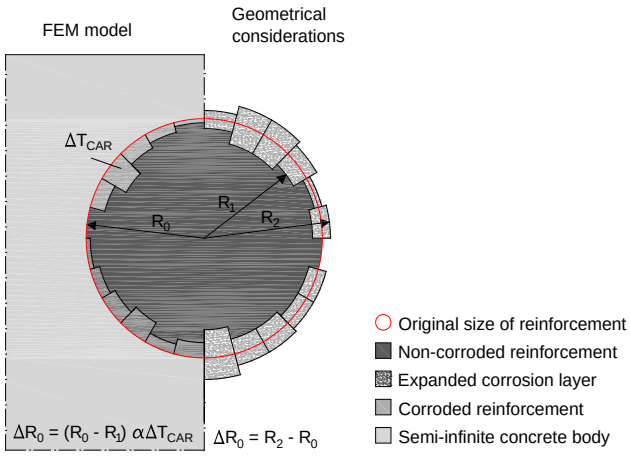

Figure 2.5 *Load application (left) and basic geometrical considerations to model non-uniform formation of corrosion products (right) in the crack propagation model.*

2.3 Comparison of Numerical and Experimental Data

The ability of the proposed model to simulate deformations and crack formation, induced by non-uniform deposition of corrosion products, is verified comparing, for a concrete body, numerical results with experimental observations presented in *[Pease et al., (2012)*]. To compare numerical results with experimental results, the actual geometry of the test specimens was modeled.

In the experiment, a 23×100×100 mm^3 reinforced mortar specimen was subjected to corrosion impressing an electrical current of 100 $\mu A/cm^2$. To provide an electrical connection between working (reinforcement) and counter electrode (ruthenium/iridium electrode), the specimen was placed in tap water, which was maintained at a level of approximately 10 mm below the reinforcement, see Figure 2.6. One smooth 10 mm steel reinforcement bar was embedded in the center of the specimen and the water-to-cement ratio, w/c, of the mortar was 0.5.

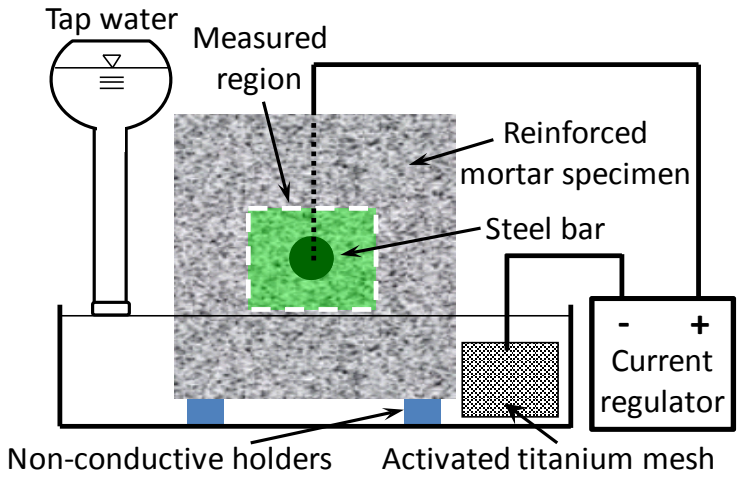

Figure 2.6 *Experimental set up for DIC, from [Pease et al., (2012)]*.

Corrosion-induced deformations and crack formation were observed by means of digital image correlation (DIC) and the experiment was stopped when the first macro-crack was observed. For more information about the experimental approach the reader is referred to [*Pease et al., (2012); Pease et al., (2006); Pereira et al., (2011)*].

To simulate corrosion-induced deformations, the commercial FEM program DIANA 9.4.2 was used. 1766 elements (10,992 DOFs) were used to discretize the interface, concrete, reinforcement and corrosion layer domain in the model. Nonlinear solution of the problem was obtained using a standard Newton-Raphson method with a displacement controlled convergence criterion.

Table 2.1 *Input parameteres.*

Parameter	Value	Dimension
Length	23	mm
Width	100	mm
Height	100	mm
Concrete cover	45	mm
d_r	10	mm
RH	65	%
M_{Fe}	55.845	g/mol
z	2	-
ρ_{steel}	7.86	g/cm^3
F	96485	A·s/mol
$mean(i_{corr})$	0.0001	A/cm^2
CAR_0	0.14	mm
CAR_{MAX}	0.28	mm
η_{lin}	0.7	-
w/c	0.5	-
f_{cm}	45	MPa
E_c	32	GPa
μ_{conc}	0.2	-
f_{ct}	4.5	MPa
τ_{conc}	4.5	MPa
E_{steel}	210	GPa
μ_{steel}	0.3	-
E_{corr}	2	GPa
μ_{corr}	0.3	-

The input parameters for the numerical simulation are provided in Table 2.1. In the model the linear expansion coefficient is set to 0.7 assuming the formation of hematite (Fe_2O_3), which was confirmed by energy dispersive spectroscopy in [*Michel et al., 2011*]. The fictitious thermal expansion coefficient was set constant, i.e. 1, while the adjusted temperature increment, ΔT_{CAR}, accounted for the non-uniform deposition of corrosion products.

The experimental data was fitted adjusting the corrosion current density vector, $\overrightarrow{i_{corr}}$, in the FEM model. As starting point for the estimation of $\overrightarrow{i_{corr}}$, DIC measured deformations (after three days of accelerated corrosion) in the concrete/reinforcement interface were used. The resulting non-uniform $\overrightarrow{i_{corr}}$ around the circumference of the reinforcement (see Figure 2.7) provided a unique solution for all measurement times, see Figure 2.8.

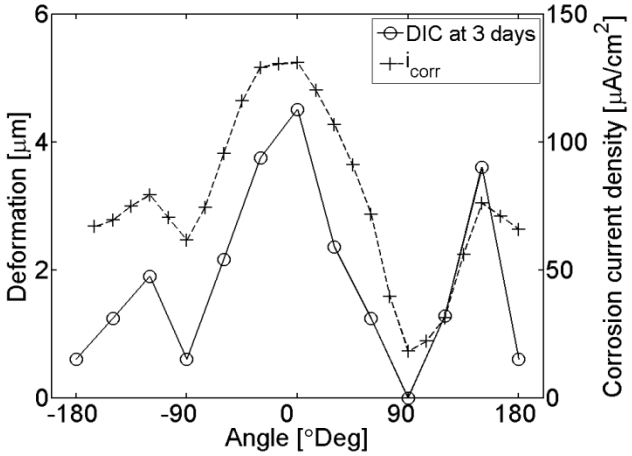

Figure 2.7 *Illustration of measured deformations (dashed line) around the circumference of the reinforcement (solid line) at three days and the corresponding non-uniform corrosion current density.*

Figure 2.8 illustrates a comparison of the modeled deformations at the concrete/reinforcement interface and experimentally measured deformations by DIC. In the figure, locations are described by polar coordinates where 90° marks the location of the predefined crack path. For the three different measurement times illustrated in the figure, the model predicts the corrosion-induced deformations very well. In general, the deviations at the different locations are less than 1 μm after six and nine days. When comparing the numerical and measured results for three days, higher deviations are found i.e. around 1 μm, which was accepted as the deviation decreased with time. For one point (150°) higher deviations between experimental and numerical results were found for three and six days. However, the deviation was not found after nine days and was therefore neglected. In the modeling approach it was assumed that the shape of the corrosion layer, i.e. non-uniform formation of corrosion products, is constant with time, which seems to be a fair assumption considering the comparison of the modeled and DIC measured deformations. The deviations that are seen for three days in general and at 150° for three and six days may be explained by small changes in the shape of the corrosion layer over time and due to micro-cracking, which is not included in the model.

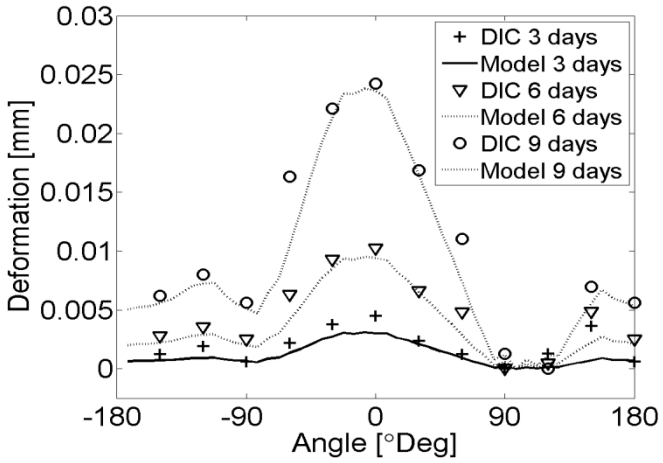

Figure 2.8 *Modeled corrosion-induced deformations (lines) and corrosion-induced deformations measured by DIC (markers).*

In Figure 2.9, the predicted corrosion-induced crack width is compared to the experimentally measured crack width. It should be noted that numerical predictions of the crack width are a result of the fitted corrosion-induced deformations at the concrete/reinforcement interface presented in Figure 2.7 and the material properties defined in Table 2.1. No additional fitting was performed.

To correspond to the location of the measured DIC crack width, the model predicted crack width was taken 1.4 mm from the reinforcement surface. In general, it is seen from the presented results that the modeled crack width corresponds well to the measured crack width. Both results, i.e. numerical and experimental, show a crack width of approximately 0 μm until six days after which the model predicted crack width rapidly increases. In contrast, the measured crack width starts to increase rapidly at approximately 7.5 days. Although, the numerical results do not capture the time-to crack initiation exactly, the model predicted crack width depicts the measured crack width well, as the slope of the two curves are approximately the same after 7.5 days. A reason for the deviation is most likely that micro-cracking is neglected in the present model. In the experiment two micro-cracks were observed and the formation of these micro-cracks has most likely postponed the initiation of the third crack (macro-crack).

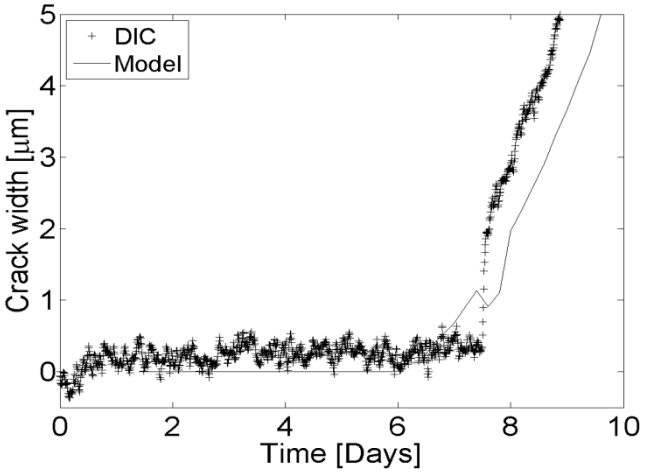

Figure 2.9 *Modeled corrosion-induced crack width (line) and crack width measured by DIC (markers) at 1.4 mm from the reinforcement surface.*

Additional uncertainty in the model is the Young's modulus of corrosion products. In the present model a value of 2.0 GPa was used as proposed in *[Pease et al., (2012)*]. Furthermore, it should be noted that studies in [*Pease et al., (2012)*] showed a weak dependence of corrosion-induced deformations on the Young's modulus of corrosion products.

2.4 Influence of Modeling Non-uniform Corrosion on Surface Cracking

To demonstrate the impact of non-uniform deposition of corrosion products on the time-to crack initiation and crack propagation, a numerical example is given. In the example, the crack width at the concrete surface (CWCS) is compared for four different scenarios, which are illustrated in Figure 2.10 and defined in Table 2.2. The different scenarios represent situations in which the main part of corrosion products accumulate in one area and are subsequently compared to a scenario assuming uniform deposition of corrosion products. For each scenario the model is set to simulate 40 days of impressed current. Parameters used for the simulations are provided in Table 2.1. The width and height of the concrete body were changed to 210 mm and 155 mm, respectively. The values for the width and height of the concrete (assuming semi-infinite behavior) were based on a study presented in [*Michel et al., 2010*].

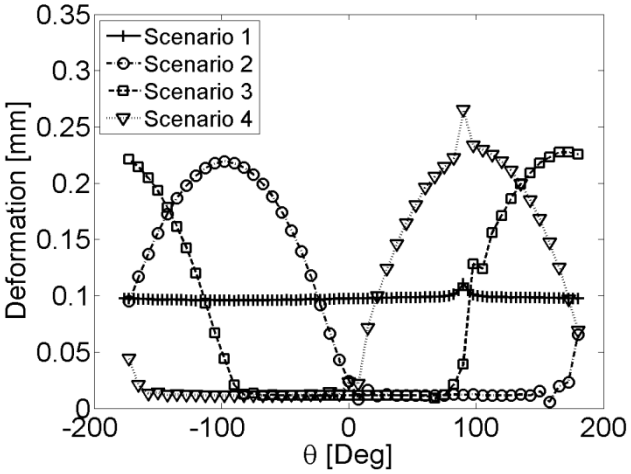

Figure 2.10 *Illustration studied scenarios. θ describes the location around the circumference of the reinforcement in polar coordinates. Please note: the figure illustrates corrosion-induced deformations at 40 days.*

Locations around the circumference of the reinforcement are described in polar coordinates in Figure 2.11 along with a clock reference (numbers inside circle) and placement of the predefined corrosion-induced crack path.

Table 2.2 *Scenarios investigated.*

Scenario	Characteristic
1	Uniform shape
2	Vertex at 6 o'clock
3	Vertex at 9 o'clock
4	Vertex at 12 o'clock

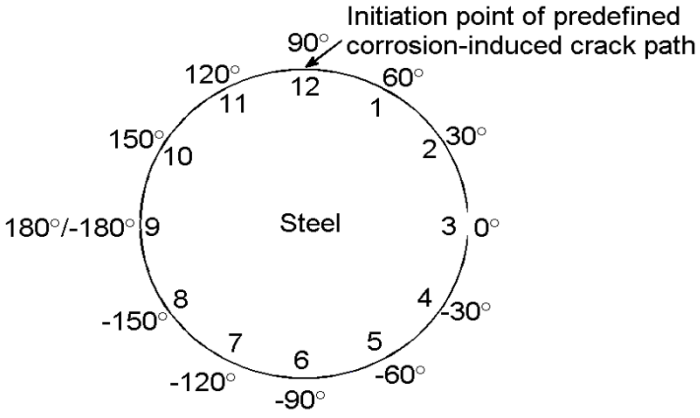

Figure 2.11 *Placement of angles (numbers outside circle) in the circumference of the reinforcement together with a clock reference (numbers inside circle). The crack initiates at 12 o'clock (90°).*

2.5 Results

In Figure 2.12, the crack width at the concrete surface is illustrated as a function of time for the four different scenarios.

In general, a considerable difference is seen regarding both time-to cover cracking and crack width for the investigated scenarios. For scenario 2, the crack is initiated after approximately 14 days, which is six days later than for scenario 3 and eight days later than for scenario 4. It should be noted that under natural conditions the difference in time-to cover cracking could in fact be years instead of days as the corrosion current density under natural conditions is considerably smaller. Also, the crack width at the concrete surface for scenario 4 is 21% bigger than for scenario 3 and 63% bigger than for scenario 2, see Table 2.3. Comparing scenario 1 (uniform formation of corrosion products) with the three other scenarios, it is seen that the assumption of uniform corrosion can lead to considerable underestimations of the time-to corrosion-induced cover cracking. Both the comparison of the time-to corrosion-induced cover cracking and crack widths illustrate the importance of understanding and modeling non-uniform deposition of corrosion products. A realistic method to implement this mechanism could be a probabilistic modeling approach. The presented results may thereby be seen as a first step illustrating extreme scenarios and providing impertinent information on the uncertainty of time-to corrosion-induced cracking.

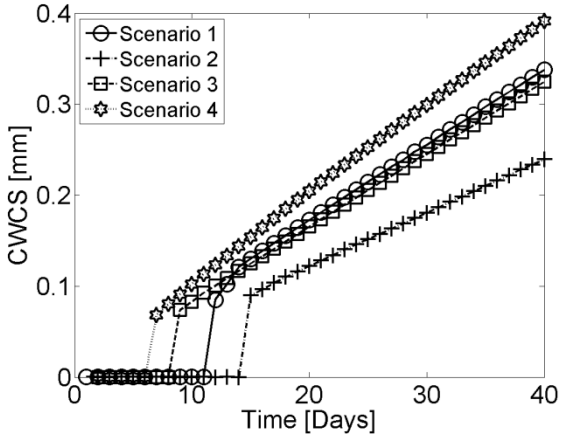

Figure 2.12 *Crack width at concrete surface, CWCS, as a function of time.*

Table 2.3 *Time-to cover cracking and crack width at the concrete surface after 40 days.*

Scenario	Initiation of CWCS [Days]	Final CWCS [mm]
1	11	0.3377
2	14	0.2394
3	8	0.3245
4	6	0.3912

2.6 Summary and Conclusions

In the present paper, the non-uniform deposition behavior of corrosion products is included in the modeling scheme of an existing deterministic finite element fracture model. The non-uniformity was implemented varying the corrosion current density along the circumference of the reinforcement. In the model, penetration of corrosion

product was included but micro-cracking and the influence of cracks on transport properties of the concrete was not considered.

To verify the model, digital image correlation measurements of deformations and crack widths were compared to simulated results. Comparisons between experimental observations and numerical results showed that the model simulates both deformations and crack width in accordance with measured data.

To investigate the influence of non-uniform deposition of corrosion products, a numerical example was given. In the example four different scenarios (accumulation of corrosion products at different locations along the circumference of the reinforcement) were studied. Comparison between the studied scenarios, showed considerable differences in the time-to cover cracking and the crack width at the surface. For scenario 4 (accumulation of corrosion products at crack initiation point) the shortest time-to cover cracking and largest final crack width was found. Based on the results presented in this study, it is recommended that future investigations and modeling of corrosion-induced cracking should focus on non-uniform deposition of corrosion products.

2.7 Acknowledgments

The authors gratefully acknowledge the financial support of the Danish Expert Centre for Infrastructure Constructions. Further, the authors would like to thank Bradley J. Pease for contributing with experimental data.

Chapter 3

Sustainability Assessment of Concrete Structure Durability under Reinforcement Corrosion (Paper II)

Anna Emilie A. Thybo

Department of Civil Engineering, Technical University of Denmark, Kgs. Lyngby, Denmark

Alexander Michel

Department of Civil Engineering, Technical University of Denmark, Kgs. Lyngby, Denmark

Henrik Stang

Department of Civil Engineering, Technical University of Denmark, Kgs. Lyngby, Denmark

Proceedings of First International Conference on Concrete Sustainability 2013

Abstract

In the present paper a parametric study is conducted based on an existing finite element based model. The influence of cover layer, reinforcement diameter and water-to-cement ratio is compared to a possible scatter in the results due to insufficient knowledge about the distribution of the corrosion current density along the circumference of the reinforcement. Simulations show that the scatter has a greater influence on the results than changing the parameters wherefore it is concluded that further investigation of the non-uniform deposition of corrosion products is essential to better understand and predict the durability of a given structure.

Keywords

Non-uniform corrosion, reinforced concrete, concrete cover cracking, numerical modeling, parameter study, finite element method.

3.1 Introduction

Infrastructure construction is important in society and therefore a tremendous amount of money is spent on new construction and the maintenance of older ones. In addition to this lots of resources are used on research and development to improve the understanding of the durability of structures and thereby improve the sustainability.

One main factor to improve the sustainability is to better understand and describe the service life and associated deterioration mechanisms of a given structure. A major part of the infrastructures are made of reinforced concrete and one of the most important deterioration mechanisms in reinforced concrete structures is reinforcement corrosion [*Rendell et al., 2002*]. Reinforcement corrosion induces deterioration mechanisms such as concrete cracking and cross sectional reduction of the reinforcement both decreasing the load bearing capacity and thereby affecting the serviceability of a structure. Based on this, especially corrosion-induced cover cracking has been studied, see e.g. [*Alonso et al., 1998*; *Andrade et al., 1993*], and various models such as analytical, see e.g. [*Liu and Weyers, 1998*; *Chernin et al., 2010*], empirical, see e.g. [*Molina et al., 1993*; *Noghabai, 1999*], and finite element based, see e.g. [*Biondini and Vergani, 2012*; *Isgor and Razaqpur, 2006*; *Michel et al., 2010*; *Solgaard et al., 2013*], models have been suggested over the years.

Recent experimental investigations such as x-ray attenuation *[Michel et al., (2012); Pease et al., (2012); Michel et al., (2011)*] and digital image correlation *[Pease et al., (2012)*] have shown that a) corrosion products deposit non-uniformly along the circumference of the reinforcement and b) corrosion products penetrate into the concrete matrix. Motivated by these observations an existing finite element based

model [*Solgaard et al., 2013*] simulating the expansion of uniformly deposited corrosion products along the circumference of the reinforcement and predicting the propagation of corrosion-induced cracking was taken a step further implementing at first the penetration of corrosion products into the concrete matrix [*Pease et al., (2012)*] and subsequently implementing the non-uniform formation of corrosion products in the modeling scheme [*Thybo et al., 2013*]. The non-uniformity of the distribution of corrosion products was found to have a significant influence on the corrosion-induced fracture process.

In the present paper the updated finite element based model [*Thybo et al., 2013*] was used to study the influence of different geometrical and material parameters on the service life. To get a better feel for the importance of the non-uniformity of corrosion products three parameters were chosen for the parametric study; a) the cover layer, b) the reinforcement diameter and c) the water-to-cement ratio. The parametric study was performed for two different distributions of the corrosion current density.

3.2 Model Approach

In the following a short description of the applied model is given. Further details regarding the modeling are found in [*Solgaard et al., (2013); Pease et al., (2012); Thybo et al., (2013)*].

An existing finite element (FE) based corrosion-induced cracking model was used to simulate the expansion of corrosion products and the subsequent crack propagation applying a discrete cracking approach. The model simulates non-uniform corrosion in a semi-infinite defect free reinforced concrete body. Micro-cracking and the influence of cracks on transport properties of the concrete was not considered.

In the model the system is divided into five distinct domains; concrete, reinforcement, corrosion layer, cracking, and a debonding domain (crack opening and sliding at reinforcement surface). In Figure 3.1 the five domains are illustrated for two different times, t_1 (damage phase in service life design) and t_2 (cracking phase in service life design). As shown in Figure 3.1 the crack initiates at or near the surface of the reinforcement and propagates towards the concrete surface which is consistent with observations in [*Michel et al., 2012*; *Bradley Justin Pease et al., 2012*; *Michel et al., 2011*; *B. . Pease et al., 2012*].

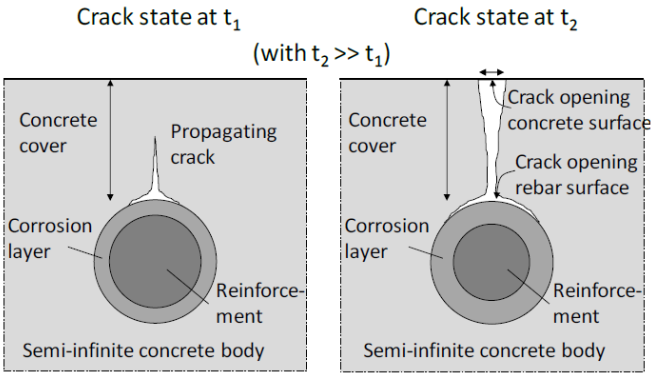

Figure 3.1 *Crack propagation - damage (left) and cracking (right) phase - in applied FE model, from* [*Michel et al., 2010*].

The concrete region is defined by a semi-infinite concrete body with elastic material behaviour.

Based on experimental investigations [*Alonso et al., 1998*; *Andrade et al., 1993*] of corrosion-induced crack patterns, the zero-thickness cohesive interface elements were implemented perpendicular (simulating mode-I crack propagation in the concrete cover) and circumferential (simulating mixed-mode crack propagation) to the reinforcement allowing only for crack propagation in the implemented interface elements.

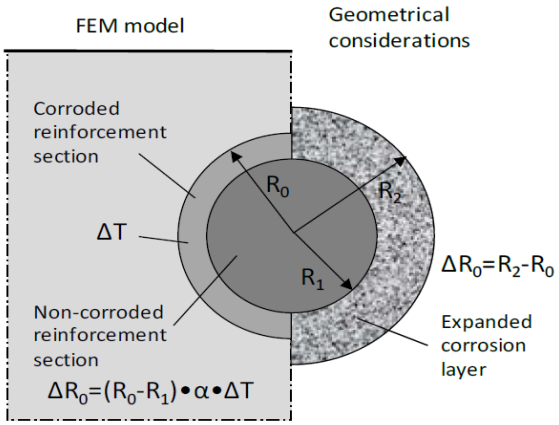

Figure 3.2 *Load application in FE model (left) and basic geometrical considerations to model uniform formation of corrosion products (right) in the crack propagation model, from* [*Michel et al., 2010*].

In [*Thybo et al., 2013*] the model was taken a step further implementing non-uniform deposition of corrosion products in the modeling scheme i.e. going from the situation illustrated in Figure 3.2 to the situation illustrated in Figure 3.3. In the figures R_2 is the free expanding radius of the corroded reinforcement, R_1 the radius of the non-corroded part of the reinforcement and R_0 the radius of the original non-corroded reinforcement. In Figure 3.3 R_1 and R_2 vary along the circumference of the reinforcement due to the non-uniform formation of corrosion products.

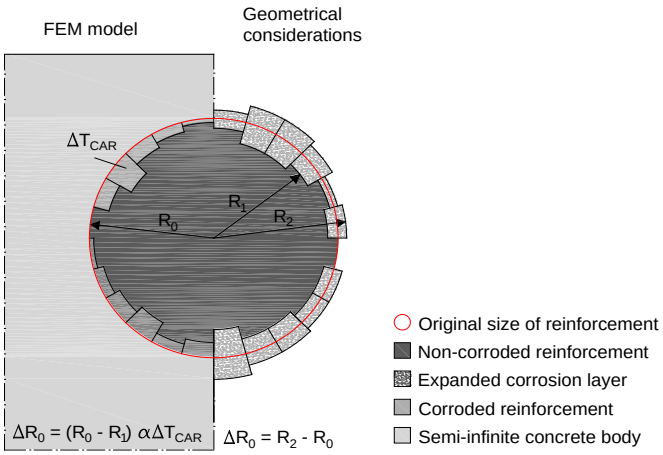

Figure 3.3 *Load application (left) and basic geometrical considerations to model non-uniform formation of corrosion products (right) in the crack propagation model, from* [*Thybo et al., 2013*].

Due to the expansion of the corrosion products tensile stresses are developed. Cracking in the concrete cover layer is induced once the tensile stresses exceed the tensile strength of the concrete.

The expansive nature of the corrosion products was modeled determining the reduction of reinforcement area and subsequently calculating the expansion of the corrosion products.

Faraday's law was used to determine the reinforcement radius reduction due to corrosion i.e. the size of the corrosion layer. To account for the variation of R_1 and R_2, the corrosion current density along the circumference of the reinforcement was varied generating different degrees of corrosion of the reinforcement - maintaining the same total corrosion current as in the uniform case. Mathematically the non-uniformity was modeled changing the corrosion current density from a scalar to a vector. The following expression of Faraday's law was applied in the modeling:

$$\overrightarrow{X(t)} = \overrightarrow{R_0} - \overrightarrow{R_1} = (M \overrightarrow{i_{corr}} \Delta t)/(z F \rho) \tag{3.1}$$

Where M is the molar mass of the metal [g/mol], i_{corr} the corrosion current density [A/mm2], Δt the duration of current application [s], z the anodic reaction valence [-], F Faraday's constant [96485 As/mol] and ρ the density of the metal [g/mm3].

To account for the expansion the linear expansion coefficient was introduced:

$$\eta_{lin}(\overrightarrow{R_0} - \overrightarrow{R_1}) = \overrightarrow{R_2} - \overrightarrow{R_0} \tag{3.2}$$

$$\eta_{lin} = \alpha \Delta T \tag{3.3}$$

where α *is a* fictitious thermal expansion coefficient [K^{-1}] and ΔT is the temperature increment [K].

3.2.1 Penetration of Corrosion Products into the Concrete Matrix

In experimental data obtained from x-ray attenuation [*Michel et al., 2012*; *Bradley Justin Pease et al., 2012*; *Michel et al., 2011*] and digital image correlation measurements [*Pease et al., (2012)*] it was observed that corrosion products penetrated into the concrete matrix delaying the stress formation and thereby the initiation of cracking. Therefore, based on the conceptual model in Figure 3.4, the mechanism was implemented in the modeling scheme in [*Michel et al., (2012); Pease et al., (2012)*] reducing the effect of corrosion-induced expansion.

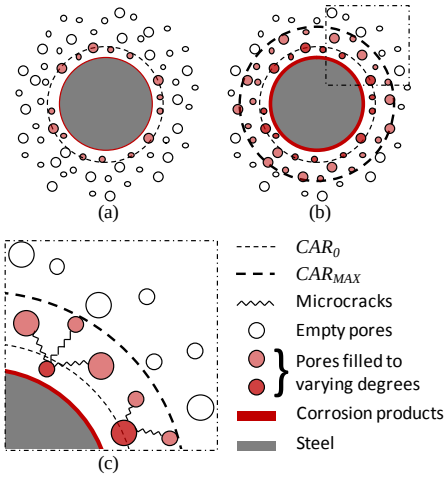

Figure 3.4 *Conceptual schematic of idealized filling process of capillary porosity with corrosion products: (a) shows the initial CAR, CAR_0, (b) the subsequent increase in CAR size to a maximum, CAR_{MAX} and filling of additional pores due to (c) formation of micro- cracks between pores allowing movement of corrosion products, from [Pease et al., 2012].*

In Figure 3.4 the penetration of corrosion products into the cementitious matrix is illustrated. Based on experimental observations, the model describes the development and expansion of a so-called corrosion accommodating region (CAR) - a region in which corrosion products penetrate the concrete matrix filling pores and moving in developed micro-cracks. A minimum (CAR_0) and a maximum (CAR_{MAX}) CAR was observed. Based on this knowledge it was possible to describe an adjusted temperature increment, see e.g. Eq. (3.4) and applying it in the modeling scheme instead of ΔT.

$$\overrightarrow{\Delta T_{CAR}} = \overrightarrow{\lambda_{CAR}}\,\Delta T \tag{3.4}$$

λ_{CAR} describes the penetration of corrosion products into the accessible space of the cementitious matrix and was determined following Eq. (3.5):

$$\overrightarrow{\lambda_{CAR}} = \left(\overrightarrow{V_{cp}} / \overrightarrow{V_{CAR}}\right)^n \; if \; \overrightarrow{V_{cp}} < \overrightarrow{V_{CAR}}$$

$$\overrightarrow{\lambda_{CAR}} = \vec{1} \qquad if \; \overrightarrow{V_{cp}} \geq \overrightarrow{V_{CAR}} \tag{3.5}$$

where n is an empirical parameter estimated to be 1.3 in [*Pease et al., 2012*], V_{cp} the volume of corrosion products and V_{CAR} the volume of the CAR.

$$\overrightarrow{V_{CAR}} = \varphi \overrightarrow{V_{CM}} \tag{3.6}$$

where φ is the capillary porosity of the concrete material, V_{CM} the accessible volume of the concrete depending on the size of CAR.

3.2.2 Creep

The effect of creep was implemented in the model in [*Pease et al., (2012)*] according to [*Eurocode, 2008*] where the effective modulus of elasticity of the concrete matrix is adjusted at each time step following Eq. (3.7).

$$E_{c,eff} = E_c / (1 + \varphi(t,t_0)) \tag{3.7}$$

where $E_{c,eff}$ is the effective modulus of elasticity [MPa], E_c the tangent modulus of elasticity [MPa], $\varphi(t,t_0)$ the creep coefficient [-], t the age of the concrete [days] and t_0 the time at loading [days].

3.3 Numerical Simulations

In the numerical simulation, the cover layer (C), the reinforcement diameter (D) and the water-to-cement ratio (w/c) were varied to study the influence of geometrical and material properties on two different limits states – damage limit (DL) and cracking limit (CL).

In Table 3.1 and Table 3.2, a schematic illustration of the investigated values of the cover layer, the reinforcement diameter and the water-to-cement ratio are given.

Table 3.1 *Overview of parametric study for S90.*

Identification	C [mm]	D [mm]	w/c [-]
Ref_{S90}	45	10	0.4
$C25_{S90}$	25	10	0.4
$C65_{S90}$	65	10	0.4
$R5_{S90}$	45	5	0.4
$R20_{S90}$	45	20	0.4
$WC03_{S90}$	45	10	0.3
$WC05_{S90}$	45	10	0.5

Table 3.2 Overview of parametric study for S270.

Identification	C [mm]	D [mm]	w/c [-]
Ref_{S270}	45	10	0.4
$C25_{S270}$	25	10	0.4
$C65_{S270}$	65	10	0.4
$R5_{S270}$	45	5	0.4
$R10_{S270}$	45	20	0.4
$WC03_{S270}$	45	10	0.3
$WC05_{S270}$	45	10	0.5

The damage and cracking limit were original defined in [*Tuutti, 1982*; *fib, 2006*] and related to service life design as a part of the propagation phase describing corrosion-induced structural consequences in the concrete, see e.g. Figure 3.1 and Figure 3.5.

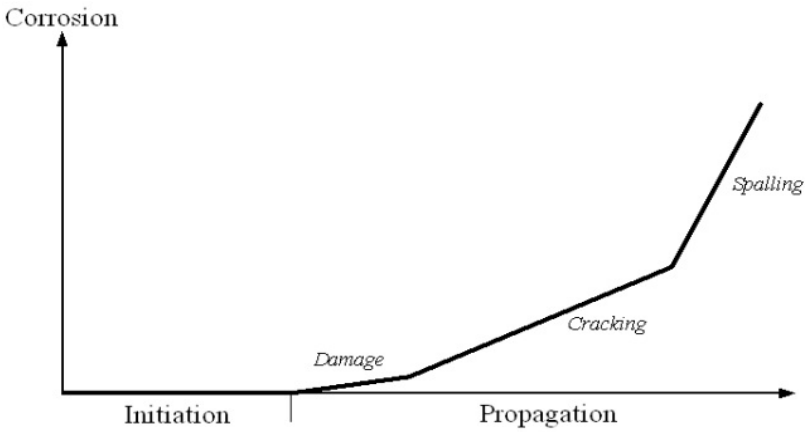

Figure 3.5 *Model for corrosion initiation and propagation and the terminology used in the current study for characterizing the propagation phase, from [Solgaard et al., (2013); Tuutti, (1982); fib Bulletin No. 34, (2006)].*

Normally the end of the initiation phase - de-passivation of the reinforcement - defines the end of service life, however this limit state is difficult to find (as it is not visible) and measure, hence great uncertainty is connected to it. Thus, it was suggested in [*Solgaard et al., 2013*] to base the end of damage and cracking phase on the size of the crack width at the cover surface. Based on a literature study and experimental observations the two crack widths, 50 μm and 0.2 mm, were applied in [*Solgaard et al., 2013*] as limits for DL and CL, respectively as these crack widths are possible to both measure and observed with the naked eye. On the basis of [*Solgaard et al., 2013*] these two values were also used as limit states in this study.

Investigating the influence of non-uniform corrosion a considerable scatter was observed in [*Thybo et al., 2013*] when considering crack width and time-to cover cracking. To investigate the influence of the scatter compared to the influence of varying C, R and w/c, the parameters were studied for two distinct situations; a)

accumulation of the corrosion products at the initiation point of the predefined corrosion-induced crack path (S90) b) accumulation of the corrosion products at the opposite site of the initiation point of the predefined corrosion-induced crack path (S270). The two situations (S90 and S270) are illustrated in Figure 3.6 and Figure 3.7 showing the variation in corrosion current density along the circumference of the reinforcement. The degrees referred to in the figures are polar angle coordinates which are shown together with the location of the initiation point of the predefined corrosion-induced crack path in Figure 3.8.

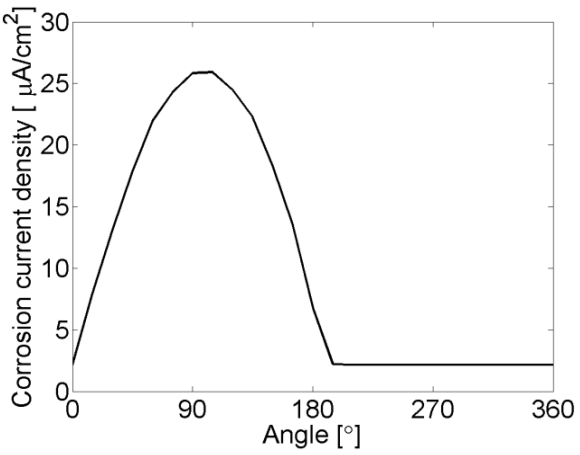

Figure 3.6 *Variation of the corrosion current density along the circumference of the reinforcement for S90.*

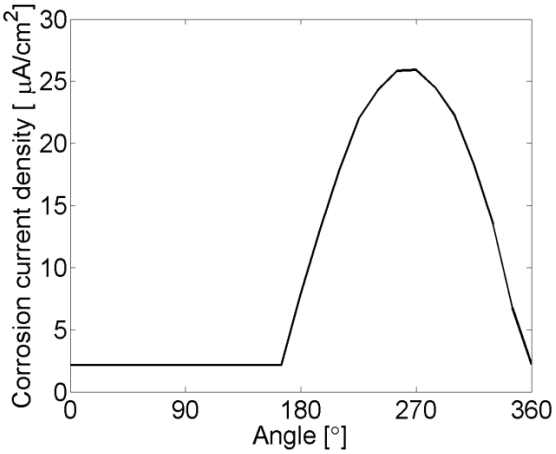

Figure 3.7 *Variation of the corrosion current density along the circumference of the reinforcement for S270.*

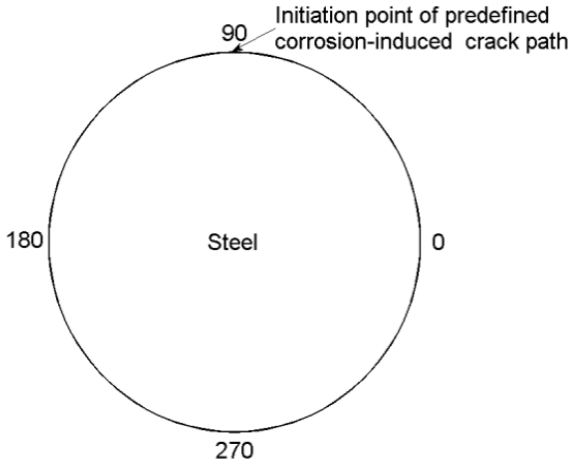

Figure 3.8 *Polar angle coordinates held together with location of initiation point of predefined corrosion-induced crack path.*

Table 3.3 *Input parameters.*

Parameter	Value	Dimension
Length	23	mm
Width	210	mm
Height	155	mm
C	45	mm
D	10	mm
w/c	0.4	-
f_{cm}	60	MPa
f_{ctm}	4.1253	MPa
τ_c	4.1253	MPa
E_c	39.542	GPa
μ_c	0.2	-
E_s	210	GPa
μ_s	0.3	-
E_{corr}	2	GPa
μ_{corr}	0.3	-
RH	65	%
M_{Fe}	55.845	g/mol
z	2	-
ρ_{steel}	7.86	g/cm^3
F	96485	A·s/mol
i_{corr_mean}	0.00001	A/cm^2
CAR_0	0.14	mm
CAR_{MAX}	0.28	mm
η_{lin}	0.7	-
α	1	-

In Table 3.3 the input parameters used in the analysis are provided. The geometrical values of the concrete were (assuming semi-infinite behavior) based on a study presented in [*Michel et al., 2010*] and the linear expansion coefficient for the corrosion products was set to 0.7 assuming the formation of hematite (Fe_2O_3), which was observed by energy dispersive spectroscopy in [*Michel et al., 2011*]. A mean

value of 10 μA/cm^2 was applied as corrosion current density as values of this size have been observed for actual structures subjected to corrosion in [*Tuutti, 1982*].

When varying w/c material properties as compression and tensile strength as well as the modulus of elasticity of concrete were changed according to Table 3.4. The relation between the three parameters in Table 3.4 was based on guidelines given in [*Eurocode, 2008*; *Aalborg Portland, 2012*].

Table 3.4 *Characteristics of concrete for w/c = 0.3 and w/c = 0.5.*

Identification	f_{cm} [MPa]	f_{ctm} [MPa]	E_c [GPa]
WC03	85	4.7727	43.897
WC05	45	3.3311	36.272

To simulate corrosion-induced crack propagation, the commercial FEM program TNO DIANA 9.4.2 was used. 2316-2984 elements (4838-6192 nodes) were used to discretize the interface, concrete, reinforcement and corrosion layer domain in the model depending on the geometry. Nonlinear solution of the problem was obtained using a standard Newton-Raphson method with a displacement controlled convergence criterion.

3.4 Results

Figure 3.9 illustrates numerical results of the time to reach the damage (DL) and cracking limit (CL) state for S90 and S270 (varying location of corrosion products see Figure 3.6 and Figure 3.7) for different cover layers. Generally it is seen that both the time to reach DL and CL depend on the size of the cover layer. Although, the effect is reverse comparing DL and CL. Increasing the cover layer increases the time to reach DL but decreases the time to reach CL i.e. the larger the cover layer the faster the crack width increases once the crack has reached the surface which corresponds well to results found in [*Solgaard et al., 2013*].

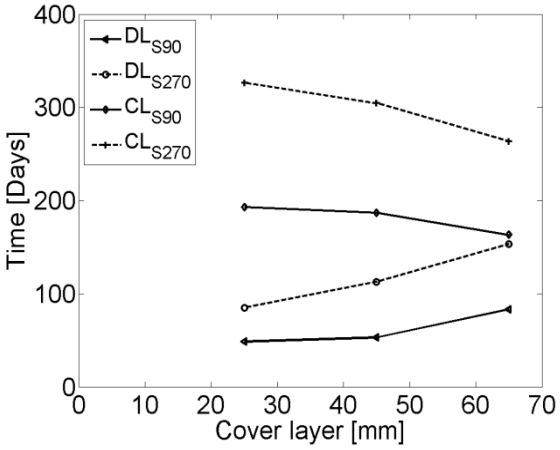

Figure 3.9 *Time to reach damage and cracking limit comparing S90 and S270 for different cover layers.*

Considering the two results for DL it is seen that increasing the cover layer from 25 mm to 65 mm increases the time to reach DL with 73% and 80% for S90 and S270, respectively. Furthermore the figure shows that changing the situation from S90 to S270 increases the time to reach DL with 77% and 84% for 25 mm and 65 mm, respectively. This indicates that the time to reach DL can be the same for a 25 mm cover layer and a 65 mm cover layer depending on the corrosion conditions and thereby the distribution of the corrosion current density along the circumference of the reinforcement.

Considering the results for CL it is seen that increasing the cover layer from 25 mm to 65 mm decreases the time to reach CL with 15% and 19% for S90 and S270, respectively. This implies that the influence of size of the cover layer is more pronounced for DL than CL.

For both DL and CL one break in each curve for S90 and S270 is observed indicating that the relation between the cover layer and time to reach DL and CL is non-linear. To determine this non-linearity other values of the cover layers should also be studied. Further, the slope of the curves is steeper for S270 than S90 implying that the lower corrosion current density the more pronounced is the influence of changing the cover layer.

In Figure 3.10 the results of the time to reach damage and cracking limit state for different reinforcement diameters for the two situations S90 and S270 are illustrated. Opposite to variations of the cover layer varying the reinforcement diameter affects DL and CL in the same way as all four curves descends asymptotically – the bigger the reinforcement diameter the earlier the limit state is reached indicating that for a given reinforcement diameter the influence of increasing the reinforcement diameter on DL/CL is limited. Considering the two results for DL it is seen that increasing the reinforcement diameter from 5 mm to 20 mm decreases the time to reach DL with 52%

and 36% for S90 and S270, respectively. The two results for CL show that the time to reach CL is decreased with 54% and 50 % for S90 and S270, respectively. This indicates that the influence of the reinforcement diameter is less pronounced for DL for lower corrosion current densities. However, further studies of this effect should be conducted to reinforce the observations of this study.

Comparing S90 and S270 show that DL increases with 80% and 139% and CL increases with 61% and 72% for 5 mm and 20 mm indicating that generally DL is more susceptible to changes in reinforcement diameter than CL and the effect gets more pronounced for larger reinforcement diameters. It is seen, comparing the different percentages, that the influence of the distribution of the corrosion current density, in this case, is greater than the influence of the reinforcement diameter.

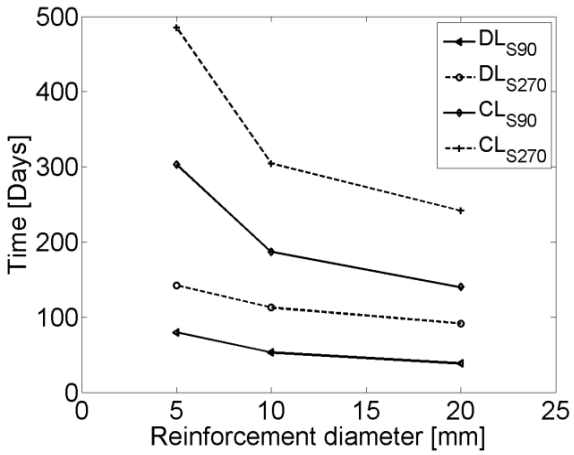

Figure 3.10 *Time to reach damage and cracking limit comparing S90 and S270 for different reinforcement diameters.*

Figure 3.11 illustrates the modeled time to reach the damage and cracking limit states for different water-to-cement ratios. Generally it is seen that varying w/c affects the results less than varying the cover layer and the reinforcement diameter. One reason for this is most likely that w/c affects other material parameters, which may counteract each other, e.g. tensile strength and the modulus of elasticity, when considering the propagation of cracks. However, a main aspect in this paper is to compare the influence of certain parameters (i.e. water-to-cement ratio, cover layer, reinforcement diameter and distribution of corrosion current density) on DL and CL - whereby a detailed sensitivity analysis of other affected material parameters, such as tensile strength and modulus of elasticity, has not been conducted.

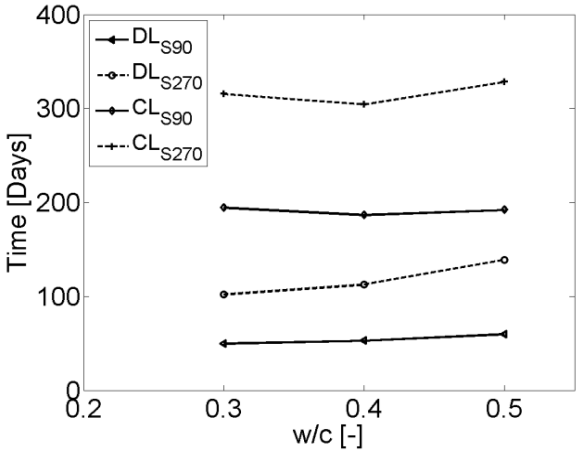

Figure 3.11 *Time to reach damage and cracking limit comparing S90 and S270 for different w/c.*

Increasing the w/c from 0.3 to 0.5 increases the time to reach DL viz. 20% for S90 and 36% for S270. Considering CL; S90 decreases with 2% and S270 increases with 4% indicating that the influence of w/c on CL is insignificant. It is seen that the slope of S270 is changing from negative to positive, however this is neglected as the decrease and increase is only 3% and 8%, respectively.

Comparing S90 and S270 the time to reached both DL and CL is significantly improved for S270 as the time is raised with more than 50% in average. This clearly shows that the uncertainty of the distribution of the corrosion current density is more decisive than varying w/c.

To create an overview, the results from the parametric study are arranged in tabular form in Table 3.5.

Table 3.5 *Time to reach damage and cracking limit based on Faraday's law.*

Identification	DL [days]	CL [days]
Ref_{S90}	52	186
Ref_{S270}	112	304
$C25_{S90}$	48	192
$C25_{S270}$	85	326
$C65_{S90}$	83	163
$C65_{S270}$	153	263
$R5_{S90}$	79	302
$R5_{S270}$	142	485
$R20\_{}_{S90}$	38	140
$R20_{S270}$	91	241
$WC03_{S90}$	49	194
$WC03_{S270}$	102	315
$WC05_{S90}$	59	191
$WC05_{S270}$	139	328

3.5 Summary and Conclusions

In the present paper an existing finite element based model simulating the expansion of non-uniformly deposited corrosion products - taking into account the penetration of corrosion products into the concrete matrix and predicting the propagation of corrosion-induced cracking was used to investigate the influence of cover layer, reinforcement diameter and water-to-cement ratio on the damage and cracking limit state. The importance of three parameters was shown together with the influence of uncertainty of the distribution of the corrosion current density varying the parameters for two different situations; a) accumulation of corrosion products at the initiation point of the predefined corrosion-induced crack path b) accumulation of corrosion products at the opposite site of the initiation point of the predefined corrosion-induced crack path. On the basis of the presented results the following was concluded:

(1) In the parametric range investigated, the uncertainty observed due to insufficient knowledge about the distribution of the corrosion current density along the circumference of the reinforcement overrules the effects of changing the studied parameters, i.e. cover layer thickness, reinforcement diameter, and water-to-cement ratio.

(2) Increasing the cover layer increases the time to reach the damage limit but decreases the time to reach the cracking limit, although the damage limit seems to be more susceptible to changes.

(3) Varying the cover layer affected the curves representing situation b) (accumulation of corrosion products at the opposite site of the initiation point of the predefined corrosion-induced crack path) the most indicating that the lower corrosion current density the more pronounced is the influence of varying the cover layer.

(4) Increasing the reinforcement diameter results in an asymptotically descending curve indicating that for a given reinforcement diameter the influence of increasing the reinforcement diameter on damage and cracking limit is limited.

(5) The influence of changing the water-to-cement ratio is limited.

Based on the conclusions the importance of investigating the distribution of the corrosion current density along the circumference of the reinforcement is visualized. As the distribution appears to be random, a probabilistic approach may be used to implement the uncertainty. Implementation of such a probabilistic modeling approach in the modeling scheme would give a more realistic estimate of the durability of a given structure and thereby improve the sustainability of the structure.

3.6 Acknowledgement

The authors gratefully acknowledge the financial support of the Danish Expert Centre for Infrastructure Constructions.

Chapter 4

Smeared Crack Modelling Approach for Corrosion-induced Concrete Damage (Paper III)

Anna Emilie A. Thybo

Department of Civil Engineering, Technical University of Denmark, Kgs. Lyngby, Denmark

Alexander Michel

Department of Civil Engineering, Technical University of Denmark, Kgs. Lyngby, Denmark

Henrik Stang

Department of Civil Engineering, Technical University of Denmark, Kgs. Lyngby, Denmark

Published in the journal “Materials and Structures”

MaterStruct (2017) 50: 146. doi:10.1617/s11527-017-0999-5

Abstract

In this paper a smeared crack modelling approach is used to simulate corrosion-induced damage in reinforced concrete. The presented modelling approach utilizes a thermal analogy to mimic the expansive nature of solid corrosion products, while taking into account the penetration of corrosion products into the surrounding concrete, non-uniform precipitation of corrosion products, and creep. To demonstrate the applicability of the presented modelling approach, numerical predictions in terms of corrosion-induced deformations as well as formation and propagation of micro- and macrocracks were compared to experimental data obtained by digital image correlation and published in the literature. Excellent agreements between experimentally observed and numerically predicted crack patterns at the micro and macro scale indicate the capability of the modelling approach to accurately capture corrosion-induced damage phenomena in reinforced concrete. Moreover, good agreements were also found between experimental and numerical data for corrosion-induced deformations along the circumference of the reinforcement.

Keywords

Concrete cracking, Smeared crack modelling approach, FEM, Corrosion

Introduction

4.1 Introduction

Along with globalisation, increase in population, and streamlining of transportation the demand for new infrastructures and, in general, the demand for sustainability of structures is expanding and, thereby, having a great effect on socio-economics. Understanding of structural performance as well as material behaviour is, therefore, of great importance and research within these fields has grown during the last decades *[Andrade et al. 1993; Cabrera 1996; Molina et al. 1993; Alonso et al. 1998; Noghabai 1999; Solgaard et al. 2013; Michel et al. 2013]*.

A leading deterioration mechanism, in reinforced concrete structures, is corrosion [*Rendell et al., 2002*], which may cause debonding/delamination in the concrete/reinforcement interface, cracking in cover layer, and decrease in durability due to corrosion of steel. Several studies have focused on modelling corrosion-induced damage leading to a variety of modelling approaches, e.g. finite element (FE) based [*Biondini and Vergani, 2012*; *Solgaard, 2013*] and analytical [*Bazant, 1979*; *Liu and Weyers, 1998*; *Chernin et al., 2010*; *Bohner E., 2010*]. Recent studies [*Bradley Justin Pease et al., 2012*; *Michel et al., 2013*] have shown that corrosion products precipitate non-uniformly (even under accelerated conditions applying direct current)

and penetrate into the surrounding concrete, which may have an influence on state-of-the-art FE modelling approaches dealing with corrosion-induced concrete damage.

Within this paper a FE modelling approach based on a discrete crack modelling that includes the penetration of corrosion products into the surrounding concrete *[Michel et al. 2013]* is further developed. The development includes the formulation of corrosion-induced concrete damage within a smeared crack modelling approach, which takes into account the penetration of corrosion products into the available pore space surrounding the reinforcement, non-uniform precipitation of corrosion products, and creep. The developed smeared crack modelling approach was then used to investigate the influence of the penetration of corrosion products into the surrounding concrete and the elastic modulus of corrosion products on corrosion-induced concrete damage. Finally, numerical results of the smeared crack modelling approach, i.e. modelled crack patterns, deformations near the concrete/reinforcement interface, and surface crack width, were compared to experimental observations obtained from accelerated corrosion experiments and data provided in the literature.

4.2 Introduction to corrosion-induced crack modelling

Once corrosion is initiated, electrochemical half-cell reactions are taking place along the reinforcement surface. The ionic reaction products of those half-cell reactions may further react and form solid corrosion products in the vicinity of the reinforcement. The type of corrosion products formed depends on the thermodynamic conditions present in the vicinity of the reinforcement [*Küter et al., 2008*]. Apart from solid corrosion products, soluble iron-chloride complexes (also referred to as green rust) may form in an oxygen-deprived environment in which chlorides are present [*Küter et al., 2008*; *Koleva et al., 2006*]. Such soluble iron-chloride complexes may not necessarily form in the vicinity of the reinforcement surface, as shown e.g. in [*Küter et al., 2008*]. However, independent of the type of iron oxides formed as a result of active corrosion, iron oxides occupy a larger volume than the initial iron that is consumed during the corrosion reaction; see e.g. [*Alonso et al., 1998*]. The increased volume of corrosion products causes tensile stresses in the surrounding concrete and may lead to concrete cracking, spalling, or delamination, if the tensile capacity of the concrete is exceeded.

To model the expansive nature of corrosion products, a thermal analogy may be used as shown in *Figure 4.1*. To mimic the increased volume of corrosion products, a ‘fictitious’ thermal load is applied to the corroded reinforcement section. Basic geometrical considerations and finite element method load application are illustrated in *Figure 4.1*. The thickness of the corroded reinforcement section, *X(t)*, may be determined using Faraday’s law, which describes the reduction in reinforcement radius due to corrosion:

$$X(t) = \frac{M i_{corr} \Delta t}{zF\rho} \tag{4.1}$$

M is the molar mass of the metal [g/mol], i_{corr} the corrosion current density [A/mm^2], Δt the duration of current application [s], z the anodic reaction valence [-], F Faraday's constant [96485 As/mol] and ρ the density of the metal [g/mm^3].

The thickness of the free expanding corrosion products can be expressed as (see e.g. Figure 4.1):

$$\Delta R_0 = R_2 - R_0 \tag{4.2}$$

Based on this, a 'fictitious' thermal load is applied to the corroded reinforcement section accounting for the expansion of corrosion products:

$$\Delta R_0 = X(t)\eta_{lin} = (R_0 - R_1)\eta_{lin} \tag{4.3}$$

where η_{lin} is the linear expansion coefficient [-] depending on the type of corrosion products formed and described by a 'fictitious' thermal expansion coefficient, α [K^{-1}], and a corresponding temperature increment, ΔT [K]. Assuming a constant coefficient of thermal expansion, α, the applied temperature increment, ΔT, represents then the type of solid corrosion product. Assuming further isotropic material properties of the corrosion products, the linear expansion coefficient may be obtained as one third of the volume expansion coefficient:

$$\eta lin = \alpha \Delta T \tag{4.4}$$

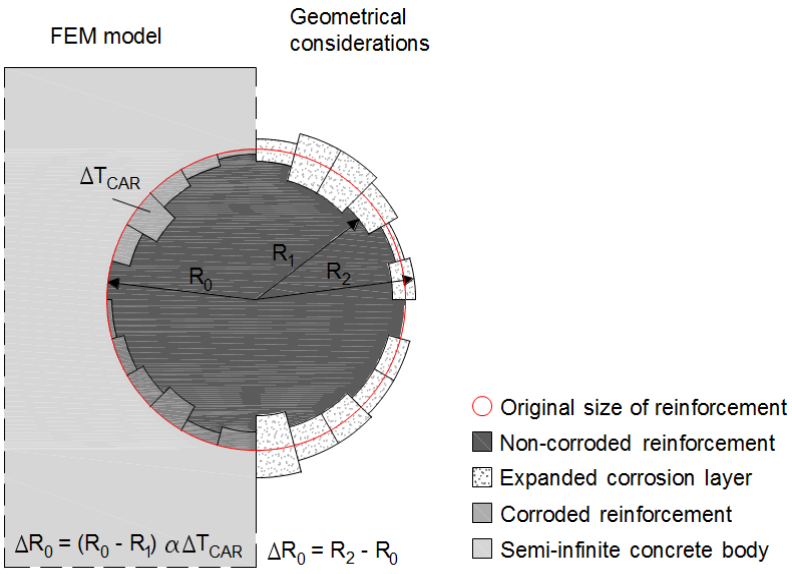

Figure 4.1 *Load application (left) and basic geometrical considerations to model non-uniform formation of corrosion products (right) in the smeared crack model, from* [*Thybo et al., 2013*]

4.3 Discrete Crack Modelling Approach

The foundation for the smeared crack modelling approach developed in this study is a FE based modelling approach in which corrosion-induced concrete damage is simulated by means of a discrete crack modelling approach [*Michel et al., 2010*; *Solgaard et al., 2013*; *B. . Pease et al., 2012*; *Michel et al., 2013*].

In general, five distinct regions (concrete, reinforcement, corrosion layer, and a cracking and debonding domain) form the modelled system, which simulates corrosion-induced cracking. In the model, uniform corrosion was assumed along the length and along the circumference of the reinforcement, for which a 2D plain strain formulation may be used. Cracking of the cementitious matrix was considered along a predefined crack path including delamination at the concrete/reinforcement interface, the former was modelled according to mode-I fracture and the latter was modelled according to mixed-mode (combined modes I and II) fracture. The initial model further assumed corrosion products form exclusively at the concrete/reinforcement interface. The penetration of corrosion products, non-uniform precipitation of corrosion products, and creep were not accounted for in the initial modelling approach presented in [*Michel et al., 2010*; *Solgaard et al., 2013*]. The implementation of these reinforcement corrosion related phenomena within a smeared crack modelling approach, are outline in the following sections.

4.4 Smeared Cracking Modelling Approach

To overcome the limitations of the discrete crack modelling approach, in particular, the predefined crack path and direction of a single corrosion-induced crack, the model was further developed within a smeared crack modelling approach. However, the formulation of smeared crack approaches in terms of continuous stress-strain relations (for a discontinuous phenomenon such as a corrosion-induced crack) is associated with drawbacks when dealing with time-dependent problems such as reinforcement corrosion. As, the nucleation of one or more corrosion-induced cracks leads to a deterioration of the current stiffness and strength of the concrete domain, subsequent stress and strain distribution depend on the stress and strain history (referred to as history dependency in the present paper).

In this study, the commercial finite element program TNO DIANA was used to simulate crack initiation and propagation using a smeared crack modelling approach. Within the model a multi-directional fixed cracking (MDFC) model was used, which can be combined with time dependent material models, such as e.g. creep. The MDFC model describes cracking using properties regarding tension cut-off, shear retention, and tension softening. In the present study linear tension cut-off was chosen viz. cracking occurs when the major principal tensile stress is larger than the minimum of either tensile strength or a ratio between the tensile and compressive strength.

Following the previously developed discrete cracking approach, the shear modulus after cracking was kept constant during simulation and multi-linear softening relations (adopted from [*Skocek, 2010*]) are used to describe tension softening. A standard Newton-Raphson method with an energy convergence criterion was used to obtain a solution of the nonlinear problem.

The implementation of penetration of corrosion products into the available pore space of the cementitious matrix surrounding the reinforcement, non-uniform precipitation of corrosion products, and creep within the smeared crack modelling approach is provided in the following sections.

4.4.1 Penetration and non-uniform precipitation of corrosion products and creep

Results of several experimental investigations described in the literature e.g. [*Liu and Weyers, 1998*; *Val et al., 2009*; *Michel et al., 2011*; *B. . Pease et al., 2012*] indicate both the penetration of corrosion products into the surrounding concrete and non-uniform precipitation of the corrosion products. The penetration of corrosion products into the available pore space of the cementitious matrix surrounding the reinforcement can be attributed to the porous nature of concrete, which allows precipitation of corrosion products to a certain degree without inducing tensile stresses in the concrete. Based on these observations [*Michel et al., 2011*], penetration and non-uniform precipitation of corrosion products and the effect of creep was implemented in a FE based discrete cracking modelling approach e.g. [*B. . Pease et al., 2012*; *Michel et al., 2013*; *Thybo et al., 2013*], which can be adapted for smeared crack modelling approach.

4.1.1.1 Penetration of corrosion products

With the help of x-ray attenuation and digital image correlation measurements [*Michel et al., 2011*; *B. . Pease et al., 2012*] were able to directly observe the penetration of corrosion products into the cementitious matrix surrounding the reinforcement reducing the effect of corrosion-induced expansion and, thereby, delaying the stress formation and initiation of cracking. Based on these observations, a conceptual approach to account for the penetration of corrosion products into the available pore space of cementitious material surrounding reinforcement was developed and presented in [*Michel et al., 2013*]. It is assumed that a corrosion accommodating region (*CAR*) around the reinforcement exists, initially denoted CAR_0, which delays stress formation while filling with corrosion products. Once this initial CAR_0 is filled with corrosion products, tensile stresses in the surrounding cementitious material increase and potentially lead to the formation of microcracks. These microcracks allow solid corrosion products to penetrate additional pore spaces and further delay corrosion-induced stresses. At some point a maximum size of the *CAR*,

denoted as CAR_{MAX}, is reached. No corrosion products can penetrate the matrix of the cementitious material beyond that point and all additionally formed corrosion products will introduce tensile stresses and potentially lead to the formation of a macrocrack.

The relationship between *CAR*, CAR_0, and CAR_{MAX} was described in [*Michel et al., 2013*] :

$$CAR = CAR_0 + (CAR_{MAX} - CAR_0)\kappa \tag{4.5}$$

κ is a dimensionless coefficient describing the change in connectivity of accessible pore space inside the *CAR* [-] and is assumed to vary between 0 and 1 according to:

$$\kappa = 0 \qquad if\ V_{cp} \le V_{cp,min}$$

$$\kappa = \frac{V_{cp} - V_{cp,min}}{\left(V_{cp,max} - V_{cp,min}\right)^{fp1}} \qquad if\ V_{cp,min} < V_{cp} \le V_{cp,max} \tag{4.6}$$

$$\kappa = 1 \qquad if\ V_{cp} > V_{cp,max}$$

where V_{cp} is the expanded volume of corrosion products [mm^3], $V_{cp,min}$ is the minimum volume of corrosion products [mm^3] (Eq. (4.6) and $V_{cp,max}$ the maximum volume of corrosion products that can be accommodated in the *CAR* [mm^3] (Eq. (4.8)), and *fp1* a fitting parameter set to 1 [-].

The values of *t* in Eq. (4.6) and (4.7) are based on experimental observations from x-ray described in [*B. . Pease et al., 2012*].

$$V_{cp,min} = 3\Delta T \pi l_A \left(R^2 - \left(R - X(t = 1.5)\right)^2\right) \tag{4.7}$$

$$V_{cp,max} = 3\Delta T \pi l_A \left(R^2 - \left(R - X(t = 5)\right)^2\right) \tag{4.8}$$

[*B. . Pease et al., 2012*] introduced an adjusted temperature increment, ΔT_{CAR}, instead of ΔT (see Eq. (4.4)) to account for the penetration of corrosion products.

$$\Delta T_{CAR} = \lambda_{CAR} \Delta T \tag{4.9}$$

λ_{CAR} describes the partial penetration of corrosion products [-] into the accessible (pore) space of the cementitious matrix and is defined as follows:

$$\lambda_{CAR} = \left(\frac{V_{cp}}{V_{CAR}}\right)^n \qquad if\ V_{cp} < V_{CAR}$$

$$\lambda_{CAR} = 1 \qquad if\ V_{cp} \ge V_{CAR} \tag{4.10}$$

where *n* is an empirical parameter discussed in [*B. . Pease et al., 2012*] [-] and V_{CAR} the volume of the *CAR* [mm^3]. The volume of the *CAR* is depending on the porosity and accessible volume of the concrete matrix:

$$V_{CAR} = \varphi V_{CM} \tag{4.11}$$

where φ is the capillary porosity of the concrete material [-], V_{CM} the accessible volume of concrete [mm^3] depending on the size of *CAR*, see Eq. (4.5), the radius of the reinforcement, *R* [mm], and the length of the reinforcement which is corroding, l_A [mm].

$$V_{CM} = \pi l_A((R + CAR)^2 - R^2) \tag{4.12}$$

4.1.1.2 Non-uniform precipitation of corrosion products

Among others, [*Michel et al., 2012*; *Bradley Justin Pease et al., 2012*; *B. . Pease et al., 2012*] observed that the precipitation of corrosion products was non-uniform along the circumference of the reinforcement although an impressed current was used to enhance the corrosion process. To account for the non-uniform precipitation of corrosion products within a discrete crack modelling approach, a corrosion current density vector, $\boldsymbol{i_{corr}}$, was introduced in [*Thybo et al., 2013*]. By varying the corrosion current density along the circumference of the reinforcement, see Figure 4.1, different degrees of reinforcement corrosion were generated i.e. the reduction in reinforcement radius (as well as the partial penetration coefficient (Eq. (4.10)) and the adjusted temperature increment (Eq. (4.9)) depend on both time and location. Introducing $\boldsymbol{i}_{corr}$ Eq. (4.1), (4.3), and (4.4) are replaced by Eq. (4.13), (4.14), and (4.15), respectively. A detailed explanation of the non-uniform precipitation of corrosion products is presented in [*Gebreyouhannes and Maekawa, 2016*] where the variation is explained as the result of the variation in the diffusion properties in the surrounding concrete resulting in a varying penetration of corrosion products into the concrete along the interface and thus resulting in varying stresses, deformations and consequently varying conditions for the corrosion process.

$$\boldsymbol{X(t)} = \boldsymbol{R_0} - \boldsymbol{R_1} = \frac{M \ \boldsymbol{icorr}\, \Delta t}{(z\, F\, \rho)} \tag{4.13}$$

$$\eta_{lin}(\boldsymbol{R_0} - R_1) = \boldsymbol{R_2} - \boldsymbol{R_0} \tag{4.14}$$

$$\eta_{lin} = \alpha\, \Delta T \tag{4.15}$$

4.1.1.3 Creep

To account for creep within the FE based smeared crack modelling approach, an effective modulus of elasticity for concrete was used according to [*Eurocode, 2008*],

see Eq. (4.16). The implementation of creep was based on the assumption that the models concerning creep in larger volumes of concrete are also applicable for the volume size considered in the present study.

$$E_{c,eff} = \frac{E_c}{1 + \varphi\left(t_{age}, t_0\right)} \tag{4.16}$$

Where $E_{c,eff}$ is the effective modulus of elasticity [MPa], E_c the tangent modulus of elasticity [MPa], $\varphi(t_{age},t_0)$ the creep coefficient [-], t_{age} the age of the concrete [days] and t_0 the time at loading [days].

4.4.2 Convergence of mesh

To investigate the impact of number of elements in the concrete domain and the number of corroding steel elements along the circumference of the reinforcement on corrosion-induced crack widths, a convergence analysis was carried out. Figure 4.2 illustrates a plot of the mesh highlighting the concrete, steel, and corroding steel domain. Three nodded triangular plane stress elements were used to discretize both the concrete and steel domain, while four-nodded quadrilateral plane stress elements where used to discretize the corroding steel domain. A zoom of the corroding steel domain is illustrated underlining that the corroding steel domain consists of several elements in the radial direction. The number of elements in radial direction depends on the number of 'time steps' selected during the simulation (see section 4.4.3).

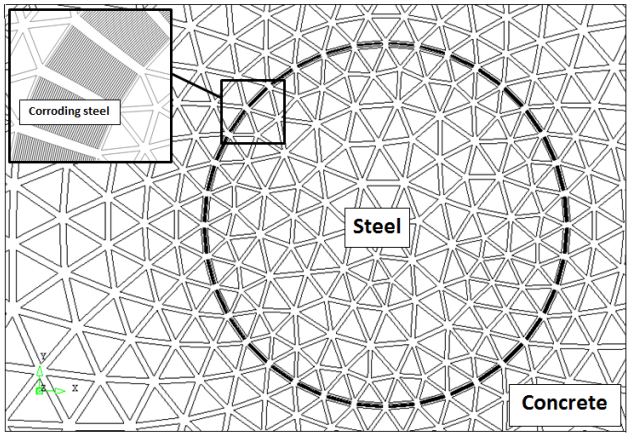

Figure 4.2 Plot of mesh

For the convergence analysis the number of elements within the concrete domain was varied between approximately 4000 and 49000 elements. Results of the analysis for a thickness of the corroding steel domain of 0.035 mm are presented in Figure 4.3 and have been normalised with respect to the results for 49082 elements. A maximum deviation of approximately 2 % is observed when increasing the number of elements from around 30000 to 49082. Thus, it was concluded that approximately 30000 elements in the concrete domain are sufficient to model corrosion-induced cracking

and it is actually possible to reduce the number of elements to optimize computational time without compromising accuracy of the simulations significantly. For the convergence analysis of the number of elements along the circumference of the reinforcement, 24, 36, 48, 148, and 192 elements were chosen to discretize the corroding steel domain. Results of the analysis are illustrated in Figure 4.4 for a thickness of the corroding steel domain of 0.035 mm and were normalised with respect to the results for 192 elements. It is seen that between 48 and 192 elements a deviation of less than 2% is observed. Therefore, it was concluded that 48 elements along the circumference of the reinforcement are sufficient for modelling corrosion-induced cracking without compromising accuracy. The influence of number of corroding steel elements in radial direction and the effect of number of elements in the steel domain was not investigated.

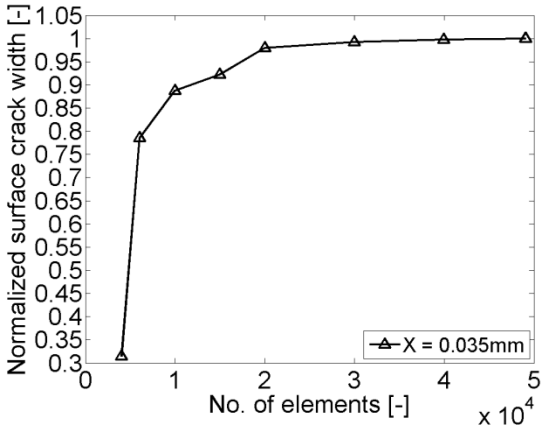

Figure 4.3 Convergence plot of elements in concrete

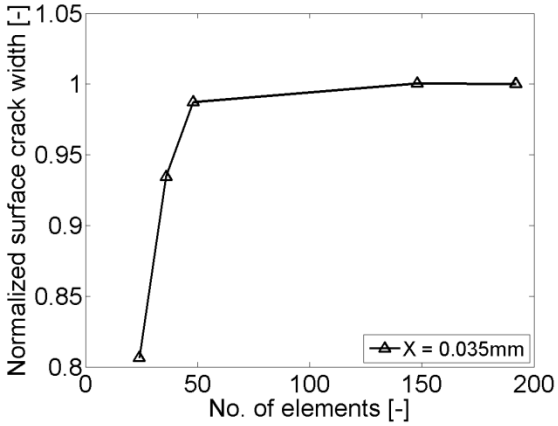

Figure 4.4 Convergence plot of elements along perimeter of reinforcement

4.4.3 History dependency

In the following the 'history dependency' of the developed smeared crack modelling approach was investigated comparing initiation time and surface crack widths varying

the number of intermediate 'load steps'. In the following the number of intermediate 'load steps' is referred to as 'time steps'. The applied number of 'time steps' for the various simulations, is schematized in *Table 4.1*, along with results of surface crack width, which are also visualised in *Figure 4.5*. The input parameters for the various simulations are given in *Table 4.2*.

Table 4.1 *Overview of time-to crack initiation and surface crack width after 20 days for varying numbers of 'time steps'.*

No. of 'time steps'	Time to crack initiation [days]	Deviation of time at first given crack value [%]	Deviation of surface crack width after 20 days [%]
1	-	-	29.1
3	12*	20.0	5.4
5	12*	20.0	5.1
20	11*	10.0	2.5
40	10.5	5.0	2.0
80	10.25	2.5	1.0
200	10	0	0

*In Figure 4.5 it is seen that the crack initiates earlier, however this is the first given value due to the low number of 'time steps'.

Table 4.2 *Input parameters for smeared crack modelling approach to investigate varying number of 'time steps'.*

	Parameter	Value	Dimension
Length	L	23	mm
Width	W	100	mm
Height	H	100	mm
Cover layer	C	45	mm
Reinforcement diameter	D	10	mm
Water-to-cement ratio	w/c	0.5	-
Concrete compressive strength	f_{cm}	45	MPa
Tangent modulus of elasticity - concrete	E_c	36.272	GPa
Shear stiffness	G_c	10	GPa
Poisson ratio - concrete	μ_c	0.2	-
Modulus of elasticity - steel	E_s	210	GPa
Poisson ratio - steel	μ_s	0.3	-
Modulus of elasticity - corrosion products	E_{corr}	2	GPa
Poisson ratio - corrosion products	μ_{corr}	0.2	-
Relative humidity	RH	65	%
Molar mass – steel	M_{Fe}	55.845	g/mol
Valence	z	2	-
Steel density	ρ_{steel}	7.86	g/cm^3
Faraday's constant	F	96485	A·s/mol
Mean corrosion current density	$i_{corr\ mean}$	0.0001	A/cm^2
Min. corrosion accommodating region	CAR_0	0.14	mm
Max. corrosion accommodating region	CAR_{MAX}	0.28	mm
Min. volume of corrosion products in *CAR*	$V_{cp,min}$	7.15	mm^3
Max. volume of corrosion products in *CAR*	$V_{cp,max}$	23.8	mm^3
Linear expansion coefficient	η_{lin}	0.7	-
Fictitious thermal expansion coefficient	α	1	-

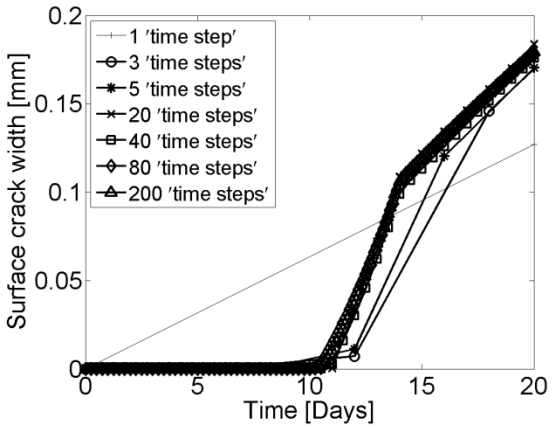

Figure 4.5 *Modelled corrosion-induced surface crack widths for varying number of 'time steps'*

From the results presented in *Figure 4.5* it can be seen that both surface crack width and time-to crack initiation depend on the number of 'time steps' (deformation history) in the smeared crack modelling approach. In general, it is observed that with decreasing number of 'time steps' insufficient and incorrect information on time-to crack initiation, crack width development over time, and final crack width are obtained. More realistic crack width development and final crack width are obtained with the modelling approach, when more than three 'time steps' are used. However, larger deviations with respect to the time-to crack initiation are still observed for an insufficient number of 'time steps'. This relation is highlighted in *Table 4.1*, where it can be observed that the final surface crack width (surface crack width at 20 days) is less affected by the number of 'time steps' compared to the time-to crack initiation. The results presented in *Table 4.1* indicate that the number of 'time steps' should be based on desired accuracy with respect to crack width development and time-to crack initiation. In order to minimise computational time and at the same time maintain an acceptable accuracy it was chosen to run simulations in the following with 40 'time steps'. For this number of 'time steps', approximately 5% and 2 % deviation with respect to time-to crack and final surface crack width are expected, respectively (compared to 200 'time steps').

4.5 Comparison between experimental and numerical results

To demonstrate the applicability of the developed FE based smeared crack modelling approach (including the penetration of solid corrosion products into the cementitious matrix, non-uniform precipitation of corrosion products, and creep) to predict corrosion-induced deformations and crack formation, numerical simulations were compared to two experimental studies: (1) results of digital image correlation (DIC) measurements presented in [*B. . Pease et al., 2012*; *Michel et al., 2013*] and (2) experimental observations from [*Vu et al., 2005*]. In addition, results of the previously

developed discrete crack modelling approach were also compared to predictions of the smeared crack modelling approach.

4.5.1 Experimental investigations

[*B. . Pease et al., 2012*] used digital image correlation (DIC) measurements to study the formation of corrosion products and corrosion-induced deformation in reinforced mortar specimens (w/c = 0.5) under accelerated corrosion conditions. Each specimen was 23 mm × 100 mm × 100 mm and a smooth 10 mm steel rod was placed in the centre as reinforcement. During the experiments, the specimens were placed in an acrylic pond containing tap water and a volumetric flask was used to maintain the water level at about 1 cm below the reinforcement. To enhance the reinforcement corrosion process, a DC regulator was used to impress a constant electrical current (100 $\mu A/cm^2$) through the counter electrode (activated titanium mesh). Deformations were measured using DIC technique allowing for crack measurements on the specimen surface, see e.g. [*B.Pease et al., 2012*].

For the DIC measurement technique, digital images were repeatedly captured at 10 minute intervals using a Nikon D3X 24.5 megapixel (6048×4032 pixel) camera body with a 60 mm focal length macro lens (AF-S Micro Nikkor 60mm f/2.8G ED). Prior to initiation of accelerated corrosion testing, three images were captured of the specimen surface, with a fourth image including a scale. The lens was placed 60 mm from the specimen surface, resulting in images with dimensions of approximately 31×41 mm^2, with each pixel representing 7.8×7.8 μm^2 of physical space [*B. . Pease et al., 2012*].

Captured images were input into a commercially available software package [*GOM, 2009*], which utilizes a previously applied stochastic speckle pattern to identify unique regions, called facets, on the specimen surface at each measurement time. The software tracks the movements of the facets and utilizes standard DIC techniques to compute deformations of the specimen surface. Additional information on the hardware used and the DIC technique is available in [*Pereira et al., 2011*] and [*Pease et al., 2006*], respectively [*B. . Pease et al., 2012*].

In addition, a trial test, to assess DIC measurement accuracy, was conducted by placing two mortar prisms side-by-side with flat faces touching each other. Prisms were fixed to a micrometer setup with 1 μm gradations with one prism stationary and the second moving with controlled distances. Two 2.5 mm extensiometers were used to provide comparative displacement measurements between the fixed and moving mortar prisms. The moving prism was translated by the micrometer setup to varying locations. At each location 3 digital images and 20 extensiometer measurements were recorded. A maximum difference of 0.29 μm was found for deformations from 0 to 26.2 μm comparing results of DIC measurement technique and extensiometer measurements [*B. . Pease et al., 2012*].

The accelerated corrosion test was stopped when the first macro-crack near the concrete/reinforcement interface was observed. For more information about preparation of the specimens, test setup, and measurement technique reference is made to [*B. . Pease et al., 2012*].

To fit the experimental observations, a vector describing the non-uniform corrosion along the circumference of the reinforcement was defined. The non-uniform corrosion current density along the circumference of the reinforcement was estimated using the experimental deformations after three days of accelerated corrosion as a starting point. A comparison between measured deformations after three days of accelerated corrosion and applied corrosion current density along the circumference of the reinforcement is illustrated in *Figure 4.6*. The average corrosion current density was 100 μA/cm2 and local variations may be attributed to factors such as reinforcement surface condition and moisture distribution around the reinforcement. In addition, the concrete tensile strength, f_{ctm}, was chosen to be 4.5 [MPa] and the non-physical modelling parameters *fp1* and *n* were set to 2.2 and 1.8, respectively. An overview of the input parameters for the smeared crack modelling approach is given in *Table 4.2*.

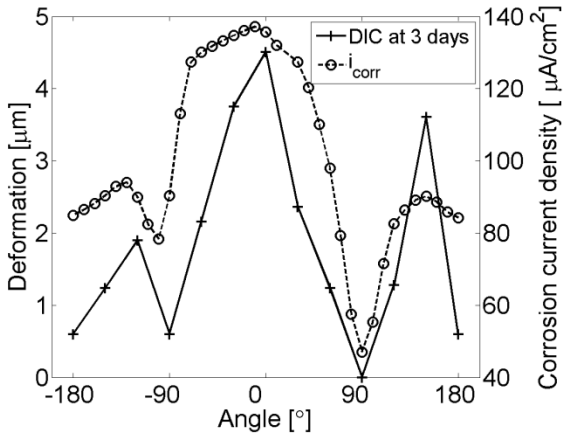

Figure 4.6 *Measured deformations (solid line) along the circumference of the reinforcement after three days of accelerated corrosion and corresponding estimated non-uniform corrosion current density (dashed line)*

Similar to [*B. . Pease et al., 2012*], [*Vu et al., 2005*] conducted accelerated corrosion tests to study the formation of corrosion-induced concrete cover cracks. Reinforced concrete slabs with w/c of 0.45, 0.5, and 0.58 were submersed in 5% sodium chloride (NaCl) solution and tested under accelerated conditions applying a constant current density of 100 μA/cm^2. Corrosion-induced cracks were measured using a combination of magnifying glass and displacement transducers. Testing was stopped when a crack width of 1.0 - 1.5 mm at the concrete surface was measured. More detailed information on specimen preparation, material properties, and experimental setup are provided in [*Vu et al., 2005*].

To simulated the experimental observations described in [*Vu et al., 2005*], i.e. time-to crack initiation and surface crack width, input parameters for the model described in *Table 4.3* were used. In addition, the concrete tensile strength compressive strength and volume expansion coefficient were set to 4.16 MPa, 43 MPa and 2,94, respectively, as provided in [*Vu et al., 2005*]. Furthermore, the non-physical modelling parameters *fp1* and *n* were set to 2.2 and 1.8, respectively. Further, Poisson's ratio and elastic modulus of corrosion products were set to 0.2 and 2 GPa, respectively, as e.g. provided in [*Solgaard et al., 2013*; *Caré et al., 2008*].

Table 4.3 *Input parameters for smeared crack modelling approach comparing to experimental data from [*Vu et al., 2005*]*.

	Parameter	Value	Dimension
Length	L	1000	mm
Width	W	156	mm
Height	H	250	mm
Cover layer	C	50	mm
Reinforcement diameter	D	16	mm
Water-to-cement ratio	w/c	0.5	-
Tangent modulus of elasticity - concrete	E_c	36.272	GPa
Shear stiffness	G_c	10	GPa
Poisson ratio - concrete	μ_c	0.2	-
Modulus of elasticity - steel	E_s	210	GPa
Poisson ratio - steel	μ_s	0.3	-
Relative humidity	RH	65	%
Molar mass – steel	M_{Fe}	55.845	g/mol
Valence	z	2	-
Steel density	ρ_{steel}	7.86	g/cm^3
Faraday's constant	F	96485	A·s/mol
Mean corrosion current density	$i_{corr\ mean}$	0.0001	A/cm^2
Min. corrosion accommodating region	CAR_0	0.14	mm
Max. corrosion accommodating region	CAR_{MAX}	0.22	mm
Min. volume of corrosion products in *CAR*	$V_{cp,min}$	2351	mm^3
Max. volume of corrosion products in *CAR*	$V_{cp,max}$	705	mm^3
Fictitious thermal expansion coefficient	α	1	-

4.6 Results and discussion

The ability of the presented smeared crack modelling approach is discussed with respect to three criteria: 1) corrosion-induced deformations near the concrete/reinforcement interface, 2) corrosion-induced crack patterns, and 3) time-to surface crack initiation and surface crack width. To quantify the ability of the model to simulate corrosion-induced deformations and cracks in the vicinity of the concrete/reinforcement interface, experimental results of digital image correlation measurements presented in [*Michel et al., 2013*] were used. Numerical predictions of time-to surface crack initiation and surface crack width were compared to experimental data presented in [*Vu et al., 2005*].

Comparisons between experimentally observed corrosion-induced deformations along the circumference of the reinforcement and numerical predictions using the presented smeared crack modelling approach and the previously developed discrete crack

modelling approach [*B. . Pease et al., 2012*; *Thybo et al., 2013*] are presented in Figure 4.8. Numerical and experimental results are given after three, six, and nine days of accelerated corrosion in polar coordinates (see also Figure 4.7). As can be seen from the results presented in Figure 4.7, excellent agreement (with respect to shape and magnitude) between experimentally observed and numerically predicted corrosion-induced deformations is found for six and nine days of accelerated corrosion.

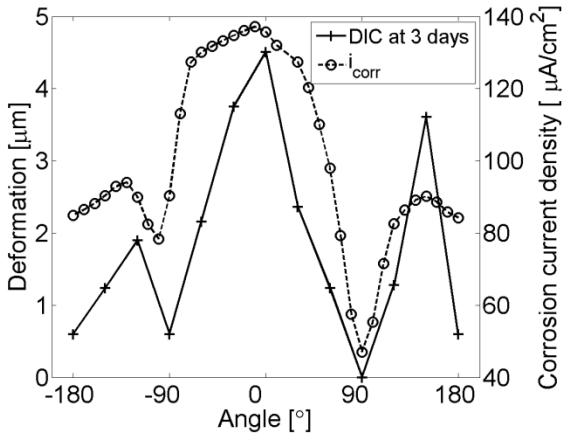

Figure 4.7 *Comparison of corrosion-induced deformations measured by DIC with numerical results obtained from a previously developed discrete cracking modelling approach* [*Michel et al., 2013*] *and the presented smeared crack modelling approach assuming non-uniform corrosion*

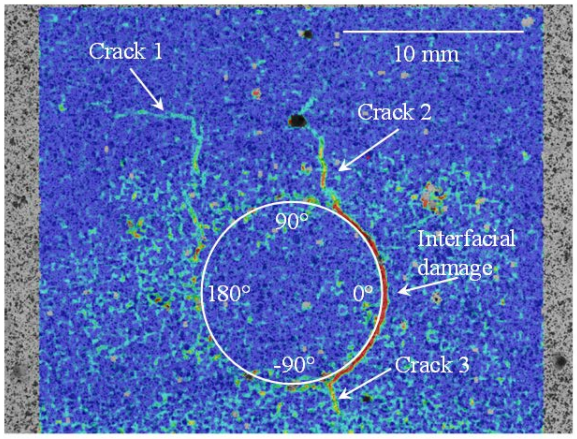

Figure 4.8 *Corrosion-induced cracks in reinforced specimens after nine days of accelerated corrosion, please note: only part of the test specimen is illustrated*

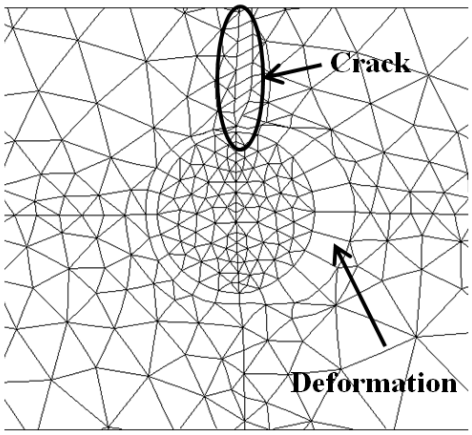

Figure 4.9 *Modelled crack development using the discrete crack modelling approach*

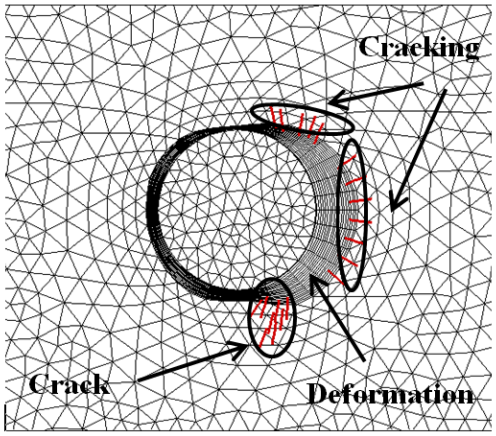

Figure 4.10 *Modelled crack development using the smeared crack modelling approach*

In addition, experimentally observed microcracks (by means of DIC) due to accelerated corrosion are illustrated in Figure 4.8. DIC allows thereby for identification of cracks as zones with localized strain, i.e. areas in red and light blue in Figure 4.8. Three corrosion-induced microcracks (with crack widths between approximately two and ten μm) and considerable damage along the circumference of the reinforcement can be identified in Figure 4.8. The microcracks formed at the reinforcement, extend around 10 to 15 mm in the mortar, and propagated towards the surface over time. For comparison, the crack pattern obtained by the presented smeared crack modelling approach and previously developed discrete crack modelling approach is given in Figure 4.10 and Figure 4.9, respectively. Similar crack pattern and corrosion-induced damage along the circumference of the reinforcement are obtained with the smeared crack modelling approach, while only one corrosion-induced crack is formed along the predefined crack path in the discrete crack modelling approach. Furthermore, extensive damage along the circumference of the reinforcement, in particular on the right side, and micro-cracking are observed in the

smeared crack modelling approach (see Figure 4.10), which is not captured by the discrete crack modelling approach (see Figure 4.9). In particular, three microcracks, which formed at the reinforcement and propagate towards the surface, can be observed in Figure 4.10. While the direction of the microcracks is not completely in agreement with the experimental observations, the extent of the microcracks is in good agreement with numerical predictions of the smeared crack modelling approach. However, it should be noted that results of the presented DIC measurement technique only provide information on corrosion-induced deformations and cracking on the specimen surface, i.e. details on corrosion-induced deformations and cracking within the specimen cannot be obtained with DIC. For additional validation of the presented modelling approach (accelerated) corrosion test may be undertaken in e.g. a µ-CT allowing for the observation of corrosion-induced deformations and cracking within the specimen.

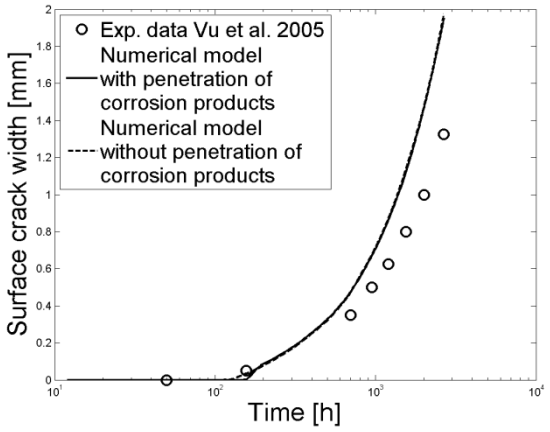

Figure 4.11 *Comparison of corrosion-induced surface cracking presented in [*Vu et al., 2005*] with Comparison of corrosion-induced surface cracking presented in [*Vu et al., 2005*] with numerical results applying the presented smeared crack modelling approach (with and without penetration of corrosion products into the surrounding concrete)*

Finally, Figure 4.11 illustrates a comparison of experimentally observed corrosion-induced surface crack width [*Vu et al., 2005*] and numerical predictions with the presented smeared crack modelling approach (taking into account and neglecting the penetration of corrosion products into the surrounding concrete). It can be clearly seen from the presented results that the model is able to accurately capture the time-to crack initiation when the penetration of corrosion products into the surrounding concrete is taken into account. Larger deviations between experimental observations and numerical predictions with respect to the time-to crack initiation are found when the penetration of corrosion products into the surrounding concrete is neglected; please note the logarithmic time scale in Figure 4.11. While the time-to crack initiation is accurately captured with the presented smeared crack modelling approach, some deviations are found between experimentally observed and numerically

predicted surface crack opening. Those deviations maybe be explained due to lacking information on fracture mechanical properties, in particular, the softening behaviour of the concrete material, as only the tensile strength was provided in [*Vu et al., 2005*].

4.6.1 Influence of elastic modulus of corrosion products

Deterioration models, such as the presented smeared crack modelling approach, developed to better understand corrosion-induced cracking processes in reinforced concrete, have highlighted a key parameter in the cracking process - namely, the elastic properties of reinforcement corrosion products [*Molina et al., 1993*; *Solgaard, 2013*]. Citing a lack of experimental observations [*Molina et al., 1993*] assumed water comprised the majority of corrosion products and therefore used water's elastic properties (2 GPa elastic modulus, 0.5 Poisson's ratio) to characterize the mechanical properties of corrosion products. Direct measurement of elastic properties of corrosion products is complicated due to the materials' stratified lamina nature. However, recently works attempted to quantify properties of reinforcement corrosion products [*Ouglova, Berthaud, et al., 2006*; *Caré et al., 2008*; *B. . Pease et al., 2012*]. Generally it was concluded that the elastic properties depend on the type and conditions under which corrosion products are formed e.g. degree of confinement, supply of oxygen, etc. In [*B. . Pease et al., 2012*] a discrete crack modelling approach was used to compare experimental observations of crack widths near the concrete/reinforcement interface (obtained by means of digital image correlation) with numerical predictions. Within their studies, [*B. . Pease et al., 2012*] found that elastic properties of the corrosion products between 2 and 20 GPa provided the best fit for the experimental data. Similar to [*B. . Pease et al., 2012*], the smeared crack modelling approach presented in this study was used to investigate the influence of the elastic properties of corrosion products on the time-to corrosion-induced cracking and development of surface cracks comparing numerical predictions and experimental observations from [*Vu et al., 2005*], see Figure 4.11. Elastic properties of corrosion products were thereby varied between 0.2 and 200 GPa.

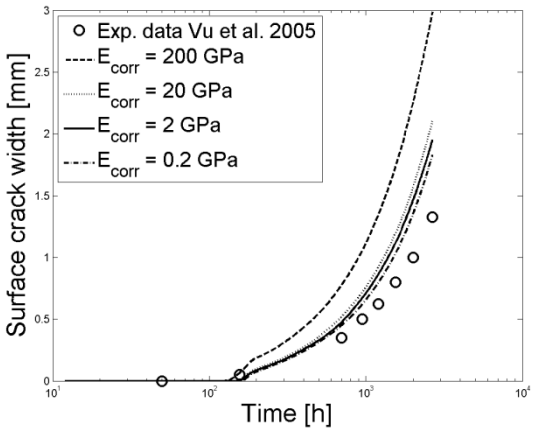

Figure 4.12 *Comparison of corrosion-induced surface crack widths for different elastic moduli of corrosion products using a smeared crack modelling approach*

Figure 4.12 illustrates numerical results of the smeared crack modelling approach and experimental results for varying elastic properties of the corrosion products. From the presented results in Figure 4.12, it can be seen that the elastic properties of the corrosion products affect both time-to corrosion-induced cracking and development of surface crack width. However, the impact on the time-to corrosion-induced cracking is lower than the influence on the development of the surface crack width, in particular for elastic properties in the range of 0.2 to 20 GPa. Significant changes in the time-to crack initiation and development of surface crack width are observed for elastic properties in the range of 200 GPa, in which case the smeared crack modelling approach considerably overestimates the experimental observations both with respect to time-to crack initiation and development of surface crack width.

4.7 Summary and Conclusions

In the present paper a finite element based smeared crack modelling approach was introduced to simulate corrosion-induced concrete damage. The presented modelling approach utilizes a thermal analogy to mimic the expansive nature of solid corrosion products and furthermore takes into account the penetration of corrosion products into the surrounding concrete, non-uniform precipitation of corrosion products, and creep. To demonstrate the applicability of the presented modelling approach, numerical predictions in terms of corrosion-induced deformations as well as formation and propagation of micro- and macrocracks were compared to experimental data obtained by digital image correlation and published in the literature. From the presented studies using the developed smeared crack modelling approach it may be concluded that:

1 The time-to crack initiation depends on the number of ‘time steps’ (deformation history) in the smeared crack modelling approach. In general, it is observed that with decreasing number of ‘time steps’ insufficient and incorrect information on

time-to crack initiation, crack width development over time, and final crack width are obtained. Preliminary modelling results indicate that the chosen number of 'time steps' should be based on desired accuracy with respect to crack width development and time-to crack initiation.

2 Excellent agreements between experimentally observed and numerically predicted crack patterns at the micro and macro scale indicate the capability of the modelling approach to accurately capture corrosion-induced damage phenomena in reinforced concrete. Moreover, good agreements were also found between experimental and numerical data for corrosion-induced deformations along the circumference of the reinforcement. In particular, the assumption of non-uniform corrosion around the circumference of the reinforcement let to a considerable improvement of numerical predictions concerning corrosion-induced deformations in comparison to previously presented modelling approaches.

3 The penetration of corrosion products into the available pore space of the cementitious matrix surrounding the reinforcement has a considerable effect on the time-to crack initiation. While in the present study the effect was demonstrated for accelerated corrosion conditions, the influence is even more pronounced under natural corrosion conditions, where corrosion current densities in the range of approximately 0.1 to 1 $\mu A/cm^2$ can be expected. It should be noted that in the present study homogeneous diffusion properties governing the penetration of corrosion products into the concrete were applied, while a more detailed study [*Gebreyouhannes and Maekawa, 2016*] applied inhomogeneous diffusion properties providing an underlying explanation for the varying precipitation of corrosion properties along the circumference of the reinforcement.

4 The elastic properties of the corrosion products affect both time-to corrosion-induced cracking and development of surface crack width. However, the impact on the time-to corrosion-induced cracking is lower than the influence on the development of the surface crack width, in particular for elastic properties in the range of 0.2 to 20 GPa. Within the present study values for the elastic modulus of corrosion products between 2.0 and 20.0 GPa provided most accurate fits to experimental results both with respect to time-to crack initiation and development of surface crack width.

Despite the good results found in the present study, future investigations should focus on improving modelling considerations regarding among others 3D analyses including non-uniform corrosion along the reinforcement as well as the inhomogeneous nature of concrete.

4.8 Acknowledgements

The authors gratefully acknowledge the financial support of the Danish Expert Centre for Infrastructure Constructions. Further, the authors would like to thank Bradley J. Pease for contributing with experimental data.

Compliance with Ethical Standards

The first author has received funding from the Danish Expert Centre for Infrastructure Constructions. No grant number exists.

Conflict of Interest Statement

The authors declare that they have no conflict of interest.

Chapter 5

Corrosion-induced Cover Cracking - effect of reinforcement arrangement (Paper IV)

Anna Emilie A. Thybo

Department of Civil Engineering, Technical University of Denmark, Kgs. Lyngby, Denmark

Alexander Michel

Department of Civil Engineering, Technical University of Denmark, Kgs. Lyngby, Denmark

Hikaru Nakamura

Department of Civil Engineering, Nagoya University, Nagoya, Japan

Henrik Stang

Department of Civil Engineering, Technical University of Denmark, Kgs. Lyngby, Denmark

Keywords

Keywords: Cover cracking, parametric study, numerical modelling, smeared cracking approach

5.1 Introduction

Civil infrastructure constructions (*e.g.* bridges, tunnels, roads, and buildings) are essential for the functionality and development of modern societies. However, deterioration of civil infrastructure together with increasing loads (*e.g.* traffic load and intensity) present major challenges to society in most developed countries; see *e.g.* [*Koch et al., 2002*; *ASCE, 2013*; *Giorno, 2011*; *Stevens et al., 2011*]. Renovation, renewal, and maintenance of existing civil infrastructures is thereby one of the primary challenges and research and experience from the past 20 years shows that the initial costs are often dwarfed by the costs of repairing, inspecting, and maintaining a civil infrastructure over its useful life, see *e.g.* [*Lepech et al., 2014*]. Reinforcement corrosion, causing concrete cover cracking and cross sectional reduction of the reinforcement both decreasing the structural performance and at worst causing total structural collapse, destroys thereby more than three per cent of the world's GDP [*Koch et al., 2002*]. At present, visual inspections generally form the basis for the assessment and maintenance planning of civil infrastructure. In particular, the presence of corrosion-induced cracks is commonly used to define service limit states for civil infrastructure - often relating corrosion-induced crack width and corrosion rate. However, the influence of governing parameters such as arrangement of reinforcement, geometry of concrete member, distribution of corrosion products, *etc.* affecting the corrosion process and subsequent formation of corrosion-induced damages are not taken into account, which may lead to erroneous conclusions with respect to the structural assessment of civil infrastructure. Thus, modelling is needed to assist visual inspection to understand and capture underlying mechanisms of corrosion-induced cracking in the civil infrastructure allowing for reliable assessment of structural performance and efficient maintenance planning of civil infrastructure.

While engineering tools and methods are well developed for the structural design of new structures, tools for assessing current and predicting the future condition of reinforced concrete structures are less advanced. Existing prediction tools are largely empirical, and thus limited in their ability to predict the performance of new materials, structural, or maintenance solutions. As such, the inability to reliably assess the long-term future ramifications of today's design decisions poses a major obstacle for the design of reinforced concrete structures. A primary reason for the lack of reliable modelling tools is that deterioration mechanisms are highly complex, involve numerous coupled phenomena that must be evaluated across a range of scales, and often cut across several academic disciplines. Despite the challenges, attempts to

improve the current tools and methods as well as studies regarding durability, sustainability, and service life design have increased considerably during the last decades. In particular, research focusing on the mechanisms behind and parameters affecting corrosion-induced cracking in reinforced concrete structures has received attention. Numerical [*Thybo et al., 2013*; *Bohner E., 2010*] and experimental [*Michel et al., 2011*; *B. Pease et al., 2012*] investigations have shown that reinforcement corrosion in concrete structures causes cracking in the concrete cover layer and cross sectional reduction of the reinforcement both mechanisms decreasing the structural performance and at worst causing total structural collapse. Finite element method (FEM) [*Isgor and Razaqpur, 2006*; *Suda et al., 1993*] analytical [*Bazant, 1979*; *Chernin et al., 2010*; *Liu and Weyers, 1998*] and empirical [*Alonso et al., 1998*; *Andrade et al., 1993*] approached have been proposed to predict corrosion-induced concrete damage.

In this paper, a finite element (FE) based modelling approach for the simulation of corrosion-induced damage in reinforced concrete is presented. The modelling approach accounts for the penetration of solid corrosion products into the available pore space of the surrounding cementitious materials, non-uniform distribution of corrosion products along the circumference of the reinforcement, and creep. Within the present study, focus is placed on the effect of various parameters, *i.e.* concrete cover layer thickness, reinforcement diameter, arrangement of reinforcement, and distribution of corrosion current density along the circumference of the reinforcement, on corrosion-induced damage phenomena, *i.e.* cover cracking, cross sectional reduction, and delamination.

5.2 Modelling approach

To investigate the effects of concrete cover layer thickness, reinforcement diameter, arrangement of reinforcement, and distribution of corrosion current density along the circumference of the reinforcement on corrosion-induced damage phenomena in civil infrastructure, corrosion-induced stresses and subsequent cracking was modelled using a smeared crack modelling approach [*Thybo et al., 2017*]. The present approach is thereby accounting for the penetration of solid corrosion products into the available pore space of the surrounding concrete, non-uniform precipitation of corrosion products along the circumference of the reinforcement, and creep - all three mechanisms affecting crack initiation and crack propagation [*Thybo et al., 2017*]. The modelling of corrosion-induced cracking and the implementation of the three mechanisms affecting crack initiation and crack propagation is briefly presented in the following, for further details the reader is referred to [*Michel et al., 2012*; *Michel et al., 2013*; *Thybo et al., 2013*; *Thybo et al., 2017*].

Non-linear fracture mechanical theory forms the basis of the model, which was divided into three different modelling domains a) concrete, b) corroding steel, and c)

steel, see Figure 1. Both the concrete and the steel region were discretized using three nodded triangular plane stress elements. The corroding steel region was discretized using four-nodded quadrilateral plane stress elements. The finite element (FE) model allows for predictions of time-to crack initiation and surface crack width using the commercial finite element program TNO DIANA. Solution of the highly non-linear problem is obtained using a standard Newton-Rapson method with an energy convergence criterion set to 10^{-2}.

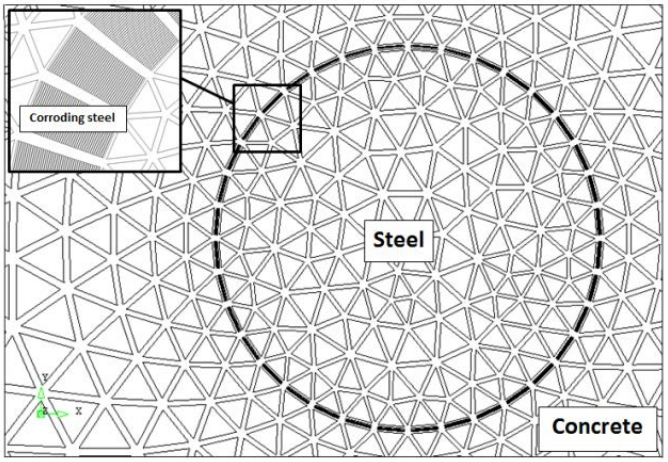

Figure 5.1 *Domains in the fracture mechanical model from* [*Thybo et al., 2017*].

5.2.1 Corrosion-induced cracking

Once corrosion is initiated, electrochemical half-cell reactions are taking place along the reinforcement. The ionic reaction products of those half-cell reactions may further react and form solid corrosion products in the vicinity of the reinforcement. Corrosion-induced cracking in reinforced concrete occurs, as the solid corrosion products occupy a larger volume than the steel consumed in the corrosion process [*Alonso et al., 1998*]. The increased volume of corrosion products leads to radial tensile stresses in the surrounding concrete. With ongoing corrosion these stresses increase reaching, at some point, a value corresponding to the tensile strength of concrete, initiating cracking in the concrete. With continuing development of the corrosion process, cracks propagate leading to *e.g.* debonding between concrete and reinforcement and cracking in the concrete cover layer.

Corrosion-induced cracking was modelled in two steps in the present modelling approach *i*) reduction of reinforcement radius and *ii*) expansion of corroded reinforcement. The reduction of reinforcement radius, *i.e.* the thickness of the corrosion layer (see also Figure 5.1), was determined applying Faraday's law. To mimic the expansive nature of solid corrosion products, a 'fictitious' thermal expansion coefficient and a corresponding temperature increment was applied to the corrosion layer. During simulations, a constant coefficient of thermal expansion was assumed along with isotropic material properties of the corrosion products *viz.* the

linear expansion coefficient was considered one third of the volume expansion coefficient. For more detailed information on the use of a thermal analogy to model the expansive nature of solid corrosion products, reference is made to e.g. [*Michel et al., 2013*].

5.2.2 Mechanisms related to corrosion initiation and propagation

Penetration of corrosion products into the available pore space of the surrounding concrete and non-uniform precipitation of corrosion products along the circumference of the reinforcement – affecting both crack initiation and propagation - have been observed in previous studies, see *e.g.* (Michel et al. 2013; Pease et al. 2012; Pease et al. 2012).

Due to the penetration of corrosion products into the available pore space of the surrounding concrete the radial pressure, *i.e.* corrosion-induced stresses and cracking caused by the corroding steel are delayed [*Michel et al., 2013*]. The influence of penetration of corrosion products into the surrounding concrete was experimentally observed (Pease et al. 2012; Michel et al. 2013). Based on the experimental results presented in [*Michel et al., 2011*] a conceptual model was established in [*Michel et al., 2013*] describing the penetration of corrosion products into the available pore space of cementitious materials comparing the volume of a defined corrosion accommodating region (CAR) and the volume of corrosion products. This conceptual model, adjusting the 'fictitious' temperature increment (applied to the corrosion layer) in relation to the amount of corrosion products and available pore space, is implemented in the present modelling approach.

Among others, [*Gebreyouhannes and Maekawa, 2016*] found that corrosion products precipitate non-uniformly along the circumference of the reinforcement. In [*Gebreyouhannes and Maekawa, 2016*] the process was explained due to variation in the diffusion properties in the surrounding concrete. However, focusing on fracture mechanics, in the present modelling approach non-uniform precipitation of corrosion products along the circumference of the reinforcement was accounted for varying the corrosion current density along the circumference of the reinforcement [*Thybo et al., 2013*]. Due to the correlation between the thickness of the corrosion layer and corrosion current density, non-uniform tensile stresses along the circumference of the reinforcement were obtained.

Considering among others the creep coefficient and the age of concrete, creep was accounted for in the modelling following instructions regarding the elastic modulus of concrete in Eurocode (1993). It was assumed that the described models related to creep in greater concrete regions are also applicable when considering concrete regions as applied in the present study.

5.2.3 Mesh

In the present modelling approach, the number of elements discretizing the corrosion layer in radial direction (see also Figure 5.1) is related to 'history dependency' - a term introduced in [*Thybo et al., 2017*]. The discretization of the corrosion layer in the radial direction accounts for the fact, that within a smeared cracking approach the stress and strain distribution at each calculated step depends on the previous stress and strain distribution when time-dependent problems are considered. Therefore, the number of corroding steel elements in radial direction is dependent on the deterioration time considered. The number of elements in the steel domain was, in this context, presumed less important and was not investigated.

A convergence analysis was conducted, optimising the mesh with respect to both accuracy and computational time. A mesh consisting of approximately 30,000 elements in the concrete domain and 48 elements in the corroding steel domain along the circumference of the reinforcement was found in [*Thybo et al., 2017*] to give a deviation of less than 2% with respect to crack width at the concrete surface.

5.3 Parametric Study

The objective of the parametric study was to investigate the effects of *i*) geometrical parameters, *i.e.* concrete cover layer thickness, reinforcement diameter, and arrangement of reinforcement and *ii*) distribution of corrosion current density along the circumference of the reinforcement on corrosion-induced damage phenomena in civil infrastructure, above all corrosion-induced cover cracking and delamination. In particular, the distribution of the corrosion current density along the perimeter of the reinforcement presents an important parameter, which is often unknown in experiments. It is expected that the parametric investigation in this study can shed light on the phenomenon and help to understand the uncertainty with respect to corrosion-induced cracking overserved during experimental investigations. Constants and parameters related to the geometry and distribution of the corrosion current density along the perimeter of the reinforcement are described in the following.

5.3.1 Geometrical parameters

To investigate the influence of geometry on the dominating corrosion-induced cracking mechanism, *i.e.* corrosion-induced cover cracking and delamination, geometrical parameters were varied throughout the parametric study. In general, three different geometrical scenarios were investigated as illustrated in Figure 5.2: *a*) the cover layer thickness is larger than the distance from the reinforcement to the remaining boundaries, *b*) the cover layer is equal to the distance from the reinforcement to the remaining boundaries, and *c*) the cover layer is smaller than the distance from the reinforcement to remaining boundaries. In addition, cover layer thickness, *C*, and reinforcement diameter, *D*, were varied. The size of both cover layer

and reinforcement diameter were chosen within the range used in the industry depending on demand with respect to structural performance and environmental exposure. To reduce computational time symmetry boundary conditions were applied also assuming that neighbouring reinforcement bars are under the same (corrosion) conditions and the width of the specimen equals the distance between reinforcement. The height (h) of the specimen was adjusted in proportion to the concrete cover layer and the reinforcement diameter. The height of the specimen was chosen to reflect a situation where the reinforcement is embedded in a semi-infinite concrete specimen limiting the potential numbers of cracked surfaces. An overview of the chosen geometrical parameters is given in Table 5.1 and illustrated in Figure 5.3.

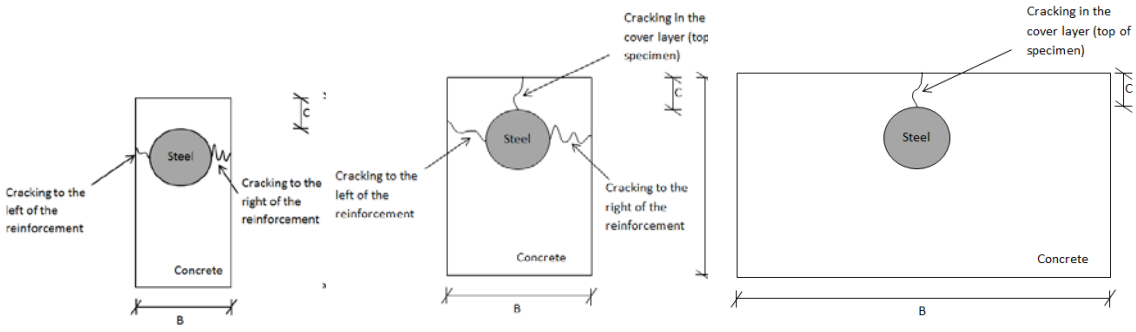

a) b) c)

Figure 5.2 *Illustration of geometrical scenarios studied to investigate dominating corrosion-induced cracking mechanism, i.e. corrosion-induced cover cracking and delamination: a) the distance from reinforcement to each side of the specimen is smaller than the cover layer, b) the distance from reinforcement to each side of the specimen is equal the cover layer, and c) the distance from reinforcement to each side of the specimen is larger than the cover layer. Please note: not to scale.*

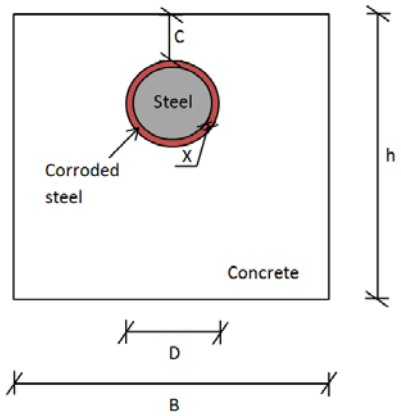

Figure 5.3 *Illustration of geometrical parameters. Please note: not to scale.*

Table 5.1 *Range of geometrical parameters.*

Concrete cover layer [mm] C	Reinforcement diameter [mm] D	Width [mm] B	Height [mm] h
20	5	C+D	
50	*10*	2C+D	100+C+D
80	*20*	3C+D	

5.3.2 Distribution of corrosion current density along the circumference of the reinforcement

Four cases were chosen to study the influence of non-uniform precipitation of corrosion products on corrosion-induced cracking mechanisms in reinforced concrete. The variation of the corrosion current density was described applying a distribution with one maximum (one vertex), which can be seen as extreme cases of potential distributions along the circumference of the reinforcement. The cases were chosen to simulate three different situations of which two were diametrically opposed and the third was representing a situation in-between. The fourth situation was chosen to compare results assuming uniform precipitation as a vast amount of models [*Solgaard et al., 2013*; *Suda et al., 1993*; *El Maaddawy and Soudki, 2007*] assume this situation. In Figure 5.4 the variation of corrosion current density along the circumference of the reinforcement for each case is illustrated. Figure 5.5 is sketching the use of polar angles as reference along the circumference of the reinforcement. Case 1 (dashed dotted line in Figure 5.4) represents a situation with uniform corrosion current density. Case 2 (solid line in Figure 5.4) represents a situation with the highest corrosion current density closest to the concrete surface. Case 3 (dashed line in Figure 5.4) represents a situation with the highest corrosion current density at the right side of the reinforcement. Case 4 (dotted line in Figure 5.4) represents a situation with the highest corrosion current density at the bottom of the reinforcement. The average corrosion current density, i_{corr_mean}, for all cases was chosen to 1 $\mu A/cm^2$ corresponding to an intermediate to high corrosion current density following general categorisation. Bigger infrastructure constructions such as bridges are often situated in aggressive or extra aggressive environments exposed to *e.g.* splashing from seawater (even partly submerged in seawater) and de-icing agents and therefore i_{corr_mean} = 1 $\mu A/cm^2$ was considered reasonable.

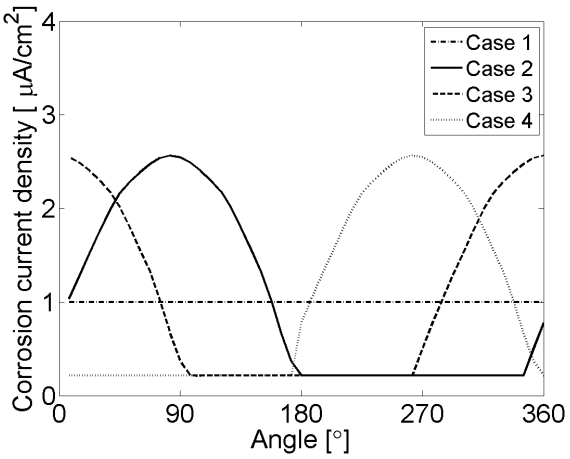

Figure 5.4 *Variation of corrosion current density along the circumference of the reinforcement for four different cases.*

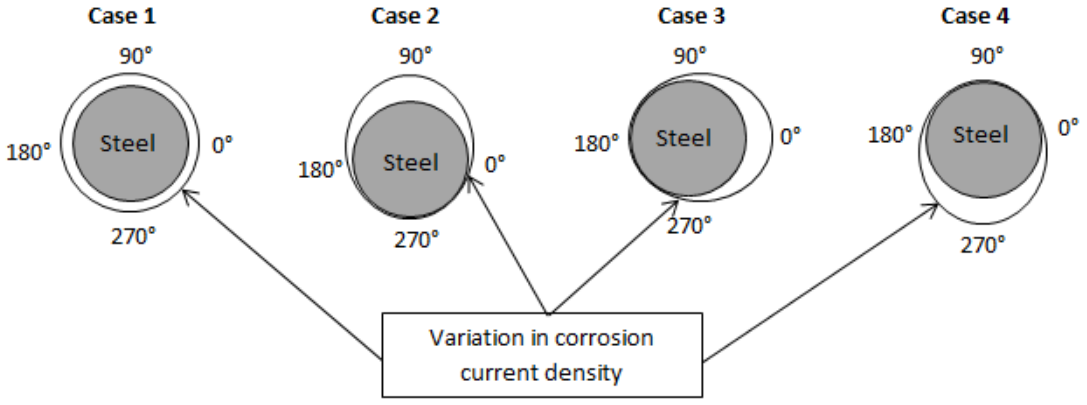

Figure 5.5 *Sketch of polar angles as reference along the circumference of the reinforcement and variation of corrosion current density for four cases.*

5.3.3 Constants

During all numerical simulations a number of material parameters, given in Table 5.2, were applied. Typical values for the mechanical properties of concrete and steel were chosen as given in *e.g.* [*Solgaard et al., 2013*].

The simulated type of corrosion products were hematite corresponding well to observations in *e.g.* [*Michel et al., 2011*]. Aside from the type of corrosion products, the mechanical properties of corrosion products depend on various factors such as for example the degree of confinement and availability of oxygen. Due to the complex nature of direct measurement of the elastic material properties of corrosion products, different suggestions of the elastic material properties for the corrosion products can be found the literature [*Molina et al., 1993*; *Suda et al., 1993*; *Caré et al., 2008*]. Based on studies [*Ouglova, François, et al., 2006*; *Michel et al., 2012*] an elastic

modulus of 2.1 GPa and a Poisson ratio of 0.2 were chosen to define elastic material properties of the corrosion layer in the present study. Isotropic material properties of the corrosion products were assumed and the linear expansion coefficient was obtained as one third of the volume expansion coefficient.

Table 5.2 *Applied material parameters during all numerical simulations.*

Parameter	Identification	Value	Unit
Concrete:			
Water-to-cement ratio	w/c	0.5	-
Tensile strength	f_{ctm}	4.5	MPa
Poisson ratio	μ_c	0.2	-
Steel:			
Modulus of elasticity	E_s	210	GPa
Poisson ratio	μ_s	0.3	-
Corrosion products:			
Modulus of elasticity	E_{corr}	2.1	GPa
Poisson ratio	μ_{corr}	0.2	-
Linear expansion coefficient	η_{lin}	0.7	-

5.3.4 Limit states

Considering service life design, the corrosion process may be divided into two phases: *i*) initiation and *ii*) propagation phase [*Tuutti, 1982*]. The propagation phase starts when corrosion takes place, *i.e.* when depassivation of the reinforcement has occurred. Following the terminology in Solgaard et al. (2013) the propagation process may be further divided into three different stages, *i.e.* damage, cracking, and spalling. Solgaard et al. (2013) defined the transition between damage and cracking limit as the first crack reaching the concrete surface. As the exact time at which this occurs is difficult to identify, due to the microscopic scale, a surface crack width of 0.05 mm was used in Solgaard et al. (2013) as indication of that transition, *i.e.* the damage limit state. Transition between cracking and spalling (the concrete is pushed off), was defined when the surface crack width reaches a value of 0.2 mm, *i.e.* the cracking limit state is defined for crack width of 0.2 mm. The damage and cracking limit state suggested in Solgaard et al. (2013) were applied in the this study, to enable a comparison between limit state and extent of corrosion (reduction in reinforcement radius) for all parameters investigated.

5.4 Experimental Data

In addition to results of the numerical simulations, findings from two experimental studies on corrosion-induced concrete cracking provided in the literature [*Tran, 2012*; *Andrade et al., 1993*] are presented in the following to reinforce observations from the parametric study on the dominating corrosion-induced cracking mechanism. In the following two subsections the two studies are briefly described, for further details the reader is referred to the specific studies.

5.4.1 Tran (2012)

Results of accelerated corrosion tests are presented in [*Tran, 2012*] including studies on the influence of varying concrete cover layer, reinforcement diameter, and specimen size on corrosion-induced cracking in reinforced concrete. The w/c ratio of the concrete was 0.56. The specimens used in the experimental setup, divided in series according to geometry, were immersed in a 3% NaCl solution while a current density of 900 μA/cm^2 was applied. Corrosion-induced concrete surface crack widths were measured during testing using displacement transducers. Upon testing, crack pattern, reduction in reinforcement diameter, amount of corrosion, and cross sectional reduction along the circumference of the reinforcement were studied. An overview of selected experimental series from [*Tran, 2012*], which were used in this study are shown in Table 5.3. An example of observed cross sectional reduction along the circumference of the reinforcement for various degrees of corrosion is given in Figure 5.6.

Table 5.3 *Testing series from* [*Tran, 2012*] *applied in the present study.*

Concrete cover layer [mm] C	Reinforcement diameter [mm] D	Width [mm] B	Height [mm] h
15	19	150	150
30	*19*	150	150
45	*19*	150	150
30	*19*	400	400

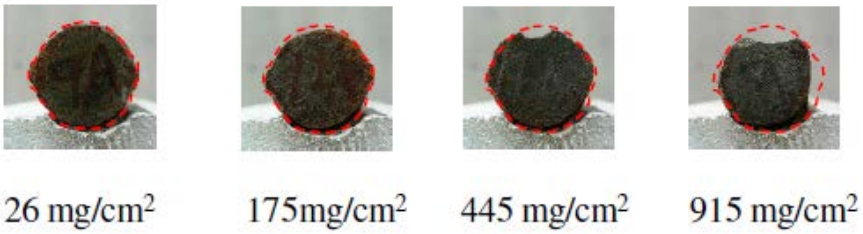

Figure 5.6 *Example of cross sectional reduction for different degrees of corrosion for series 150×150×30 mm3 (width×height×cover), from* [*Tran, 2012*]. *Dotted red line indicates initial size/shape of reinforcement.*

5.4.2 Andrade et al. (1993)

[*Andrade et al., 1993*] conducted accelerated corrosion tests investigating the effect of concrete cover layer (see Table 5.4) on corrosion-induced cracking in reinforced concrete. The specimens, with a w/c ratio of 0.5, were cured under water for at least 28 days and a tensile strength of 3.55 MPa was reported. A direct current of 100 μA/cm^2 was applied during testing where a galvanostat applied the current through a counter electrode located underneath the specimen. A sponge provided electrical contact between specimen and counter electrode. Strain gauges, attached to the

reinforced concrete specimens, were used to measure deformations and estimate the surface crack width during accelerated corrosion testing.

Table 5.4 *Testing series from* [*Andrade et al., 1993*] *applied in the present study.*

Concrete cover layer [mm] C	Reinforcement diameter [mm] D	Width [mm] B	Height [mm] h
20	16	30*	150
20	*16*	150	150
30	*16*	150	150

*Boundary to one side.

5.5 Numerical Results and Experimental Data

In the following, results of the parametric study with the developed numerical approach are presented to study the relationship between defined limit states (see section 5.3.4) and cross sectional reduction of the reinforcement in dependence of various geometrical parameters, *i.e.* concrete cover layer/reinforcement diameter ratio (C/D) and specimen width (B), as well as distribution of corrosion current density along the circumference of reinforcement. For comparison of the various results, the largest cross sectional reduction of the reinforcement, X_{max}, was chosen, see Figure 5.5. To determine X_{max}, Faraday's law was used, which also provides a direct relation to corrosion time. In addition, to the numerical results, experimental data provided in [*Tran, 2012*; *Andrade et al., 1993*] are presented for comparison and discussion of governing corrosion-induced cracking mechanisms, *i.e.* corrosion-induced cover cracking and delamination. It should be noted that for all numerical simulations the mechanical properties of concrete, reinforcement, and corrosion products are defined as given in Table 5.2. Furthermore, the experimental investigations presented in [*Tran, 2012*; *Andrade et al., 1993*] concern a single rebar, while symmetry boundary conditions were chosen in the numerical approach. However, for the geometries investigated in this study (see section 5.3.1), it may be assumed that the effect of chosen boundary conditions on crack initiation and propagation can be neglected. Finally, it should be mentioned that the experimental investigations were conducted under accelerated conditions, *i.e.* a direct current was applied enforcing reinforcement corrosion, with corrosion current densities in the order of several 100 $\mu A/cm^2$ compared to 1 $\mu A/cm^2$ chosen for the numerical studies. Thus, to enable a comparison between experimental observations and numerical results, all results are presented with respect to cross sectional reduction determined by means of Faraday's law. However, it should be kept in mind that the presented modelling approach accounts for the effect of creep, which is time dependent, *i.e.* cross sectional reductions of several hundred microns can be observed within a couple of weeks under accelerated corrosion, while it may take several decades to obtained a similar cross section reduction under natural conditions.

In all figures, the naming convention was based on specimen geometry, *i.e. D19_B150_C30* (see *e.g.* Figure 5.7) refers to a specimen with a reinforcement diameter, D = 19 mm, specimen width, B = 150 mm, and concrete cover layer, C = 30 mm.

5.5.1 Influence of concrete cover layer and reinforcement diameter

The influence of geometry, *i.e.* concrete cover layer and reinforcement diameter, as well as distribution of corrosion current density around the circumference of the reinforcement on the largest cross sectional reinforcement reduction, X_{max}, for two defined limit states, *i.e.* damage and cracking limit state, are presented in Figure 5.7. The damage limit state, *DL*, defines thereby a crack width of 0.05 mm, while the cracking limit state, *CL*, is defined for a crack width of 0.20 mm.

In general, increasing values for X_{max} are observed for increasing C/D considering both the damage and cracking limit state. However, the curves are considerably steeper for cases of non-uniform corrosion (case 2 to 4), see Figure 5.7 b) to d), compared to uniform corrosion (case 1), see Figure 5.7 a). At the same time, similar values of X_{max} are found for all cases of non-uniform corrosion with respect to the damage and cracking limit state for the investigated geometries, *i.e.* similar correlations between X_{max} and defined limit states were found irrespective of the distribution of corrosion current densities around the reinforcement. Moreover, an increase in difference of X_{max} between the damage and cracking limit state is observed comparing results for uniform and non-uniform corrosion. Furthermore, the numerical studies show that the influence of the reinforcement diameter on the damage and cracking limit state is limited for small covers, *i.e.* similar X_{max} initiate the crack at the concrete surface, in particular, for uniform corrosion, see Figure 5.7 a). However, increasing the concrete cover thickness, results in a more pronounced dependence of X_{max} on the reinforcement diameter. The effect is considerably more prominent for non-uniform corrosion compared to uniform corrosion, see Figure 5.7 b) to d). Finally, it can be noticed that for the non-uniform corrosion case 4 (see Figure 5.7 d)) neither the cracking nor the damage limit state was reached for geometries with a reinforcement diameter of 20 mm and a maximum concrete cover of 80 mm.

In addition to the numerical results, experimental observations from [*Tran, 2012*; *Andrade et al., 1993*] are presented in Figure 5.7. Experimental results from [*Andrade et al., 1993*] are given for values of X_{max} corresponding to crack widths of 0.05 mm, *i.e.* the damage limit state, and 0.15 mm, respectively. Experimental findings from [*Tran, 2012*] are given for values of X_{max} corresponding to crack widths of 0.15 mm, 0.14 mm, and 0.13 mm, respectively. Comparison of numerical results and experimental observations illustrate a good correlation for the data presented in [*Andrade et al., 1993*] assuming uniform corrosion, while the assumption of uniform corrosion considerable underestimates X_{max} for the data presented in [*Tran, 2012*].

Better correlation between experimental data from [*Tran, 2012*] and numerical simulations are found assuming non-uniform corrosion, *i.e.* case 2, which is also in good agreement with the visual observations of the reinforcement after accelerated corrosion reported in [*Tran, 2012*], see Figure 5.6.

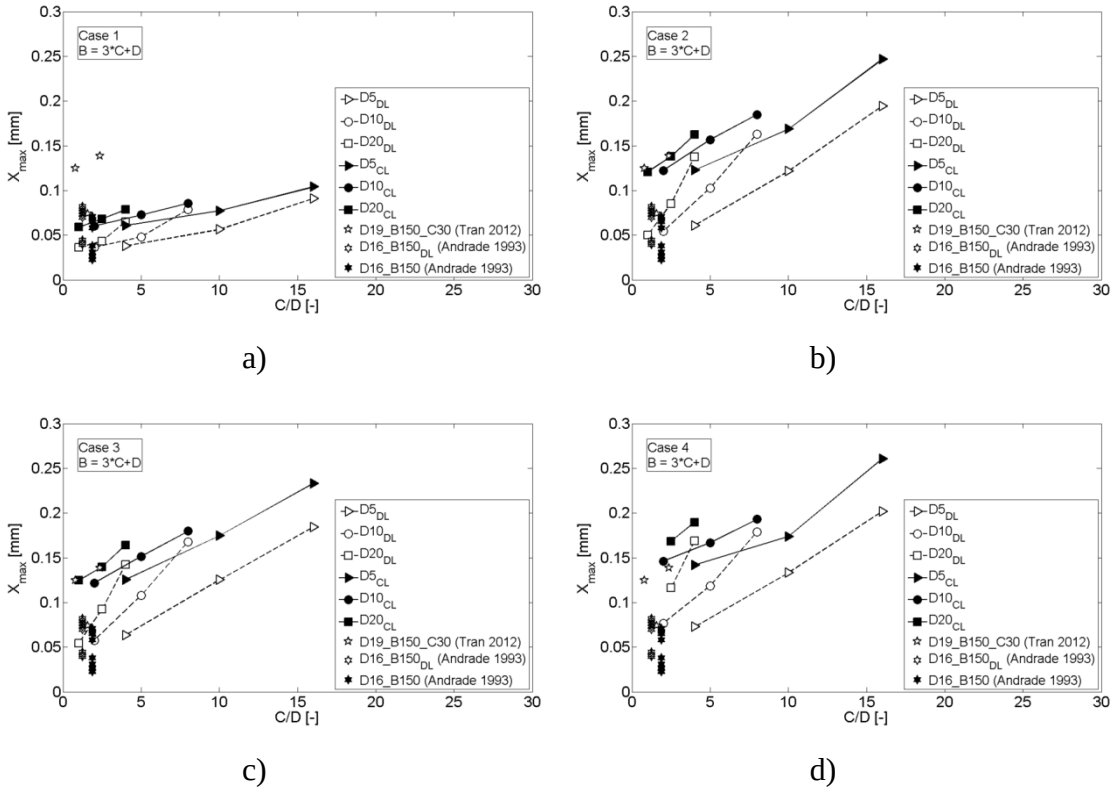

Figure 5.7 *Influence of C/D on Xmax for damage (DL) and cracking (CL) limit state assuming a) uniform corrosion (case 1) and b), c), and d) noon-uniform corrosion. Dashed lines indicate results of numerical simulations for Xmax with respect to damage limit state, while solid lines indicate results for cracking limit state. Markers represent experimental results obtained by* [*Tran, 2012*; *Andrade et al., 1993*].

5.5.2 Influence of distance between reinforcement bars and distribution of corrosion current density

Results of numerical simulations investigating the influence of the distance between reinforcement bars (specimen width) and distribution of corrosion current density along the circumference of the reinforcement on the dominating corrosion-induced cracking mechanism, *i.e.* corrosion-induced cover cracking and delamination, are presented in Figure 5.8. Figure 5.8 illustrates thereby the relation between the largest cross sectional reinforcement reduction, X_{max}, and surface crack width for varying reinforcement diameters, *i.e.* 5 mm, 10 mm, and 20 mm, distances between reinforcement bars, *i.e.* $B = C+D$, $B = 2C+D$, and $B = 3C+D$, a cover layer of 50 mm, and four different corrosion distribution scenarios, see Figure 5.5.

In general, results of the parametric study show that the dominating corrosion-induced cracking mechanism is cover cracking for specimens with $B = 3C+D$, while delamination is the governing mechanism for specimens with $B = C+D$. These observations on the governing cracking mechanism are independent of reinforcement diameter, cover thickness, and distribution of corrosion current density. For specimen geometries of $B = 2C+D$, the dominating cracking mechanism is highly dependent on the distribution of the corrosion current density along the circumference of the reinforcement. For example, for non-uniform corrosion case 2 ((Figure 5.8 b)), surface cracking is observed as the dominating cracking mechanism for all geometries with $B = 2C+D$, while delamination is the governing mechanism for these geometries for case 3 (Figure 5.8 c)). A mix of governing cracking mechanisms is observed for uniform corrosion and the non-uniform corrosion case 4. Assuming uniform corrosion, for reinforcement diameters larger than 10 mm surface cracking is observed, while for smaller diameters delamination appears to be the governing cracking mechanism. Similar observations can be made for the non-uniform corrosion case 4, in which surface cracking appears to be the dominating cracking mechanism for reinforcement diameters of 5 and 20 mm, respectively. Moreover, in case of cover cracking as governing mechanism, results of this study indicate that an increase in reinforcement diameter leads to increasing crack widths. The effect appears to be more pronounced for non-uniform corrosion, see Figure 5.8 b) and c), compared to uniform corrosion, see Figure 5.8 a). Results for non-uniform corrosion, furthermore, indicate that the effect is amplified with decreasing specimen width, see Figure 5.8 b). Finally, results clearly show that time-to surface crack initiation is affected by the distribution of corrosion current along the circumference of the reinforcement and thus X_{max}. Surface cracking is observed considerably earlier (and lower values of X_{max}) for uniform corrosion compared to non-uniform corrosion.

In addition to the numerical results, experimental observations from accelerated corrosion studies presented in [*Tran, 2012*] and [*Andrade et al., 1993*] are given in Figure 8. Results presented in [*Tran, 2012*] concern specimen with a single rebar, reinforcement diameter of 19 mm, cover layer of 30 mm, and a specimen width of 150 and 400 mm, respectively. Observations provided in [*Andrade et al., 1993*] are for specimens with a single rebar, reinforcement diameter of 16 mm, cover of 20 mm and specimen width of 30 mm and 150 mm, respectively. Comparison between experimental data and results of the numerical modelling approach indicate a good correlation between X_{max} and surface crack width for the data presented in [*Andrade et al., 1993*] assuming uniform corrosion, see Figure 5.8 a). However, the surface crack width as well as X_{max} is considerably underestimated for the data presented in [*Tran, 2012*] assuming uniform corrosion, see Figure 5.8 a). Better agreement between numerical and experimental results is found assuming non-uniform corrosion; in particular, for a distribution of corrosion products as assumed for case 2, see Figure

5.8 b). This is consistent with experimental observations provided in [*Tran, 2012*] on cross sectional reduction of the reinforcement as *e.g.* presented in Figure 5.6.

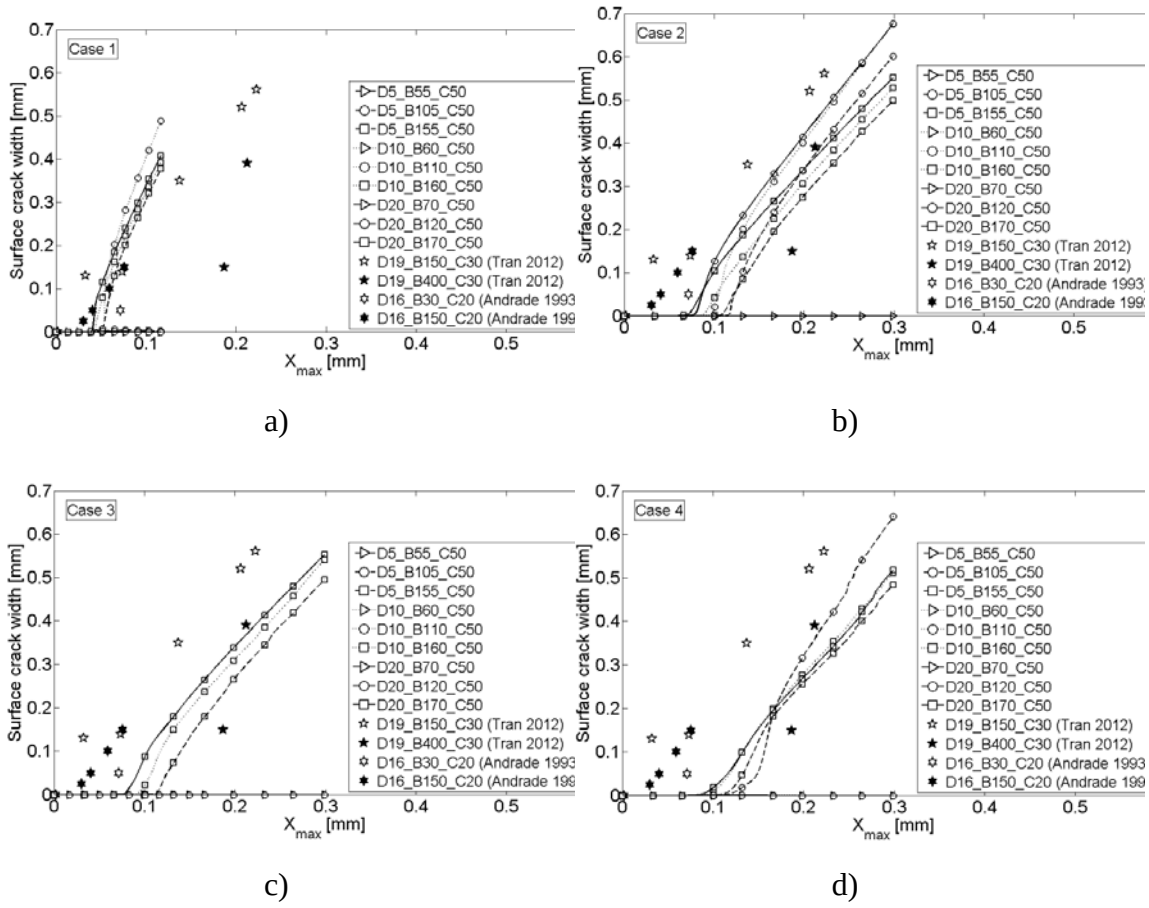

Figure 5.8 *Influence of specimen width on surface crack width for varying reinforcement diameter simulating a) uniform corrosion (case 1) and b), c), and d) non-uniform corrosion. The modelled results are compared to experimental data provided in* [*Tran, 2012*; *Andrade et al., 1993*].

5.6 Discussion

In general, experimental results reported in the literature concerning corrosion-induced cracking are provided in terms of cross sectional reduction of reinforcement, X_{max}, and related crack width, W, at the concrete surface, *e.g.* X_{max} = 15–18 µm for W ≈ 50 µm [*Andrade et al., 1993*], X_{max} = 10–65 µm for W ≈ 50 µm [*Vu et al., 2005*], and X_{max} = 15–30 µm for W ≈ 50 µm [*Alonso et al., 1998*] for varying tensile strength of concrete, concrete cover thickness, and reinforcement diameter. These values for X_{max} are thereby in general calculated based on Faraday's law, assuming 100 % current efficiency, and furthermore assuming uniform corrosion, which may be incorrect and thus used as an explanation for the scatter of the results. Nevertheless, similar results in terms of X_{max} and W are observed in this study assuming uniform

corrosion for varying geometrical parameters of reinforced concrete members, see Figure 5.7.

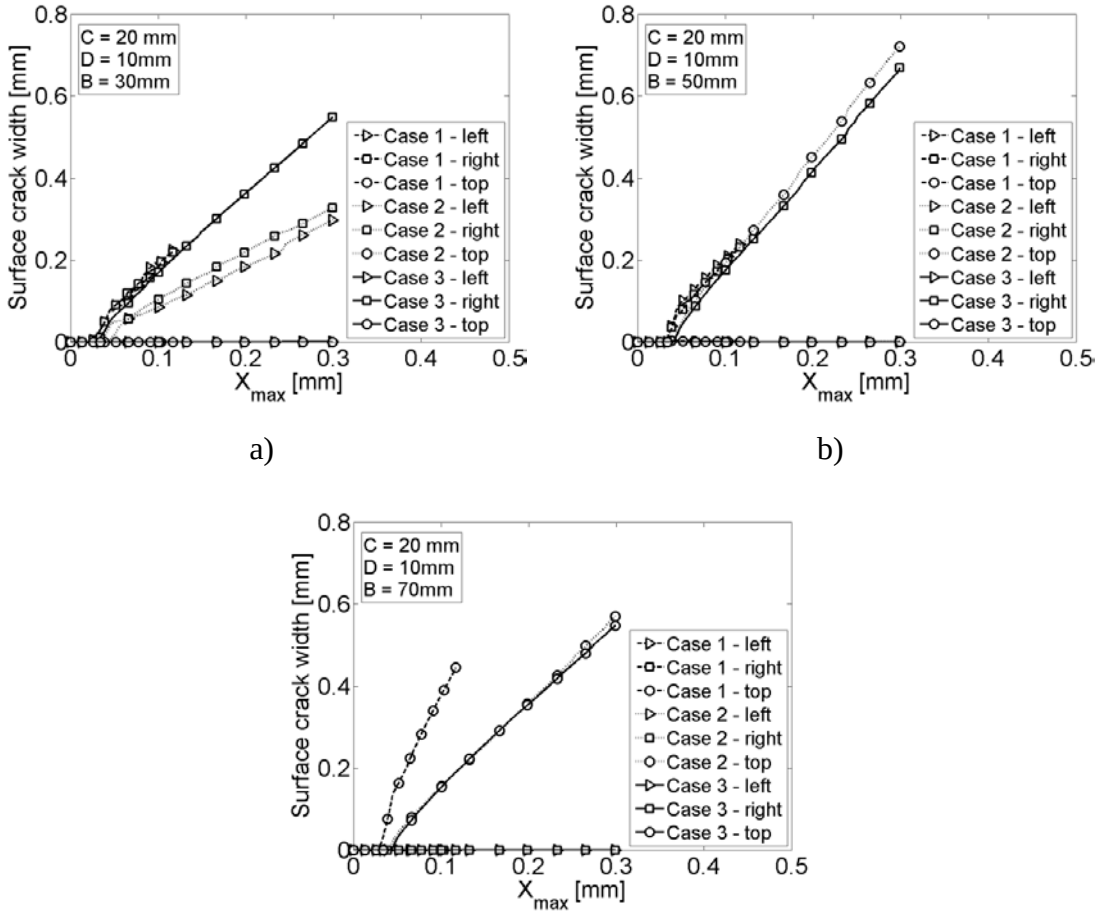

Figure 5.9 *Influence of distribution of corrosion current density along the circumference of the reinforcement on surface crack width for specimens with a) B = C+D, b) B = 2C+D, and c) B = 3C+D.*

Results of the parametric study indicate increasing values for X_{max} for increasing C/D considering both the damage and cracking limit state, which is consistent with observations presented in *e.g.* [*Alonso et al., 1998*]. In general, tensile strength of concrete, reinforcement diameter, and cover thickness (apart from electrochemical parameters controlling the corrosion process itself) determine the time-to crack initiation at the concrete surface. Assuming stable corrosion-induced crack propagation, as *e.g.* shown in [*Solgaard et al., 2013*], the observed relation between C/D and X_{max} may be attributed to the fact that increasing C/D result in a larger resistance to corrosion-induced tensile stresses of the reinforced concrete member, *i.e.* increasing cover for the same reinforcement diameter and constant corrosion rate leads to larger X_{max} and time-to crack detection at the surface. The results further show that the curves are considerably steeper for cases of non-uniform corrosion (case 2 to 4), see Figure 5.7 b) to d), compared to uniform corrosion (case 1), see Figure 5.7 a).

No considerable difference between the studied corrosion distributions and slope of the curves is thereby observed, *i.e.* the location of the largest cross sectional reduction does not seem to influence the relation between X_{max} and C/D. The observed increase in X_{max} for non-uniform distributions of corrosion along the circumference of the reinforcement may be attributed to a combination of localized and increased corrosion (see Figure 5.4) and resulting localized corrosion-induced stresses leading to crack initiation and propagation.

Moreover, results of the parametric study provide valuable insight into the dominating corrosion-induced cracking mechanism; for specimens with $B = 3C+D$ cover cracking is found to be the dominating cracking mechanism, while delamination is the governing mechanism for specimens with $B = C+D$. These observations on the governing cracking mechanism are independent of reinforcement diameter, cover thickness and distribution of corrosion current density, see Figure 5.8 and Figure 5.9. For specimen geometries of $B = 2C+D$, the dominating cracking mechanism is highly dependent on the distribution of the corrosion current density along the circumference of the reinforcement. Along with these observations, the parametric study indicates that surface cracking is observed considerably earlier (and for lower values of X_{max}) for uniform corrosion compared to non-uniform corrosion, see also Figure 5.9. These results clearly highlight the important practical implications of considering geometrical parameters as well as uniform and non-uniform corrosion on the governing corrosion-induced cracking mechanism and performance of corroding reinforced concrete elements. The distribution of corrosion products along the circumference determines the magnitude and spatial distribution of the expansive pressure applied as well as the loss of steel cross sectional area required to reach specified damage states. In particular, the relation between cross sectional reduction of reinforcement diameter and damage limit is of critical importance when attempting to estimate the residual service life of a deteriorating element. Results presented in this study clearly show that for more realistic estimations of the remaining service life of corroding reinforced civil infrastructure, visual assessment should be supported with numerical simulations.

5.7 Summary and Conclusions

As outlined in the introduction, it is currently state-of-the-art to base assessment and maintenance planning of civil infrastructure on visual inspections. In particular, the visual assessment of corrosion-induced cracks is commonly used to define service limit states for civil infrastructure - often relating corrosion-induced crack width and corrosion rate. However, the influence of governing parameters such as arrangement of reinforcement, geometry of concrete member, distribution of corrosion products, *etc.* affecting the corrosion process and subsequent formation of corrosion-induced damages are often unknown or not taken into account, which may lead to erroneous conclusions with respect to the structural assessment of civil infrastructure. In this

study, a numerical modelling approach was presented that is capable of predicting corrosion-induced cracking in reinforced concrete taking into account aforementioned governing parameters. Subsequently, a parametric study was undertaken to investigate the dominating corrosion-induced cracking phenomenon in dependence of reinforcement arrangement, geometry of concrete member, and distribution of corrosion products along the circumference of the reinforcement. From the presented results it may be concluded that:

- The presented FEM modelling approach is capable of realistically reproducing corrosion-induced cracking in reinforced concrete members taking into account geometrical parameters and distribution of corrosion products along the circumference of the reinforcement, which was demonstrated comparing numerical predictions and experimental data provided in the literature.
- Parametric studies with the presented modelling approach allowed for investigations of the governing corrosion-induced cracking mechanism, *i.e.* cover cracking and delamination, in reinforced concrete members. Results show that for specimens with $B = 2C+D$, the dominating cracking mechanism is highly dependent on the distribution of corrosion products along the circumference of the reinforcement, while cover cracking and delamination was exclusively observed for geometries with $B = C+D$ and $B = 3C+D$, respectively.
- For more realistic estimations of the remaining service life of corroding civil infrastructure, visual assessment should be supplemented with numerical simulations accounting for reinforcement arrangement, concrete member geometry, and - most important - distribution of corrosion products, which determines the local cross sectional reinforcement reduction, governs the cracking mechanism, and is vital for residual load bearing capacity estimations.

Further work is required to improve predictions of the presented FEM modelling approach including among others, extension of the modelling approach to three dimensional simulations, accounting for confinement provided by the presence of shear links, and stress fields generated by imposed loading. Moreover, establishment of a direct coupling between electrochemical and fracture mechanical simulations are needed taking into account *e.g.* temperature, relative humidity, *etc*. affecting among others electrochemical processes, to provide the basis for realistic service life predictions of civil infrastructure.

5.8 Acknowledgements

The authors gratefully acknowledge the financial support of the Danish Expert Centre for Infrastructure Constructions.

Chapter 6

Summary, Conclusions and Future Work

6.1 Summary

The aim of this work was to develop a theoretical framework for corrosion-induced damage in reinforced concrete in order to improve the basis for assessment of service life of structures based on visual assessment. Upon a review, state of the art modelling approaches for corrosion-induced damage in reinforced concrete structure, focus was in particular placed on the modelling of non-uniform distribution of corrosion products along the circumference of the reinforcement, penetration of corrosion products into the corrosion accommodating region and corrosion-induced multiple cracking in reinforced concrete structures applying a smeared cracking model. To limit the scope of the work, efforts were placed on modelling a cross section with one reinforcement bar. The complexity, when modelling corrosion-induced cracking in a cross section with multiple reinforcement bars, is increased due to the interaction between cracks and corrosion of several reinforcement bars. It was assumed that corrosion-induced damage based on corrosion of one reinforcement bar – and describing the interaction between adjacent bars implicitly – is sufficient to represent the influence on service life cracking which was studied in the present work. The applicability of the developed framework was tested by comparing numerical predictions with experimental results either obtained as part of the Ph.D. study or provided in the literature.

In a first step (Chapter 2), non-uniform distribution behaviour of corrosion products were implemented in a deterministic finite element fracture model. The model applies a discrete crack modelling approach that simulates the initiation and propagation of corrosion-induced cracking. The model is divided into five distinct regions with different material characteristics: concrete, steel, corrosion, cracking and debonding. The modelling approach includes the effect of creep and penetration of corrosion products into the surrounding concrete. However, the model simulates *uniform* corrosion along the circumference of the reinforcement i.e. corrosion elements are

subjected to the same volume expansion coefficient / same corrosion current density. Non-uniform distribution behaviour of corrosion products along the circumference of the reinforcement is typically observed due to varying corrosion current density. Therefore, in order to implement this mechanism in the modelling scheme a vector describing the variation of corrosion current density was introduced. As a first step this vector was estimated based on experimental observations of a corroded reinforcement bar. Finally, modelling results were compared to experimental observations and results from another model. As the comparison between numerical predictions and experimental results showed reliable results the influence of cover layer, reinforcement diameter and water-to-cement ratio on the damage and cracking limit state was investigated in Chapter 3. The three parameters were varied combined with two different descriptions of the corrosion current density a) accumulation of corrosion products at the initiation point of the predefined corrosion-induced crack path and b) accumulation of corrosion products at the opposite site of the initiation point of the predefined corrosion-induced crack path. The study showed that the non-uniform distribution behaviour of corrosion products along the circumference of the reinforcement had an influence on both damage and cracking limit state. Further the distribution behaviour of corrosion products along the circumference of the reinforcement proved to be comparable to the influence of cover layer, reinforcement diameter and water-to-cement ratio.

Continuing the development of the modelling scheme, a new model was established in Chapter 4. The same finite element program was used as in the original model, but instead of applying a discrete crack model approach a smeared crack model approach formed the basis of the model. By applying this approach, it was possible to account for multiple cracking including both micro and macro cracks. Mechanisms such as creep, penetration of solid corrosion products into the surrounding concrete and non-uniform distribution of corrosion products along the circumference of the reinforcement were implemented in the modelling scheme. Contrary to the previous model only three distinct regions were defined: concrete, steel and corroding steel. Thus, an initiation point of the expected crack(s) was not defined. To test the developed smeared crack model simulated results were compared to data found in the literature as well as results from simulations applying the discrete crack model approach described in Chapter 2 and 3. Both the discrete crack modelling approach and the smeared crack modelling approach provided good estimates of the experimentally corrosion induced-deformation. Including non-uniform corrosion around the circumference of the reinforcement further improved the accuracy of the numerical prediction. Considering corrosion-induced crack formation the smeared crack modelling approach particularly demonstrated good agreement with experimental results compared to the discrete crack modelling approach. Finally the penetration of corrosion products into the porous concrete had a considerable effect on the time-to crack initiation.

A parametric study of the modelling approach developed in Chapter 4 was undertaken in Chapter 5. The influence of reinforcement arrangement, geometry of the concrete member, and distribution of corrosion products along the circumference of the reinforcement on surface crack initiation and reduction in reinforcement radius was investigated. In the study, the influence of adjacent reinforcement bars was taken into account varying the geometry of the unit cell containing a single reinforcement bar. The size of concrete cover and distance between reinforcement bars combined with a varying distribution of corrosion products along the circumference of the reinforcement had a remarkable influence on the cracking mechanism. Both cover cracking and delamination was seen and in cases with cover cracking the distribution of corrosion products had a great influence on the time to crack initiation.

6.2 Conclusions

The studies presented in this work showed the fact that implementing non-uniform distribution of corrosion products along the circumference of the reinforcement in the modelling scheme along with a smeared crack modelling approach has a considerable impact when estimating the service life of reinforced concrete structures – both when it comes to time-to surface crack initiation and surface crack width.

In the following, the conclusions are related to the research questions formulated in the introduction.

Relation between the non-uniformity of distribution of corrosion products at the reinforcement/concrete interface and prediction of corrosion-induced damage in reinforced concrete structures

- Considering the corrosion-induced cracking pattern, it was shown that cracks initiate at locations with the highest accumulation of corrosion products. Assuming uniform corrosion could therefore lead to wrong conclusions with respect to service life predictions as the extent of corrosion, in reality, could be much higher if estimations are only based on visual observations such as time-to surface crack initiation and size of the surface crack width.
- Moreover, within the present framework, the influence of other variables e.g. water-to-cement ratio on the service life showed to be less important compared to the variation of corrosion current density, see e.g. Chapter 3.

Relation between the crack modelling approach and the prediction of corrosion-induced damage in reinforced concrete structures

- Applying a smeared crack modelling approach allows for prediction of both micro and macro cracks. Further, the initiation points of cracks are regulated

by material and geometrical parameters i.e. the initiation points are not predefined. Therefore, compared to earlier models, which applied a discrete crack modelling approach and assumed uniform distribution of corrosion products along the circumference of the reinforcement, the further developed model provides a considerably more realistic and precise estimate of the corrosion-induced deterioration mechanisms, see Chapter 4.

- It should however be mentioned that applying a smeared crack modelling approach compared to a discrete crack modelling approach increases complexity. The complexity is associated to the fact that every initiation and development of cracks leads to decreased stiffness in the concrete domain. The issue is referred to as history dependency in Chapter 4 and affects the number of calculation steps ('time steps') needed. Decreasing the number of 'time steps' too much results in insufficient information about the time-to surface crack initiation as well as the surface crack width. It is however possible to decrease the number of calculation steps depending on the desired accuracy with respect to crack width development and time-to crack initiation.
- Further, it is concluded that penetration of corrosion products into the surrounding concrete has an even more announced effect on the time-to crack initiation when applying a smeared crack modelling approach and accounting for a non-uniform distribution of corrosion products compared to earlier models due to the effect of non-uniform distribution of corrosion products. It is therefore strongly recommended to incorporate this mechanism in the modelling scheme.

Relation between parameters such as arrangement of reinforcement, geometry of concrete member, distribution of corrosion products, etc. and prediction of corrosion-induced damage in reinforced concrete structures when considering multiple cracking

- Based on parametric studies in Chapter 5 it was seen that the arrangement of the reinforcement has a considerable effect on the governing corrosion-induced cracking mechanism. Depending on the distance between the reinforcement and the cover layer combined with a variation in corrosion current density along the circumference of the reinforcement both cover cracking and delamination was seen. Decreasing the distance between the reinforcement eventually leads to delamination i.e. no warning of deterioration is given if only focusing on surface crack widths. Furthermore, the study showed that for certain geometries, cover cracking would eventually occur independent of corrosion distribution; however time to surface crack initiation varied remarkable depending on the distribution of corrosion products leading to uncertain estimates of the service life.
- Finally, it is concluded from the studies in Chapter 5 that for assessments of

the remaining service life of existing structures, visual assessment should be supplemented with numerical simulations accounting for reinforcement arrangement, concrete member geometry, and - most important - distribution of corrosion products, which determines the local cross sectional reinforcement reduction, governs the cracking mechanism, and is vital for residual load bearing capacity estimations.

6.3 Future Work

The work presented in this thesis has shown that it is possible to improve the existing models used for service life predictions. With the presented model and suggestions for improvements it is believed that the basis of an operational tool for service life predictions could be established. The applications of such tool are 1) design 2) a supplement to inspection and monitoring. Especially when considering condition assessments and assessment of remaining service life of existing structures this kind of model could be a useful tool. Using the observed conditions of the structure, along with known geometrical and material parameters as input, predictions regarding the condition of concrete and the state of the reinforcement (state of corrosion) are possible. Given the current condition of the structure, it is moreover possible to plan present and future precautions and/or recommendations regarding maintenance. Thus an interesting or more beneficial way of using such models is to estimate the remaining service life of structures, which according to calculations should have reached the end of service life but are still operational.

Considering a new structure it is recommend to describe a probabilistic function which defines the distribution of corrosion products. This is recommended to account for the influence of parameters which are unknown before taking the structure into operation.

The improvements not only deal with implementation of additional mechanisms but also question todays usual definitions of limit states. The studies indicate that the models have to increase the flexibility in order to improve the estimation of durability and service life of the structure. Two approaches making the models more flexible is to adjust the current limit states (e.g. allowing corrosion to a certain degree) or allow for different limit stats depending on the structure.

Besides the aforementioned recommendations, which are directly related to the work presented, additional suggestions to improve the general estimates of service life predictions are listed below.

- Changing the modelling scheme from 2D to 3D would allow the user to understand both the corrosion process and the corrosion-induced damage along the length of the reinforcement. Some presented models e.g. [*Lundgren, 2005b*; *Richard et al., 2010*; *Tran, 2012*] included a 3D modelling scheme, however [*Lundgren, 2005b*] considers uniform corrosion, [*Richard et al.,*

2010] does not consider the reduction of reinforcement radius and [*Tran, 2012*] applied a discrete crack model approach. Simulations, considering these parameters simultaneously and applying a smeared crack model approach, would provide an overall impression of the deterioration process as correlation would be accounted for. Furthermore it would help the user to determine whether or not the given area is a hot spot i.e. making it possible to define if the problem is a general problem or if maintenance and necessary precautions should only focus on a certain area.

- In addition to changing the modelling scheme from 2D to 3D a description of the inhomogeneous nature of concrete would improve the results of the simulations as it is well known that the placement of the aggregates, which is random, affects the cracking pattern.
- Ensure direct coupling between electrochemical and fracture mechanical simulations. The electrochemical process determines the corrosion process and therefore it would make the simulations more realistic. Furthermore the influence of several additional parameters such as temperature and relative humidity are included in the modelling. [*Isgor and Razaqpur, 2006*; *Ožbolt et al., 2012*; *Fahy et al., 2017*] coupled electrochemical and fracture mechanical simulations. Though, [*Isgor and Razaqpur, 2006*] applied a discrete crack model approach, [*Ožbolt et al., 2012*] neglected the effect of concrete softening and [*Fahy et al., 2017*] considered uniform distribution of corrosion products.

Bibliography

Alonso, C., Andrade, C., Rodriguez, J. and Diez, J.M. (1998), Factors controlling cracking of concrete affected by reinforcement corrosion. *Materials and Structures*, **31**(7), 435–441.

Andrade, C., Alonso, C. and Molina, F.J. (1993), Cover cracking as a function of bar corrosion: Part I-Experimental test. *Materials and Structures*, **26**(8), 453–464.

ASCE (2013), *2013 Report Card for America's Infrastructure*,

Balafas, I. and Burgoyne, C.J. (2011), Modeling the Structural Effects of Rust in Concrete Cover. *Journal of Engineering Mechanics*, **137**(3), 175–185.

Bardal, E. (2004), *Corrosion and protection*, Springer.

Bazant, Z.P. (1979), Physical Model for Steel Corrosion in Concrete Sea Structures - Theory. *Journal of the Structural Division-ASCE*, **105**(6), 1137–1153.

Bertolini, L., Elsener, B., Pedeferri, P., Redaelli, E. and Polder, R.B. (2013), *Corrosion of Steel in Concrete*, Weinheim, Germany: Wiley-VCH Verlag GmbH & Co. KGaA.

Bhargava, K., Ghosh, A.K., Mori, Y. and Ramanujam, S. (2006), Analytical model for time to cover cracking in RC structures due to rebar corrosion. *Nuclear Engineering and Design*, **236**(11), 1123–1139.

Biondini, F. and Vergani, M. (2012), Damage modeling and nonlinear analysis of concrete bridges under corrosion. In *Proc. of the 6th Inter. Conf. on Bridge Maintenance, Safety and Management*. pp. 948–957.

Bohner, D.E. (2012), Prediction Model for Concrete Cover Cracking due to Corrosion of Reinforcement. *Fib Symposium 2012: Concrete Structures for Sustainable Community - Proceedings*, (537), 1–4.

Bohner E., M.H.S.& B.S. (2010), Investigations on the mechanism of concrete cover cracking due to reinforcement corrosion. In et al. B. H. Oh, ed. *Fracture Mechanics of Concrete and Concrete Structures - Assessment, Durability, Monitoring and Retrofitting of Concrete Structures*-. Seoul, pp. 937–943. et al. B. H. Oh, ed. et al. B. H. Oh, ed.

Cabrera, J.G. (1996), Deterioration of Concrete Due to Reinforcement Steel Corrosion.

Caré, S., Nguyen, Q.T., L'Hostis, V. and Berthaud, Y. (2008), Mechanical properties of the rust layer induced by impressed current method in reinforced mortar. *Cement and Concrete …*, **38**(8–9), 1079–1091.

Chernin, L., Val, D. V and Volokh, K.Y. (2010), Analytical modelling of concrete cover cracking caused by corrosion of reinforcement. *Materials and Structures*, **43**(4), 543–556.

Dansk Betonforening (2014), *Betonhåndbogen*, Dansk Betonforening.

DuraCrete (2000), *Probabilistic performance based durability design of concrete structures*,

Eurocode, 2 (2008), *Design of Concrete Structures, Part 1 / General Rules and Rules for Buildings. (Industrial Processes: Building and Civil Engineering.).*, DS EN

1992-1-1.

Fahy, C., Wheeler, S.J., Gallipoli, D. and Grassl, P. (2017), Corrosion induced cracking modelled by a coupled transport-structural approach. *Cement and Concrete Research*, **94**, 24–35.

fib (2006), *Model Code for Structural Concrete: a new approach to structural engineering*,

Gebreyouhannes, E. and Maekawa, K. (2016), Nonlinear Gel Migration in Cracked Concrete and Broken Symmetry of Corrosion Profiles. *Journal of Advanced Concrete Technology*, **14**(6), 271–286.

Giorno, C. (2011), *Meeting Infrastructure Needs in Australia*,

GOM (2009), Aramis user manual – Software, Aramis v6.1 and higher.

Guzmán, S. and Gálvez, J.C. (2017), Modelling of concrete cover cracking due to non-uniform corrosion of reinforcing steel. *Construction and Building Materials*, **155**, 1063–1071.

Isgor, O.B. and Razaqpur, a G. (2006), Modelling steel corrosion in concrete structures. *Materials and Structures*, **53**(12), 291–302.

Jamali, A., Angst, U., Adey, B. and Elsener, B. (2013), Modeling of corrosion-induced concrete cover cracking: A critical analysis. *Construction and Building Materials*, **42**, 225–237.

Jensen, M.M. (2014), A Coupled Transport and Chem-ical Model for Durability Pre-dictions of Cement Based Ma- terials. , **321**(September), 208.

Koch, G.H., Brongers, M.P., Thompson, N.G., Virmani, Y. and Payer, J. (2002), *Corrosion costs and preventive strategies in the United States*,

Koleva, D.A., Hu, J., Fraaij, A.L.A., Stroeven, P., Boshkov, N. and de Wit, J.H.W. (2006), Quantitative characterisation of steel/cement paste interface microstructure and corrosion phenomena in mortars suffering from chloride attack. *Corrosion Science*, **48**(12), 4001–4019.

Küter, A., Geiker, M.R. and Møller, P. (2008), *Management of Reinforcement Corrosion*.

Lepech, M.D., Geiker, M. and Stang, H. (2014), Probabilistic design and management of environmentally sustainable repair and rehabilitation of reinforced concrete structures. *Cement and Concrete Composites*, **47**, 19–31.

Liu, Y. and Weyers, R.E. (1998), Modeling the Time-to-Corrosion Cracking in Chloride Contaminated Reinforced Concrete Structures. *Corrosion*, **95**(95), 675–681.

Lundgren, K. (2005a), Bond between ribbed bars and concrete. Part 1: Modified model. *Magazine of Concrete Research*, **57**(7), 371–382.

Lundgren, K. (2005b), Bond between ribbed bars and concrete. Part 2: The effect of corrosion. *Magazine of Concrete Research*, **57**(7), 383–395.

Maekawa, K., Kishi, T. and Chaube, R.. (1999), *Modelling of Concrete Performance*,

Michel, A. (2012), *Reinforcement Corrosion : Numerical Simulation and Service Life Prediction*. Technical University of Denmark.

Michel, A., Pease, B., Peterová, A. and Geiker, M. (2012), Experimental determination of the penetration depth of corrosion products and time to corrosion-induced cracking in reinforced cement based materials. In *Int. Congress on Durability of …*.

Michel, A., Pease, B.J., Geiker, M.R., Stang, H. and Olesen, J.F. (2011), Monitoring reinforcement corrosion and corrosion-induced cracking using non-destructive x-ray attenuation measurements. *Cement and Concrete Research*, **41**(11), 1085–1094.

Michel, A., Pease, B.J., Peterová, A., Geiker, M.R., Stang, H. and Thybo, A.E.A. (2014), Penetration of corrosion products and corrosion-induced cracking in reinforced cementitious materials: Experimental investigations and numerical simulations. *Cement and Concrete Composites*, **47**, 75–86.

Michel, A., Pease, B.J., Peterová, A., Geiker, M.R., Stang, H. and Thybo, A.E. a. (2013), Penetration of corrosion products and corrosion-induced cracking in reinforced cementitious materials: experimental investigations and numerical simulations. *Cement and Concrete Composites*.

Michel, A., Solgaard, A.O.S., Geiker, M.R., Stang, H. and Olesen, J.F. (2010), Modeling Formation of Cracks in Concrete Cover due to Reinforcement Corrosion. In *Proceedings of 7th International Conference on Fracture Mechanics of Concrete and Concrete Structures (FraMCoS-7)*. pp. 944–951.

Molina, F., Alonso, C. and Andrade, C. (1993), Cover cracking as a function of rebar corrosion: Part 2—Numerical model. *Materials and Structures*, **26**(9), 532–548.

El Maaddawy, T. and Soudki, K. (2007), A model for prediction of time from corrosion initiation to corrosion cracking. *Cement and Concrete Composites*, **29**(3), 168–175.

Noghabai, K. (1999), FE-Modelling of cover splitting due to corrosion by use of inner softening band. *Materials and Structures*, **32**(221), 486–491.

Ouglova, A., Berthaud, Y., François, M. and Foct, F. (2006), Mechanical properties of an iron oxide formed by corrosion in reinforced concrete structures. *Corrosion Science*, **48**(12), 3988–4000.

Ouglova, A., François, M., Berthaud, Y., Garé, S. and Foct, F. (2006), Mechanical properties of an iron oxide formed by corrosion in reinforced concrete structures. *Journal De Physique. IV : JP*, **136**, 99–107.

Ožbolt, J., Oršanić, F., Balabanić, G. and Kušter, M. (2012), Modeling damage in concrete caused by corrosion of reinforcement: Coupled 3D FE model. *International Journal of Fracture*, **178**(1–2), 233–244.

Pantazopoulou, S. J., & Papoulia, K.D. (2001), Modeling cover-cracking due to reinforcement corrosion in RC structures. *Journal of Engineering Mechanics*, **2**(April), 342–351.

Pease, B.., Michel, A., Thybo, A.E.A. and Stang, H. (2012), Estimation of elastic modulus of reinforcement corrosion products using inverse analysis of digital image correlation measurements for input in corrosion-induced cracking model. In *Bridge Maintenance, Safety, Management, Resilience and Sustainability - Proceedings of the Sixth International Conference on Bridge Maintenance, Safety and Management*. pp. 3643–3650.

Pease, B.J., Geiker, M.R., Stang, H. and Weiss, J. (2006), Photogrammetric Assessment of Flexure Induced Cracking of Reinforced Concrete Beams under Service Loads. In *Proceedings of the Second International RILEM Symposium : Advances in Concrete through Science and Engineering*.

Pease, B.J., Michel, A., Geiker, M.R. and Stang, H. (2012), Modelling Moisture Ingress through Simplified Concrete Geometries. In *International Congress on Durability of Concrete*.

Pease, B.J., Michel, A. and Stang, H. (2012), Quantifying movements of corrosion products in reinforced concrete using x-ray attenuation measurements. In *Proceedings of the 2nd International Conference on Microstructure Related Durability of Cementitious Composites*.

Pereira, E.B., Fischer, G. and Barros, J.A.. (2011), Image-based detection and analysis of crack propagation in cementitious composites. In *Proceedings of International RILEM Conference On Advances In Construction Materials Through Science and Engineering*.

Qiao, D., Nakamura, H., Kunieda, M. and Ueda, N. (2012), NUMERICAL ANALYSIS OF INFLUENCING FACTORS ON CORROSION-INDUCED CONCRETE CRACKING WITH RBSM. In pp. 1–7.

Rendell, F., Jauberthie, R. and Grantham, M. (2002), *Deteriorated Concrete: Inspection and Physicochemical Analysis*, Thomas Telford Ltd.

Richard, B., Ragueneau, F., Cremona, C., Adelaide, L. and Tailhan, J.L. (2010), A three-dimensional steel/concrete interface model including corrosion effects. *Engineering Fracture Mechanics*, **77**(6), 951–973.

Rodriguez, J., Ortega, L.M., Casal, J. and Diez, J.M. (1996), Corrosion of reinforcement and service life of concrete structures. *DURABILITY OF BUILDING MATERIALS AND COMPONENTS*, **1**, 117–126.

Sanz, B., Planas, J. and Sancho, J.M. (2017), Influence of corrosion rate on the mechanical interaction of reinforcing steel, oxide and concrete. *Materials and Structures/Materiaux et Constructions*, **50**(4), 1–14.

Skocek, J. (2010), *Fracture propagation in cementitious materials Multi-scale approach : measurements and mod- eling Jan Sko˘*. Technical University of Denmark.

Solgaard, A., Michel, A., Geiker, M. and Stang, H. (2013), Concrete cover cracking due to uniform reinforcement corrosion. *Materials and Structures*, 1–19.

Solgaard, A.O.S. (2013), Corrosion of reinforcement bars in steel fibre reinforced concrete structures.

Standard, D. and DS (1993), *Eurocode 2 / Betonkonstruktioner. - 1-1: Generelle regler samt regler for bygningskonstruktioner + Dansk supplement*,

Stevens, B., Schieb, P.-A. and Gibson, A. (2011), *Strategic Transport Infra-structure Needs to 2030: Main Findings. OECD Futures Project on Transcontinental Infrastruc-ture Needs to 2030/50*,

Strauss, A., Wendner, R., Bergmeister, K., Teplý, B. and Novák, D. (2012), Probabilistic performance assessment of concrete structures subjected to corrosion process. In F. Biondini & D. M. Frangopol, eds. *Bridge Maintenance,*

Safety, Management, Resilience and Sustainability Proceedings of the Sixth International IABMAS Conference, Stresa, Lake Maggiore, Italy, 8-12 July 2012. CRC Press, pp. 683–690. F. Biondini & D. M. Frangopol, eds. F. Biondini & D. M. Frangopol, eds.

Suda, K., Misra, S. and Motohashi, K. (1993), Corrosion products of reinforcing bars embedded in concrete. *Corrosion Science*, **35**(5–8), 1543–1549.

Synder, K.A. (2001), Validation and modification of the 4sight computer program.

Thybo, A.E.A., Michel, A. and Stang, H. (2013), Modeling of Corrosion-induced Concrete Damage. In *Proceedings of 8th International Conference on Fracture Mechanics of Concrete and Concrete Structures (FraMCoS-8).*

Thybo, A.E.A., Michel, A. and Stang, H. (2017), Smeared crack modelling approach for corrosion-induced concrete damage. *Materials and Structures*, **50**(2), 146.

Tran, K.K. (2012), *STUDY ON CRACKING BEHAVIOR OF CONCRETE DUE TO REBAR CORROSION TRAN Kim Khoa STUDY ON CRACKING BEHAVIOR OF CONCRETE DUE TO REBAR CORROSION*. Nagoya University.

Tuutti, K. (1982), *Corrosion of steel in concrete*, Stockholm, Sweden.

Val, D. V., Chernin, L. and Stewart, M.G. (2009), Experimental and numerical investigation of corrosion-induced cover cracking in reinforced concrete structures. *Journal of Structural Engineering*, **135**(4), 376–385.

Vu, K., Stewart and Mullard (2005), Corrosion-induced cracking: experimental data and predictive models. *ACI Structural Journal*, **102**(5), 719–726.

Wong, H.S., Zhao, Y.X., Karimi, A.R., Buenfeld, N.R. and Jin, W.L. (2010), On the penetration of corrosion products from reinforcing steel into concrete due to chloride-induced corrosion. *Corrosion Science*, **52**(7), 2469–2480.

Zhao, Y., Wu, Y. and Jin, W. (2013), Distribution of millscale on corroded steel bars and penetration of steel corrosion products in concrete. *Corrosion Science*, **66**, 160–168.

Aalborg Portland (2012), *Cement og Beton*,